Search for Baryon Number Violation by Two Units at Belle II

Melanie Hess

Master's Thesis
at the Faculty of Physics
Ludwig–Maximilians–Universität München
Chair of Elementary Particle Physics

Supervisors:
Prof. Dr. Thomas Kuhr
Dr. Thomas Lück

Munich, September 9, 2024

Suche nach doppelter Baryonenzahlverletzung an Belle II

Melanie Hess

Masterarbeit
an der Fakultät für Physik
Ludwig–Maximilians–Universität München
Lehrstuhl für Experimentelle Teilchenphysik

Betreuer:
Prof. Dr. Thomas Kuhr
Dr. Thomas Lück

München, den 9. September, 2024

Abstract

The origin of the matter-antimatter asymmetry in the universe still remains a mystery in physics. So far, possible explanations fail to account for the whole amount of the deviation. The concept of baryon number violation is one of the approaches for the explanation of the matter-antimatter asymmetry.
Experiments are used as an input for new theories and as a test and investigation of existing ones. This study focuses on baryon number violation by two units. The Belle II simulation is used to search for the decay channel $B^+ \to p\,\Lambda\,\pi^+\,\pi^-$ using the decay channel $B^+ \to p\,\overline{\Lambda}\,\pi^+\,\pi^-$ as a control channel.
For the reconstruction of the chosen decay channel, only hadrons are utilized. The fit is developed on the control channel and implemented as an unbinned maximum likelihood fit. In order to estimate the quality of the fit, toy studies are used. Furthermore, the impact of systematic uncertainties is estimated. Since no signal events are expected in the simulation for the decay channel $B^+ \to p\,\Lambda\,\pi^+\,\pi^-$, an upper limit is set on the branching ratio of the chosen decay channel.
As an outlook, a second interesting hadronic decay channel, namely $B^+ \to p\,\Lambda$, is introduced and some first results of the reconstruction are presented.

Contents

Chapter 1

Introduction

The Standard Model of particle physics is a widely accepted model, which can predict and explain many experimental results and observations. However, some open questions remain. They include dark matter and the possible candidates for its nature. Another persisting problem is the neutrino mass, which is confirmed in nature but not included in the Standard Model. The open question forming the background of this thesis is the observation of the matter-antimatter asymmetry.
A possible explanation for the matter-antimatter asymmetry in the universe is baryon number violation. Baryons have a baryon number of 1 and anti-baryons of -1, while the baryon number of mesons is 0 ([37], Chapter 2).
Baryon Number Violation by one unit is constrained through the proton decay [22]. In contrast to the Standard Model, where baryon number violation is a symmetry [18], Grand Unified Theories (GUT) can include proton decay [53, 18, 48]. An overview over the current status of the proton decay including experiment as well as theory can be found in ref. [53]. In ref. [22] the impact of proton decay on baryon number violating processes including the third generation of quarks and thus the b quark is discussed. They analyse the three proton decay channels $p \to \ell^+\nu_\ell\overline{\nu}$, $p \to \pi^+\overline{\nu}$ and $p \to \pi^0\ell^+$, where they define the usage of a virtual b quark as compulsory. Here, ℓ is either e or μ, but they also present results for the decay channel $p \to \ell^+\nu_\ell\overline{\nu}_\tau$. Finally, they exclude the possibility to find evidence for baryon number violation in b-hadron decays at the already existing experiments based on their results for baryon number violation favouring the third family and being highly generation-dependent [22].
However, there could be other physical phenomena suppressing this effect.
Searches for baryon number violation in B meson decays have already been performed.
An example is the search for the decays $B^0 \to \Lambda_c^+ l^-$, $B^- \to \Lambda l^-$ and $B^- \to \overline{\Lambda} l^-$ by the BaBar collaboration [31]. Here, l is either e or μ. Therefore, not only the quantity baryon number is violated, but also lepton number is not conserved. As they do not observe significant signal evidence, they set upper limits at 90% confidence level on the branching fractions resulting in $\mathcal{BR} = (3.2 - 520) \times 10^{-8}$ for the different decay channels [31].
Another search is performed by the LHCb collaboration [8]. Here, they are investigating the decay channels $B^0 \to p\mu^-$ and $B_s^0 \to p\mu^-$. In analogy to the decay channel chosen by

the BaBar collaboration, baryon number is violated as well as lepton number. As they do not find a clear signal, upper limits are set on the branching fractions. At 90% confidence level, their results are $\mathcal{BR} < 2.6 \times 10^{-9}$ for $B^0 \rightarrow p\mu^-$ and $\mathcal{BR} < 12.1 \times 10^{-9}$ for the decay channel $B_s^0 \rightarrow p\mu^-$ [8].
Baryon number violation by two units is already a part of the active research and the development of theories.
An effective Lagrangian violating baryon number by two units has been constructed by ref. [48]. The dimension of their Lagrangian is nine [48].
Citing this result, the reference [54] extends the Standard Model with gauge-invariant operators up to dimension nine in order to violate baryon number by two units. In their analysis, they focus on the deuteron and compute the ratio $R_d = \Gamma_d^{-1}/\tau_{n\bar{n}}$, where Γ_d^{-1} is the deuteron lifetime and $\tau_{n\bar{n}}$ represents the square of the neutron-antineutron oscillation time. Details on their proceeding can be found in ref. [54]. Using the lower limit on the deuteron lifetime of ref. [13], they find the neutron-antineutron oscillation time to be $\tau_{n\bar{n}} > 5.1a = 1.6 \times 10^8 s$ [54].
The possibility of neutral oscillations is a consequence of baryon number violation by two units. An overview of this topic can be found in ref. [18]. Also ref. [13] contains the topic of neutron-antineutron oscillation focusing on the deuteron.
In ref. [10] a search for $\overline{\Lambda} - \Lambda$ oscillations is reported. For the analysis, they choose the decay channel $J/\psi \rightarrow pK^-\overline{\Lambda} + c.c.$. The events are recorded with the BESIII detector and in total $1.31{\times}10^9 J/\psi$ events were analysed by them. More details on the reconstruction channel for the Λ, the selection criteria and further details can be found in ref. [10]. As a result, they calculate an upper limit at 90% C.L. on the oscillation parameter $\delta m_{\overline{\Lambda}\Lambda}$: $\delta m_{\overline{\Lambda}\Lambda} < 3.8 \times 10^{-18} GeV$. This translates to $\tau > 1.7 \times 10^{-7} s$, where τ is the oscillation time [10].
Complementing the searches of neutron-antineutron oscillation, this work focuses on the search for baryon number violation by two units in the decay of the B meson. In analogy to the suppression of baryon number violating processes by one unit in the B meson decay through the long life time of the proton, the same argument applies to baryon number violation by two units and the deuteron. However, also the same counter-argument can be used stating that the involvement of the deuteron could be suppressed.
The structure of this work is presented in the following. First of all, this chapter continues with the explanation of the strategy of the analysis and concludes with the introduction of the SuperKEKB collider and of the Belle II detector. Then, the Standard Model and the Standard Model decay channels used for this analysis as well as the contained particles are described. Afterwards, the simulated data samples, which are used for the analysis, are presented. Hereon follows a chapter focusing on the reconstruction of the events, which covers the decay channel $B^+ \rightarrow p\,\Lambda\,\pi^+\,\pi^-$ as well as the decay channel $B^+ \rightarrow p\,\Lambda$. Contrary, the analysis of these two decay channels is divided into two chapters. Starting with the analysis of the $B^+ \rightarrow p\,\Lambda\,\pi^+\,\pi^-$ in chapter 5, the second decay channel is analysed in chapter 6. Finally, the results and the outlook are recapitulated and discussed in the summary.

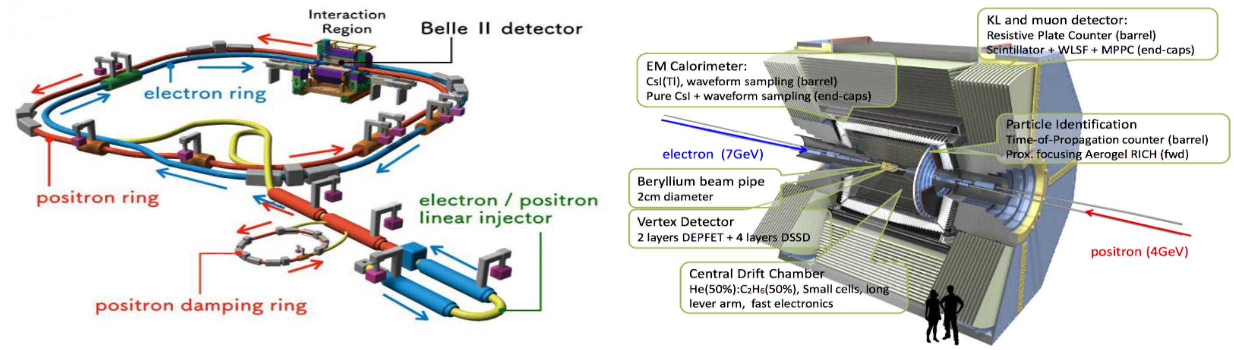

Figure 1.1: This picture is taken from ref. [49]. The left side represents the SuperKEKB collider, while the right side pictures the Belle II detector and its subdetectors. The pure Csl endcaps are not realized.

1.1 The Strategy of the Analysis

Since the properties of the beyond Standard Model decay channel $B^+ \to p\,\Lambda\,\pi^+\,\pi^-$ might contain new physics and can thus deviate from the expectations and as the simulation is based on the Standard Model, the corresponding Standard Model decay channel $B^+ \to p\,\overline{\Lambda}\,\pi^+\,\pi^-$ is used as a control channel and is included in the analysis. Since these are hadronic decays, the decay channel is reconstructed directly by reconstruction of the decay particles. During the reconstruction, loose cuts are applied to the reconstructed events. As a next step, tighter cuts are implemented in order to extract the correctly reconstructed signal events. These cuts are optimized on the Standard Model decay channel. Then, a fitting function is fitted to both decay channels to extract signal yields. For this, different methods are used. The fit itself is an unbinned maximum likelihood fit, but at first both channels are fitted separately and afterwards a simultaneous fit on both channels with a shared signal function is implemented. Both fitting functions are validated using toy studies. The systematic uncertainties are calculated and included in the simultaneous fit. For the Standard Model decay channel, the branching ratio is calculated and for the beyond Standard Model decay channel, an upper limit is set on the branching ratio. In order to calculate the upper limit, the profile negative loglikelihood is used.
In principle, the same analysis strategy can be applied to other hadronic decay channels. Thus, some preliminary results for the decay channel $B^+ \to p\,\Lambda$ are presented.

1.2 The Belle II Experiment

The Belle II experiment is an upgrade of the Belle experiment located in Japan in Tsukuba. It is a so called B factory, as it is mainly designed to produce $B\overline{B}$ pairs out of the decay of the $\Upsilon(4S)$ meson. Thus, it provides the optimal setup for a huge amount of different analyses.

1.2.1 The SuperKEKB Collider

The SuperKEKB collider is a double-ring collider with one ring for electrons at 7 GeV and another one for positrons at 4 GeV [14]. Thus, it is an asymmetric ring collider. The center-of-mass energy corresponds to the mass of the $\Upsilon(4S)$ resonance, which decays mainly into $B\overline{B}$ meson pairs [62]. The SuperKEKB collider is an upgrade of the KEKB collider with a 40 times higher design luminosity of now 8 $\times 10^{35} cm^{-2}s^{-1}$ [14]. In order to reach this increase of the luminosity, essentially the beam size is reduced to 50 nm at the collision point and the currents are doubled in comparison to the KEKB accelerator ([46], Chapter 2). A visualization of the SuperKEKB collider can be found in figure 1.1.
More details can be found for example in ref. [9], ref. [14] and in chapter 2 of ref. [46].

1.2.2 The Belle II Detector

The detector Belle II consists of many subdetectors and its symmetry is cylindrical with the beam line as symmetry axis ([23], Chapter 2). The detector components are presented in the following and are visualized in figure 1.1.
The innermost detector is a charged particle tracking system, which includes two components.

Vertex Detector
The first one is the silicon pixel detector and the silicon vertex detector ([46], Chapter 3) for measuring the quantity momentum of charged particles with low energy and for reconstructing vertices ([23], Chapter 2) out of the combination of charged tracks. It consists of six layers between 14mm and 135mm beam pipe radius ([46], Chapter 3). The first two layers belonging to the pixel detector use sensors, which are pixelated and of the DEPFET type ([46], chapter 3). The last four layers correspond to the silicon vertex detector and as the name already indicates, there are silicon strip sensors, which are double-sided ([46], chapter 3).

Central Drift Chamber
Furthermore, the second one - the Central Drift Chamber (CDC)- can reconstruct charged particle tracks and in the Central Drift Chamber the momentum and energy loss, which is given by dE/dx, are measured ([23], Chapter 2). This applies just for charged particles and the results can be taken for particle identification, which is a major goal of the detectors ([23], Chapter 2).
The CDC is a drift chamber with He-C_2H_6 as chamber gas and small drift cells leading to 3.3cm/(μs) as average drift velocity ([46], Chapter 3). Layers of sense wires, which are arranged in two different orientations, enable the reconstruction of a full 3-dimensional helix track ([46], Chapter 3).
Ionisation is caused by charged particles passing through the gas and these created charges drift to the wires ([1], Chapter 3).

Aerogel Cherenkov Counter
This detector is located in the forward endcap region and it is implemented for the identification of charged particles ([46], Chapter 3). As the name already indicates, the Cherenkov radiator is made of aerogel ([46], Chapter 3).
Making use of the Cherenkov effect, the ring of Cherenkov light is imaged, which has a characteristic radius ([1], Chapter 3). Thus, the Aerogel Cherenkov Counter is an orthogonal source for the information of the mass of particles ([1], Chapter 3).

Time-of-Propagation Counter
Located in the barrel region is the time-of-propagation counter, where the Cherenkov ring is reconstructed using the information of the Cherenkov photons arriving at the photodetector, more precisely the time of arrival and the impact position ([46], Chapter 3). This detector consists of sixteen modules with a quartz bar of a width of 45cm and a thickness of 2cm each ([46], Chapter 3).
Thus, this detector also provides information on the particle identification ([1], Chapter 3).

The following section is based on chapter 6 and 19 of ref. [35]. Most Cherenkov Counters consist of two parts - the radiator and the photodetector. The in the interaction point created charged particles propagate through the radiator and emit Cherenkov radiation, if their velocity v is bigger than the speed of light in the same medium. Thus, $v > c/n$ is required, where n is the refractive index of the medium. The Cherenkov radiation is emitted in a light cone defined by the Cherenkov angle $\Theta_c = 1/(n\beta)$. Here, β is given by v/c, meaning that by measuring the Cherenkov angle in a medium with known refractive index one can determine the velocity of the particle. Together with the momentum p of the particle, which can be determined in the tracking system, one can calculate the mass of the particle with $m = p/(\gamma\beta c)$, where γ is given by $\gamma = 1/(\sqrt{1-\beta^2})$, and thus identify it. The energy loss of the particle based on the Cherenkov radiation can be neglected.
After this general description of Cherenkov Counters based on chapter 6 and 19 of ref. [35], the next subdetector of Belle II is presented.

Electromagnetic Calorimeter
Next in line is the electromagnetic calorimeter. Roughly 90% of the total solid angle are enclosed by the calorimeter ([23], Chapter 2) ([46], Chapter 3) and its radius in the barrel region starts at 125 cm and ends at 165cm ([46], Chapter 3).
The crystals are made of CsI(Tl) and are used in the barrel, the forward endcap and the backward endcap ([46], Chapter 3). Gamma rays are detected as well as electrons in the electromagnetic calorimeter ([46], Chapter 3).

The paragraph about the calorimeter is based on chapter 21 of ref. [35]. In general, one can distinguish two calorimeters: the electromagnetic calorimeter and the hadronic calorimeter. Both types are used to determine the energy of particles. Usually, the electromagnetic calorimeter will handle the photons and electrons. Photons interact with matter via the Compton scattering and the photoelectric effect. Furthermore, they can

convert into e^+e^--pairs, if the photons have enough energy. The two first named processes dominate for low energetic photons (E<1 MeV). For electrons, the Bethe-Bloch formula describes the mean energy loss. There are many options for electrons to interact with matter, but the dominant ones for the energy loss are the bremsstrahlung and the ionization process. For the latter one, the squared values of the particle's speed v, of the particle's charge q and of the material's atomic number A are important quantities for the energy loss. In contrast, the energy loss through bremsstrahlung depends on the energy of the particle. The observed track in a calorimeter are particle showers, where interacting particles create a lot of secondary particles, which can again interact with the material and thus shower in the calorimeter. In order to determine the energy of the particle, the depth of the detector must cover the shower range. A typical variable is the radiation length X_0 defined by the average distance needed to decrease the energy of an electron or positron by bremsstrahlung to E/e. This quantity depends empirically on the charge number Z of the material and also on its atomic number A. The second important quantity for the choice of the detector material and design is the Molière radius. This quantity represents the ability to distinguish two neighboured showers. Since many particles do not penetrate through the calorimeters, only a few further detectors are needed for special particles.
After this paragraph based on chapter 21 of ref. [35] focusing on the physics of the detector, the last Belle II subdetector is presented.

$\mathbf{K_L}$ Muon Detector

The last detector is an instrumented flux return, which is the K_L^0 and μ detector ([23],Chapter 2). It is made of alternating iron plates and detector elements ([46], Chapter 3).
As can be seen in figure 1.1, the barrel region is a resistive plate counter, while the endcaps and the two inner layers of the barrel are made out of scintillator strips with fibers shifting the wavelength ([46], Chapter 3). Thus, the barrel region contains the two inner layers and afterwards twelve layers with two resistive plate chambers ([46], Chapter 3).

Typical muon detectors consist of a detector and a magnetic field ([35], Chapter 20). Thus, the track can be detected, the charge can be determined through the direction of bending and the momentum can be calculated through the track curvature ([35], Chapter 20). There exist different detector designs like the Drift-Tube Detector and the Resistive-Plate Chambers or the Multi-Wire Chambers ([35], Chapter 20).

More details on the detector elements can be found in ref. [9] and in ref. [11].

Chapter 2

Physical Background

In order to prepare the physical background information for the analysis, the following chapter is structured into three parts. At first, the particles and interactions of the Standard Model are described briefly. The second part is dedicated to the individual particles and their properties, while the third part introduces the Standard Model decay channels used for the analysis later on.
Throughout the whole document, charge conjugation is implied.

2.1 The Standard Model

This chapter is based on the historical introduction and chapter 12 and 15 of ref. [21].
At first, the particles are introduced. There are three generations of quarks and leptons. The first quark generation consists of the up quark u and the down quark d. The second quark generation contains the charm quark c and the strange quark s, while the third generation consists of the top quark t and the bottom quark b. The first named quark of each generation has charge +2/3 and the second named quark -1/3. All quarks are spin 1/2 particles. The three lepton generations are the electron e, the muon μ and the tau τ, all with charge -1, together with the corresponding neutrino ν. Also the leptons are spin 1/2 particles.
Additionally, the force carrier particles are bosons with spin one. The photon γ is the carrier of the electromagnetic force, while the $W^{\pm}$ and the Z boson are related to the weak interaction. The strong interaction is mediated via the gluon g. All of these particles are vector bosons. A scalar boson of the Standard Model is the higgs with spin zero.
Baryons are made out of three quarks. Possible combinations consisting only u and d quarks are the proton, the neutron or Δ baryons. If the baryon contains at least one s-quark, it is also called hyperon. An example is the Λ baryon. Contrarily, mesons are made out of a quark and an antiquark. Examples for mesons, which are made out of combinations of u- or d-quark and $\overline{u}$-antiquark or $\overline{d}$-antiquark, are the pions, the ρ mesons and the ω meson.
After this short introduction of the Standard Model based on ref. [21], the particles and

particle	quark content	mass [MeV]	mean life τ [s]	$c\tau$ [m]
B^+	$u\bar{b}$	5279.3	1.64×10^{-12}	$491.1\ \times10^{-6}$
p	uud	938.3		
Λ	uds	1115.76	2.63×10^{-10}	0.0789
π^+	$u\bar{d}$	139.6	2.60×10^{-8}	7.8045

Table 2.1: This table is based on ref. [62]. It summarizes some properties of the particles, which are part of the analysed decay channels.

decay channels utilized for the analysis are presented in the following.

2.2 The Particles

In total, four different particles were used for the analysis. These are the B^+, the Λ, the π^+ and the p as well as their corresponding charge-conjugated anti-particles. Some properties of them will be presented in the following subchapters.

2.2.1 The B^+ Meson

Since the analysed hadronic decay channels are decays of the B meson, some of its properties will be shortly discussed. An overview can be found in table 2.1. As the first detector element is located at a 14mm radius, the $B^\pm$ meson decays before reaching the detector. Thus, it has to be reconstructed out of its decay products and can not be measured directly. The discovery of the B meson was reported by Behrends et al. in 1983 [20].

2.2.2 The Decay Particles

Three different particles are required to reconstruct the chosen decay channels, more precisely, the proton p, the Lambda Λ and the charged pion $\pi^\pm$. Some properties of these particles can be found in table 2.1. Both the proton and the Λ are baryons, whereas the pion is a meson. The stability of the proton has already been discussed in the introduction. Also the lifetime of the pion is long enough to detect it in the detector. In contrast to them, the Λ decays early inside of the detector. Thus, a decay channel for the Λ reconstruction has to be chosen and the decay of the Λ has to be taken into account during the reconstruction of the events for the analysis, since this involves additional reconstruction tools as is explained in chapter 4.

2.3 The Decays

Throughout the analysis, different decay channels were analysed. The main decay channels of the Standard Model $B^+ \to p\,\overline{\Lambda}\,\pi^+\,\pi^-$ and $B^+ \to p\,\overline{\Lambda}$ will be introduced in the following, completed by the decay channel $\Lambda \to p\pi^-$. While the first two decay channels originate in the B meson decay, the last one depicts a possible decay for the Λ baryon. Thus, it is used for the reconstruction of the Λ particle in the main decay channels.

2.3.1 The Decay $B^+ \to p\,\overline{\Lambda}\,\pi^+\,\pi^-$

Here, the B^+ meson decays into four particles, namely $p, \overline{\Lambda}, \pi^+$ and π^-. This is an hadronic decay, since no leptons are involved. Thus, there should be no missing energy in the reconstruction due to decay particles.
In 1988, ref. [15] reported an upper limit at 90% confidence level on the branching ratio $\mathcal{BR}(B^+ \to p\,\overline{\Lambda}\,\pi^+\,\pi^-) < 1.8 \times 10^{-4}$.
The decay $B^+ \to p\,\overline{\Lambda}\,\pi^+\,\pi^-$ was discovered by Belle in 2009 [26] and is described briefly until the end of this subchapter based on ref. [26].
Their analysis includes the three decay modes $B^+ \to p\,\overline{\Lambda}\,\pi^+\,\pi^-$ and the two decays with intermediate decays $B^+ \to p\,\overline{\Lambda}\,f_2(1270)(\to \pi^+\,\pi^-)$ and $B^+ \to p\,\overline{\Lambda}\,\rho^0(\to \pi^+\,\pi^-)$. For the analysis, $657{\times}10^6 B\overline{B}$ pairs were used (integrated luminosity: 605fb^{-1}). As the main background, the continuum background $e^+e^- \to q\overline{q}$ was pointed out by them. For the background suppression, they used for example a Fisher Discriminant, based on ref. [34], as well as applied a charm veto. Afterwards, they carried out an extended unbinned maximum likelihood fit with a Gaussian to model the signal for the M_{bc} variable and a double Gaussian for the ΔE variable. Both the M_{bc} and the ΔE variable are introduced later on. Thereupon, the systematic uncertainties are studied by them, for example the tracking efficiency or the proton identification. As a result, they measure the following branching ratio $\mathcal{BR}$ for the decays [26]:

$$\mathcal{BR}_{B^+ \to p\,\overline{\Lambda}\,\pi^+\,\pi^-} = (5.92^{+0.88}_{-0.84} \pm 0.69) \tag{2.1}$$

$$\mathcal{BR}_{B^+ \to p\,\overline{\Lambda}\,\rho^0(\to \pi^+\,\pi^-)} = (4.78^{+0.67}_{-0.64} \pm 0.60) \tag{2.2}$$

$$\mathcal{BR}_{B^+ \to p\,\overline{\Lambda}\,f_2(1270)(\to \pi^+\,\pi^-)} = (2.03^{+0.77}_{-0.72} \pm 0.27) \tag{2.3}$$

The first uncertainty is the statistical uncertainty and the second one is the systematic uncertainty calculated by ref. [26]. More details on the analysis can be found in ref. [26].

2.3.2 The Decay $B^+ \to p\,\overline{\Lambda}$

In contrast to the previously described decay channel, this decay of the B meson does not contain the two pions. It is thus a two body decay of the B^+ into a proton and $\overline{\Lambda}$ and therefore also an hadronic decay channel.
The main feynman diagram for the decay $B^+ \to p\,\overline{\Lambda}$ is expected to be a $b \to s$ loop diagram, with contributions from annihilation diagrams and tree-level diagrams, but the later one is suppressed by V_{ub} [6].
Before the discovery of the decay channel, different analyses have been carried out and upper limits have been calculated for this decay channel. One is calculated for example in

ref. [15].
Another search for this decay was carried out in 2007 at Belle, ref. [58], as a part of the search for two-body decays that are purely baryonic and is described in the following based on ref. [58]. In total, they analysed three different decay channels: $B^0 \rightarrow \Lambda\,\overline{\Lambda}, B^0 \rightarrow p\,\overline{p}$ and $B^+ \rightarrow p\,\overline{\Lambda}$. The integrated luminosity of the data sample is 414fb^{-1}, which is equivalent to 449×10^6 $B\overline{B}$ events. For the analysis, they applied different cuts and for the Λ baryon reconstruction they required the p´s and π´s to have opposite charge. They define the signal region as follows [58]:

$$5.27 \text{ GeV/c}^2 < \text{M}_{bc} < 5.29 \text{ GeV/c}^2 \quad \text{and} \quad |\Delta E| < 0.05 \text{ GeV}$$

According to their analysis, the continuum background $e^+e^- \rightarrow q\overline{q}$ with $q = u, d, s, c$ dominates the background. Further optimizations of the cuts and the systematics can be found in ref. [58] itself. As a result, they calculated an upper limit of 3.2×10^{-7} at 90% confidence level [58].
The previously described analysis based on ref. [58] reported an upper limit, but there is another search for the decay channel, which is described until the end on this subchapter based on ref. [6].
The branching ratio $\mathcal{BR}$ was measured by the LHCb experiment, ref. [6] and thus, they found evidence for this decay channel. Therefore, they used the full data sample from pp collisions from the years 2011 and 2012 at LHCb. In order to suppress systematic uncertainties, they used the decay $B^+ \rightarrow K_s^0\pi^+$. For the task a data sample of the integrated luminosity of 1 fb^{-1} for 2011 (centre-of-mass energy: 7 TeV) and of 2 fb^{-1} for 2012 (centre-of-mass energy: 8 TeV) is analysed. Requirements for the data taking can be found in the reference itself (ref. [6]). For the selection, they applied different cuts. Furthermore, artificial neural networks are used as multivariate classifiers for the final selection and for the separation of signal and background by them. After the selection, an unbinned extended maximum likelihood fit with the sum of two Crystal Ball functions to describe the signal is carried out by them. The details and systematic uncertainties can be found in ref. [6]. As a result, their branching fraction for the decay $B^+ \rightarrow p\,\overline{\Lambda}$ is [6]:

$$\mathcal{BR}{=}(2.4^{+1.0}_{-0.8} \pm 0.3) \times 10^{-7}$$

The first uncertainty summarizes the statistical systematics and the second uncertainty presents the systematic uncertainties [6].

2.3.3 The Decay $\Lambda \rightarrow p\pi^-$

In addition to the two presented possible decay channels of the B meson, the main decay channel of the Λ will be introduced in this chapter. Since the Λ decays into a p and π, this is also an hadronic decay channel, which means, that inserting this Λ decay into the previously described B meson decays still preserves the properties of being a purely hadronic decay.
The decay $\Lambda \rightarrow p\pi^-$ can be visualized with a tree diagram (fig. 2.1).

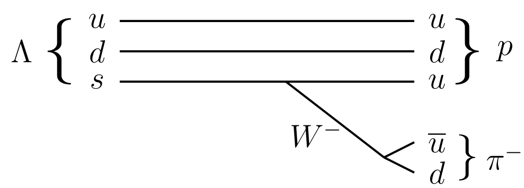

Figure 2.1: This figure visualizes a possible decay diagram for $\Lambda \to p\pi^-$.

The branching ratio $\mathcal{BR}$ of this decay channel has been determined more than once. An early measurement is presented by ref. [29]. Their result is $\mathcal{BR} = 0.624 \pm 0.030$ [29]. The latest measurement of the branching ratio [19] was carried out in an hydrogen bubble chamber with a stopping kaon (K^-) beam and resulted in a branching ratio, which agrees within one standard deviation with the one found in ref. [29]. The branching ratio is calculated as $(\Lambda \to p\pi^-)/(\Lambda \to all) = 0.646 \pm 0.008$ [19].
Another measurement was performed by ref. [39] using a hydrogen bubble chamber. The production of the Λ results out of the interaction of a kaon K^- with a proton p [39]. For the calculation of the $\mathcal{BR}$, they use the formula $(\Lambda \to \pi^- + p)/[(\Lambda \to \pi^- + p) + (\Lambda \to \pi^0 + n)]$ leading to $\mathcal{BR}$=0.643±0.016 [39]. Thus, the result agrees within one standard deviation with the two previously presented results.

Chapter 3

Data and Simulation

The whole analysis is based on simulation more precisely Monte Carlo (MC) simulation. Two different MC samples are used. On the one hand, the Monte Carlo sample provided by the Belle II Collaboration was taken and will be called MC sample in the following. On the other hand, Monte Carlo data samples containing signal were created, which will be called Signal MC in the following. Since the MC sample was produced using the Belle II software release release-06-00-08, also the Signal MC is produced with release 6.

3.1 MC Sample - Generic MC

The MC sample is a generic MC sample of Belle II. Thus, the decays of the particles are implemented according to the Standard Model decays. The generic MC sample used for this analysis represents the events from the e^+e^- collisions in the Belle II detector and is structured as explained in the following: One part consists of the so called continuum background, which is $e^+e^- \rightarrow q\overline{q}$, where $q = u, d, s, c$ meaning the colliding positron and electron create a pair of quark and anti-quark not including the bottom quark and the top quark. The simulation of these events is carried out with the Jetset generator (Pythia [57]) and KKMC[41, 42] ([46], Chapter 4). Another part of the MC sample contains the tau pair production using KKMC [41, 42]. Finally $e^+e^- \rightarrow \Upsilon(4S) \rightarrow B\overline{B}$ events are subdivided into $B^0\overline{B}^0$ and B^+B^- events. They are generated using Pythia [57] and EvtGen [50], which creates events according to a decay table and a model. In total, an integrated luminosity of $\int \mathcal{L}dt = 400fb^{-1}$ is represented in the MC sample corresponding to 216×10^6 B^+B^- events. The PHOTOS simulation package [30] is utilized to generate the radiation of the final state ([46], Chapter 4) and Geant4 [12] simulates the particle detector interaction.
The branching fraction $\mathcal{BR}$ for the Standard Model decay $B^+ \rightarrow p\,\overline{\Lambda}\,\pi^+\,\pi^-$ in the simulation of the generic samples is implemented with the value $\mathcal{BR} = 1.128 \times 10^{-5}$. In the MC simulation, this $\mathcal{BR}$ is attributed to the direct decay of the B meson into the final state alone. During the analysis, it turned out, that different decays including intermediate decays contribute to the signal events. Details are given in table 3.1 and in table 3.2 as well as in the following.

There are different remarks to be made of the decay channels contributing to the signal events. First of all, the branching ratio in the MC for the direct decay $B^+ \rightarrow p\overline{\Lambda}\pi^+\pi^-$ is too high, since the total branching ratio of the PDG [62] has been used for the simulation, which includes the intermediate decays implemented independently in the simulation and summarized in the second group of table 3.1. Secondly, the decay $B^+ \rightarrow p\overline{\Lambda}\rho^0$ and the decay $B^+ \rightarrow p\overline{\Lambda}f_2$ are implemented in the simulation with the PDG values [62]. But this ignores the fact, that the reference [26] has measured the product $\mathcal{BR}$ for the decay $B^+ \longrightarrow p\overline{\Lambda}\rho^0(\rightarrow \pi^+\pi^-)$ and the decay $B^+ \longrightarrow p\overline{\Lambda}f_2(\rightarrow \pi^+\pi^-)$, which also includes the decay of the f_2 and the ρ^0 to $\pi^+\pi^-$. As a result, ref. [26] calculated the branching ratio for $B^+ \longrightarrow p\overline{\Lambda}\rho^0(\rightarrow \pi^+\pi^-)$, which is the product of the $\mathcal{BR}$s of $B^+ \longrightarrow p\overline{\Lambda}\rho^0$ and $\rho^0 \rightarrow \pi^+\pi^-$. Thus, the implementation in the MC of $B^+ \longrightarrow p\overline{\Lambda}\rho^0$ needs to take into account the decay of the ρ^0. Unfortunately this is not the case, but the result for the product branching ratio is transfered without changes. The same applies to the intermediate decay via the f_2. Thirdly, the decay $B^+ \rightarrow p\Lambda(1520)$ corresponding to the last decay channel of the table would violate baryon number by two units. Furthermore, the implementation of the branching ratio is not consistent with the PDG [62]. Also the decay $B^+ \rightarrow \Lambda\overline{\Lambda}\pi^+$ has an outdated $\mathcal{BR}$ in the simulation. The PDG value [62] is based on the new measurement in ref. [25] and is an upper limit at $90\% CL$. The third part of table 3.1 summarizes further decay channels contributing to the signal events.

decay	product $\mathcal{BR}$
$B^+ \longrightarrow p\overline{\Lambda}\pi^+\pi^-$	1.13×10^{-5}
$B^+ \longrightarrow p\overline{\Lambda}\rho^0(\rightarrow \pi^+\pi^-)$	4.80×10^{-6}
$B^+ \longrightarrow p\overline{\Lambda}f_2(\rightarrow \pi^+\pi^-)$	1.13×10^{-6}
$B^+ \longrightarrow \Lambda(\rightarrow p\pi^-)\overline{\Xi}^+(\rightarrow \overline{\Lambda}\pi^+)$	3.19×10^{-7}
$B^+ \longrightarrow \Lambda(\rightarrow p\pi^-)\overline{\Lambda}\pi^+$	1.79×10^{-6}
$B^+ \longrightarrow \pi^+$ J/ψ $(\rightarrow \overline{\Lambda}\Lambda(\rightarrow p\pi^-))$	3.98×10^{-8}
$B^+ \longrightarrow \Delta^{++}(\rightarrow p\pi^+)\overline{\Lambda}\pi^-$	2.00×10^{-6}
$B^+ \longrightarrow p\overline{\Sigma}_c^0(\rightarrow \pi^+\overline{\Lambda}_c^-(\rightarrow \overline{\Lambda}\pi^-))$	3.15×10^{-7}
$B^+ \longrightarrow p\pi^+\overline{\Lambda}_c^-(\rightarrow \overline{\Lambda}\pi^-)$	2.41×10^{-6}
$B^- \longrightarrow \overline{p}\ \Lambda(1520)\ (\rightarrow \Lambda\pi^+\pi^-)$	1.00×10^{-7}

Table 3.1: This table summarizes the decay channels with $\mathcal{BR}$ from MC contributing to the signal events in the MC sample for the first decay.

However, there are some signal events in the MC simulation, which could not be assigned to a specified decay channel. Table 3.2 depicts the mother particles of the p, $\overline{\Lambda}$, π^+ and π^-. In total, six different combinations are found, which have not been found in the decay table for the MC. Probably, they result out of quark hadronisation processes, which are also simulated. As the branching fraction is not known, an efficiency can not be calculated for them. To sum it up, the chosen decay channel for the Standard Model decay is modelled incorrectly in the simulation and also the intermediate decays reveal problems with the branching ratio $\mathcal{BR}$.

	p	$\overline{\Lambda}$	π^+	π^-
mother particle 1	B^+	B^+	ω	ω
mother particle 2	B^+	B^+	η_c	η_c
mother particle 3	$\Delta0$	B^+	B^+	$\Delta0$
mother particle 4	B^+	$\overline{\Sigma}^{*+}$	$\overline{\Sigma}^{*+}$	B^+
mother particle 5	$B+$	B^+	$\overline{D}0$	$\overline{D}0$
mother particle 6	B^+	$\overline{\Sigma}^{*-}$	B^+	$\overline{\Sigma}^{*-}$

Table 3.2: This table summarizes signal events not directly defined in the decay file.

These differences between the MC simulation and the expected results on data are taken into account differently during the analysis. The final results are calculated on the decays based on the PDG [62] and the ref. [26] including weights to adjust the wrong branching ratios. Therefore, the MC sample is edited and weights are applied to the decay channels in order to match the true values (see Chapter 5.3.4).
For the analysis of the second decay channel $B^+ \longrightarrow p\Lambda(\overline{\Lambda})$, the implementation is also not exactly correct. Here, the Λ and $\overline{\Lambda}$ in brackets means, that second decay channel refers to both the beyond Standard Model decay channel and the corresponding Standard Model decay channel. Similarly, the first decay channel refers to the decay $B^+ \rightarrow p\,\Lambda(\overline{\Lambda})\,\pi^+\,\pi^-$. In the simulation, the value of the branching ratio for the Standard Model decay channel is $\mathcal{BR} = 3.2 \times 10^{-7}$, which is the value given in ref. [58]. But as is stated in chapter 2, this is an upper limit for the branching ratio. Another analysis succeeds in measuring the branching ratio to be $\mathcal{BR} = (2.4^{+1.0}_{-0.8} \pm 0.3) \times 10^{-7}$ [6]. Consequently, the number of events for $B^+ \longrightarrow p\overline{\Lambda}$ is overrated in the simulation. This is taken into account in the analysis of the second decay channel.

3.2 Signal MC - Creation of Simulated Data

This chapter starts with the Signal MC for the first decay.
The Signal MC for the Standard Model decay channel $B^+ \rightarrow p\,\overline{\Lambda}\,\pi^+\,\pi^-$ is generated as follows: one million $\Upsilon(4S)$ events decay to B^+B^- using the decay model vector to scalar-scalar (VSS) of EvtGen [50]. Either the B^+ decays to $B^+ \rightarrow p\,\overline{\Lambda}\,\pi^+\,\pi^-$ or the B^- decays to $B^- \rightarrow \overline{p}\,\Lambda\,\pi^-\,\pi^+$ using the phase space (PHSP) decay model and including final state radiation, while the other B meson decays generically as previously described. Also the Λ of the decay channel decays generically. Again, the used generators are EvtGen [50] for the decays and Geant4 [12] for the detector simulation. As a result, one million signal events have been generated. In principle, there could be more signal events resulting out of the generic decay, but because of the low branching fraction for this decay channel, those are negligible. In the following, charge conjugation is implied.
The Signal MC for the beyond Standard Model decay channel was created in the same way after replacing the $B^+ \rightarrow p\,\overline{\Lambda}\,\pi^+\,\pi^-$ decay with $B^+ \rightarrow p\,\Lambda\,\pi^+\,\pi^-$. In this case, the number of one million events should be accurate, since this decay is not part of the Standard Model. Both Signal MC samples include beam background.
As is already mentioned in the previous chapter, the reference reporting on the branching fraction of $B^+ \rightarrow p\,\overline{\Lambda}\,\pi^+\,\pi^-$, ref. [26], measured the direct decay and two intermediate decays to the same final state particles, namely $B^+ \rightarrow p\,\overline{\Lambda}\,\rho^0(\rightarrow \pi^+\,\pi^-)$ and $B^+ \rightarrow p\,\overline{\Lambda}\,f_2(\rightarrow \pi^+\,\pi^-)$. As they are included in the signal events in the main parts of the analysis, also the properties of these three decays are compared later on. Therefore, Signal MC is produced. The generators and the beam background stay the same.
As before one million decays of the B^+B^- were created, where one B meson always decays into the signal channel and the other one generically. In total 1×10^6 events are generated for the decay $B^+ \rightarrow p\,\overline{\Lambda}\,\rho^0(\rightarrow \pi^+\,\pi^-)$ and for the decay channel $B^+ \rightarrow p\,\overline{\Lambda}\,f_2(\rightarrow \pi^+\,\pi^-)$

each. The decay of the B meson to p, $\overline{\Lambda}$ and the intermediate particle ρ^0 or f_2 is described with the phase space decay model simulating also radiative corrections (PHOTOS [30]), while $\rho^0 \to \pi^+ \pi^-$ uses the vector to scalar scalar (VSS) decay model and $f_2 \to \pi^+ \pi^-$ the tensor to scalar scalar (TSS) decay model of EvtGen [50].
For these two decay channels, no corresponding beyond Standard Model decay channel has been created, since they are used for the systematic uncertainties and for the comparison to the direct decay channel.
Also for the second decay channel $B^+ \to p\,\Lambda(\overline{\Lambda})$, Signal MC has been created.
Here, both the creation of the Signal MC sample for the Standard Model decay channel $B^+ \to p\,\overline{\Lambda}$ and of the Signal MC sample for the beyond Standard Model decay channel $B^+ \to p\,\Lambda$ are treated the same way as the corresponding direct decay channel of the first decay and one million events each have been created. They only differ in the two pions, which are deleted for the second decay channel $B^+ \to p\,\Lambda(\overline{\Lambda})$.
Overall, six different Signal MC samples have been created, four for the first decay channel and two for the second decay channel. All of them are produced with the Belle II software [2, 47] release release 6 and the same beam background. But since they model different decay channels, they are produced using different decay models of EvtGen [50].

Chapter 4

The Event Reconstruction

This chapter presents the reconstruction of the events. The cuts included in this chapter are cuts on the event reconstruction and differ from the cuts explained in chapter 5 for the reduction of the background and the extraction of the signal. Thus, they define a pre-selection for further studies and optimization.
Now, the event reconstruction of the first decay channel is described.
Both Signal MC and MC sample are analysed using the same reconstruction. The selected decay channel includes both protons and pions from the B meson decay and from the Λ or $\overline{\Lambda}$ decay. On the proton and pion needed for the Λ or $\overline{\Lambda}$ reconstruction, which are called p_Λ and π_Λ, no cuts are implemented. Whereas on the proton and the two pions resulting directly out of the B meson decay, different cuts have been applied for example on the tracks. These cuts are summarized in table 4.1. The probability to be of a certain particle type is calculated by dividing the particles´ likelihood to be a proton or pion by the sum of the likelihoods of the particle to be a proton, electron, muon, pion, kaon and deuteron. The cut on the particle's probability is implemented in order to reduce misidentification of particles. Another cut is placed on the polar angle to restrict the angle to the CDC

p	π
probability to be a $p > 0.1$	probability to be a $\pi > 0.1$
$17° <$ polar angle $\theta < 150°$	$17° <$ polar angle $\theta < 150°$
number of hits in CDC detector>20	number of hits in CDC detector>20
dr for POCA with respect to IP<0.5cm	dr for POCA with respect to IP<0.5cm
$\lvert$dz$\rvert$ < 2cm with respect to IP	$\lvert$dz$\rvert$ < 2cm with respect to IP

Table 4.1: This table summarizes the cuts applied to the proton p and the pion π during the reconstruction. The cuts are not implemented on the particles p_Λ and π_Λ. The CDC detector is the Central Drift Chamber and dr is the transverse distance to the interaction point (IP). POCA is the abbreviation for point of closest approach. The dz has basically the same definition for the z direction. More details are given in the text and in ref. ([1], Chapter 7).

acceptance ([46], Chapter 3). The next cut is implemented on the number of hits in the CDC detector. This is the number of hits used for the fit to the track in the CDC ([46], Chapter 5). As the fit quality improves for more hits, this cut ensures the quality of the resulting particles. Finally, the last two cuts lead to the rejection of particles originating too far from the interaction point.
As the lifetime of the Λ (table 2.1) enables the particle to decay outside of the beam pipe and thus the decay particles do not originate from the interaction point, the reconstruction of this particle requires a special treatment. Therefore, two different candidate lists are loaded and the candidates are made, a fit is applied to the vertices and the invariant mass is required to be between 1.10 GeV/c^2 < M < 1.13 GeV/c^2. The first list is filled in the following way: combinations of one positive and one negative tracks are taken and a vertex fit is applied to them using RAVE [60]. Then, the invariant mass of the Λ is computed. The second list reconstructed the Λ's, which decayed inside of the beam pipe. Finally, the two lists are merged. A more detailed description can be found in ref. ([46], Chapter 5)([1], Chapter 23).
Thereupon, the B meson decay is reconstructed by combining the p, Λ, π^+ and π^- using the cut 5.2 GeV/c^2 < M$_{bc}$ and $|\Delta E| < 0.3$ GeV. The variables are given by [26] ([23], Chapter 7):

$$M_{bc} = \sqrt{E_{beam}^2 - p_B^2} \tag{4.1}$$

$$\Delta E = E_B - E_{beam} \tag{4.2}$$

Here, the center-of-mass frame is used and the beam energy is given by E_{beam}, whereas E_B and p_B are the energy and the momentum of the B meson, respectively. Due to the definition of the variables, M_{bc} peaks at the B meson mass for correctly reconstructed candidates and ΔE peaks at zero. The width of the ΔE peak is finite because of the spread of the beam energy and the energy resolution of the detector ([23], Chapter 7). Similarly, the peak of the M_{bc} variable is widened basically due to the spread in the beam energy ([23], Chapter 7). These two variables have been used in a variety of analyses. Further examples for the usage of one or both of these variables can be found in references [17, 58, 61].
At this point of the reconstruction, the decay channel is reconstructed. Thus, the reconstruction for the beyond Standard Model decay channel and the Standard Model decay channel differ at this point for the Λ particle. Then, another vertex fit is applied. Here, TreeFitter [38] is used, which is a tool that performs a fit for the whole decay chain of the B meson. Afterwards, the true Monte Carlo simulation information is extracted for the particles.
Additionally, the rest of event is included, where the rest of event contains the particles, which are not used in the signal side reconstruction. The cuts applied to the rest of event particles are summarized in table 4.2. They are divided into cuts applied to tracks and cuts applied to clusters sharing a cut on the momentum in the center of mass frame to exclude final state particles originating not in B events. Apart from that, a cut is applied to the number of hits in the CDC detector for tracks, thus again ensuring the quality of

Cuts for the rest of event	
track cuts	cluster cuts
number of hits in CDC detector > 0	momentum ≥ 0.05 GeV/c
momentum in center of mass frame ≤ 3.2 GeV/c	

Table 4.2: This table contains the cuts for the particles going into the rest of event in the reconstruction file. The CDC detector is the Central Drift Chamber.

the corresponding particle. On the cluster cut side, an additional momentum cut is implemented to reduce photons of the background.

As was already mentioned, the reconstruction for the beyond Standard Model decay channel and the Standard Model decay channel of the first decay differ only in the either Λ or $\overline{\Lambda}$ insertion in the reconstruction channel. The implemented cuts and the procedure are exactly the same. There are three Signal MC samples for the Standard Model decay channel of the first decay, more precisely the direct decay channel and the two intermediate decays via the ρ^0 and the f_2. The reconstruction of the events for all of them is exactly the same as explained before. No differences are implemented for the intermediate decays, since the aim is to estimate their impact on the correctly reconstructed signal events of $B^+ \to p\,\overline{\Lambda}\,\pi^+\,\pi^-$. The reconstruction on the MC sample is run twice, once with the Standard Model decay channel and once with the other one.

For the reconstruction of both the beyond Standard Model decay channel and the Standard Model decay channel of the second decay, basically the same reconstruction is used. However, since this decay channel does not include pions originating directly from the B meson, the cuts on the pion given in table 4.1 are unnecessary and therefore not applied to the reconstructed particles. One significant change is the usage of another release for the reconstruction, namely the light release nebelung. For the reconstruction of the decay channel $B^+ \to p\,\Lambda(\overline{\Lambda})\,\pi^+\,\pi^-$ release 6 is used. Apart from that, no changes are made for the procedure and the cuts. As for the first decay channel, the only difference between the beyond Standard Model decay channel and the Standard Model decay channel is the usage of either Λ or $\overline{\Lambda}$ in the decay string of the B meson. The Signal MC samples are handled with the corresponding beyond Standard Model decay channel reconstruction or Standard Model decay channel reconstruction, whereas the reconstruction on the MC sample is run twice and thus separately for both decay channels.

Chapter 5

Analysis of the $\mathbf{B^+ \rightarrow p\,\Lambda\,\pi^+\pi^-}$ Decay Channel

As a decay channel for the search for baryon number violation, the decay of the B meson $B^+ \rightarrow p\,\Lambda\,\pi^+\,\pi^-$ was chosen, because it offers many advantages. First of all, baryon number violation by two units is fulfilled as the baryon number of mesons is zero and both the proton p and the Lambda Λ are baryons and not anti-baryons. Thus, their baryon number is equal to one. As this decay channel is not part of the Standard Model, it will be attributed to the beyond Standard Model. Secondly, the existence of a similar Standard Model decay channel $B^+ \rightarrow p\,\overline{\Lambda}\,\pi^+\,\pi^-$ provides useful support for the development of the analysis, since it can be used as a control channel. These two decay channels differ only in the Λ for the beyond Standard Model decay and the $\overline{\Lambda}$ for the Standard Model decay. Thirdly, both decay channels are purely hadronic. Therefore, no neutrino is part of the decay, which would lead to missing energy, because the particle itself can not be reconstructed in the detector. Fourthly, as the Λ is reconstructed via the p and π, the final state particles are all charged. This is another advantage for the reconstruction.
To conclude, the decay channel $B^+ \rightarrow p\,\Lambda\,\pi^+\,\pi^-$ has a lot of advantages and will be analysed in the following.

5.1 Results of the Decay Reconstruction on the Signal MC

After the reconstruction of the events, the whole Signal MC ($1{\times}10^6$ events) is analysed. Therefore, Monte Carlo variables are used to distinguish between correctly reconstructed events and wrongly reconstructed events, which can not be done on data. First of all, the results for the Standard Model (SM) decay channel $B^+ \rightarrow p\,\overline{\Lambda}\,\pi^+\,\pi^-$ are presented in the following.
The signal region is defined for the M_{bc} variable around the B meson mass $M_B = 5.279$ GeV/c^2 [62]. Since the mass of the $\Upsilon(4S)$ is $M_{\Upsilon(4S)} = 10.58$ GeV/c^2 [62], which is connected to an upper limit at roughly $M_{bc} > 5.29$ GeV/c^2, the signal region is chosen to be $M_{bc} >$

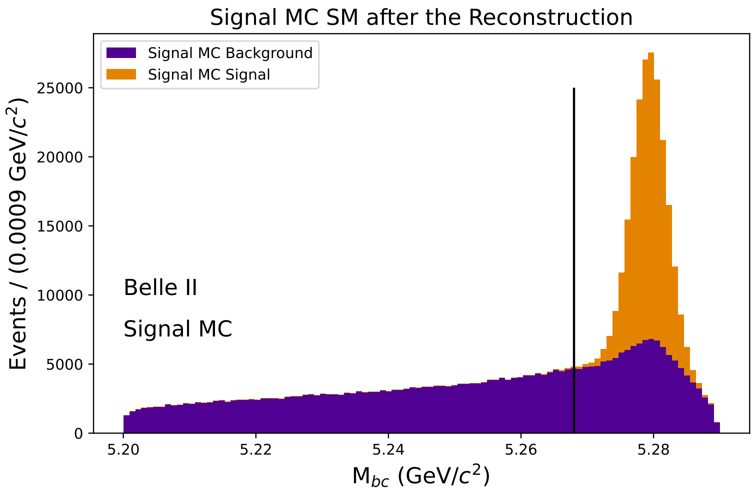

Figure 5.1: This picture visualizes the events after the reconstruction of the Standard Model (SM) decay channel on the corresponding Signal MC. Correctly reconstructed events are depicted in orange and the other events in purple. The peak in the background in the signal region $M_{bc} > 5.268$ GeV/c^2, which is indicated with the vertical black line, is visible, although the height of the signal is much bigger.

5.268 GeV/c^2. The upper limit of the signal region is not implemented by hand, but is naturally constrained by half of the center of mass energy. This definition is used for both the Standard Model decay channel and the beyond Standard Model (BSM) decay channel. Inside of the signal region 153757 correctly reconstructed particles for the Signal MC of the Standard Model decay channel are found, which corresponds to a reconstruction efficiency of $\epsilon_{rec} = N_{rec}/N_{gen} = (15.38 \pm 0.04)\%$, where N_{rec} is the number of correctly reconstructed particles and N_{gen} is the number of generated signal events. The error follows from the binomial distribution. Unfortunately, also the incorrect reconstructed events peak in the mass spectrum of the M_{bc} variable as can be seen in figure 5.1. The number of wrongly reconstructed particles was investigated for all combinations and the results are shown in figure 5.2. The peak of the wrongly reconstructed particles is ignored throughout the analysis, but is picked up again in the systematic uncertainties chapter 5.5.
Secondly, the same properties of the beyond Standard Model decay channel are analysed. With 153582 correctly reconstructed events in the Signal region, the efficiency is $\epsilon_{rec} = (15.36 \pm 0.04)\%$, which is basically the reconstruction efficiency for the Standard Model decay channel. In parallel, there is also a peak in the M_{bc} variable in the previously defined signal region. This is depicted in figure 5.3. As before, the results of the analysis of incorrectly reconstructed particles can be found in figure 5.4. The general impression is the same for Standard Model and beyond Standard Model decay channel: the reconstruction of the Lambda and its daughter particles are the main sources for wrongly reconstructed events. One difference is the number of wrongly reconstructed events for wrong $\overline{\Lambda}$ and the pions, since this is vice versa the distribution for Λ and the pions. However, this seems

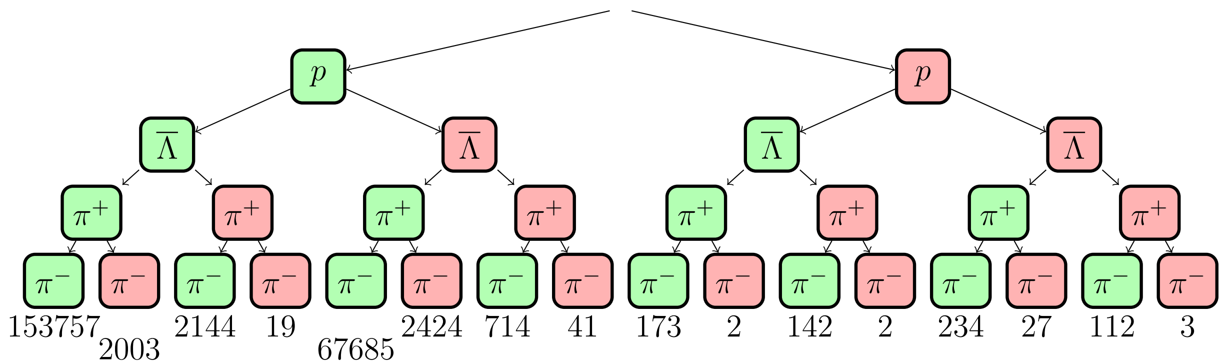

Figure 5.2: This picture visualizes the distribution of wrongly reconstructed particles in the signal region $M_{bc} > 5.268$ GeV/c^2 for the Standard Model decay channel in Signal MC. Green boxes represent correct reconstruction and red boxes indicate wrongly reconstructed particles. The daughter particles of $\overline{\Lambda}$ contain 22211 cases, where p_Λ is incorrectly reconstructed and 19057 cases, where π_Λ is wrongly reconstructed and 8014 cases where both are incorrectly reconstructed. Here, just these two particles are considered and no requirements for other particles are made. Thus, they can not be directly assigned to the graph presented here.

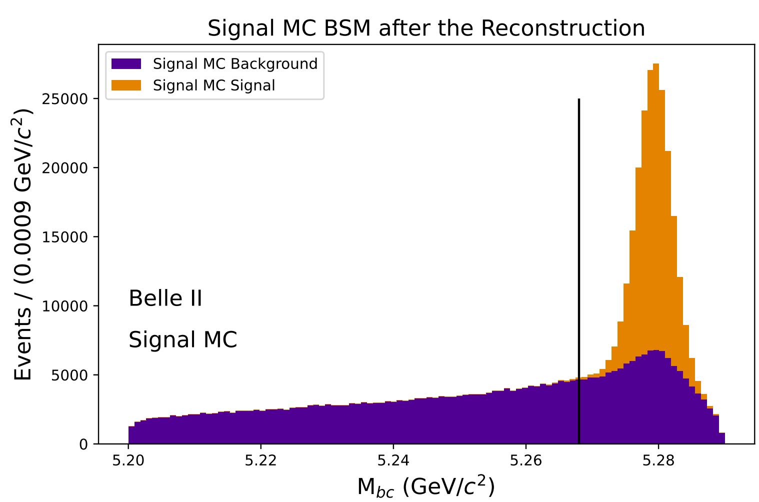

Figure 5.3: In this figure, the events after the reconstruction of the beyond Standard Model (BSM) decay on the corresponding signal MC are illustrated. In parallel to the picture for the Standard Model, the correctly reconstructed events are depicted in orange, while the others are depicted in purple. The signal region is on the right of the black line. Also for this decay, the background peak in the signal region exists.

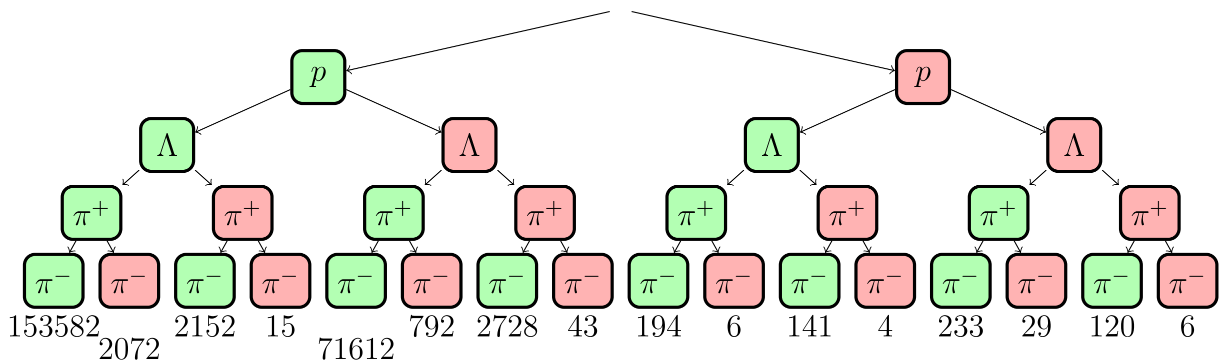

Figure 5.4: This picture visualizes the distribution of wrongly reconstructed particles in the signal region $M_{bc} > 5.268$ GeV/c^2 for the beyond Standard Model decay channel in Signal MC. As before, green boxes represent correct reconstruction and red boxes stand for wrongly reconstructed particles. The daughters of the Λ contain 20091 cases, where p_Λ is incorrectly reconstructed and 20158 cases, where π_Λ is wrongly reconstructed and 6778 cases where both are incorrectly reconstructed. Here, just these two particles are considered and no requirements for the other particles are included. Therefore, the numbers do not correspond to numbers of the presented picture.

reasonable, since the $\overline{\Lambda}$ changed from particle to antiparticle.
After looking at the signal MC for both decays separately, the shapes of the two decays are compared for different variables. This is done to verify, that the same analysis can be used for both decay channels. Here, the comparison for the M_{bc} variable is presented as an example. Overall, no huge differences have been found. To compare the two decay channels with different number of events, the beyond Standard Model decay channel is normalized to the other one. The comparison is done for correctly reconstructed signal events in the signal region. Thereupon, the p-value of the χ^2 test is calculated with only 40 bins and a normalization of the counts of the Standard Model decay channel to estimate the difference between the shapes. The results are shown in figure 5.5. This corresponds to a p-value of 0.33 for the range of 5.268 GeV/c^2 - 5.290 GeV/c^2. If the p-value is close to zero, the χ^2 indicates a bad goodness-of-fit. This p-value underlines the comparability of the two distributions.
Until the end of this subchapter, the χ^2 distribution based on chapter 2 of ref. [28], the χ^2 test based on chapter 4 of ref. [28] and the p-value based on chapter 4 of ref. [28], too, are introduced.
The χ^2 distribution is given by ([28], Chapter 2):

$$f(z,n) = \frac{1}{2^{n/2}\Gamma(n/2)} z^{n/2-1} e^{-z/n} \tag{5.1}$$

Here, Γ is the gamma function. In case of a histogram, which has many entries in each bin and whose data sample follows a Poisson distribution, the χ^2 test will follow the just

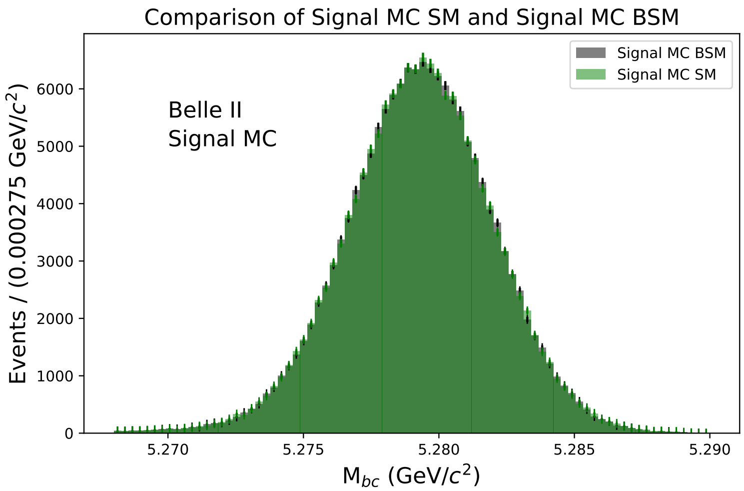

Figure 5.5: This figure presents the comparison of the Standard Model Signal MC with the beyond Standard Model Signal MC in the signal range. Here, only correctly reconstructed events are considered. Both decay channels have the same shape and mostly agree within one errorbar.

presented $f(z, n)$. The χ^2 test is defined as ([28], Chapter 4):

$$\chi^2 = \sum_{i=1}^{N} \frac{(n_i - \nu_i)^2}{\nu_i} \tag{5.2}$$

N is the number of bins of the histogram used for the test, which also represents the degrees of freedom. Then, the number of entries in the corresponding bin is given by n_i, whereas ν_i is the number of expected entries. Furthermore, the p-value is defined as ([28], Chapter 4):

$$p = \int_{\chi^2}^{\infty} f(z, N) dz \tag{5.3}$$

For equ. 5.3, N represents the degrees of freedom ([28], Chapter 4).

5.2 Results of the Decay Reconstruction on the MC sample

After working with the Signal Monte Carlo, both decay channels are reconstructed on the MC sample, which represents the Belle II data collection. The analysis is developed on the Standard Model decay channel $B^+ \to p\,\overline{\Lambda}\,\pi^+\,\pi^-$ and afterwards applied to the beyond Standard Model decay channel $B^+ \to p\,\Lambda\,\pi^+\,\pi^-$.
Starting with the Standard Model decay channel, figure 5.6 depicts all events after the reconstruction. The correctly reconstructed events are included in the purple genericB^+B^-

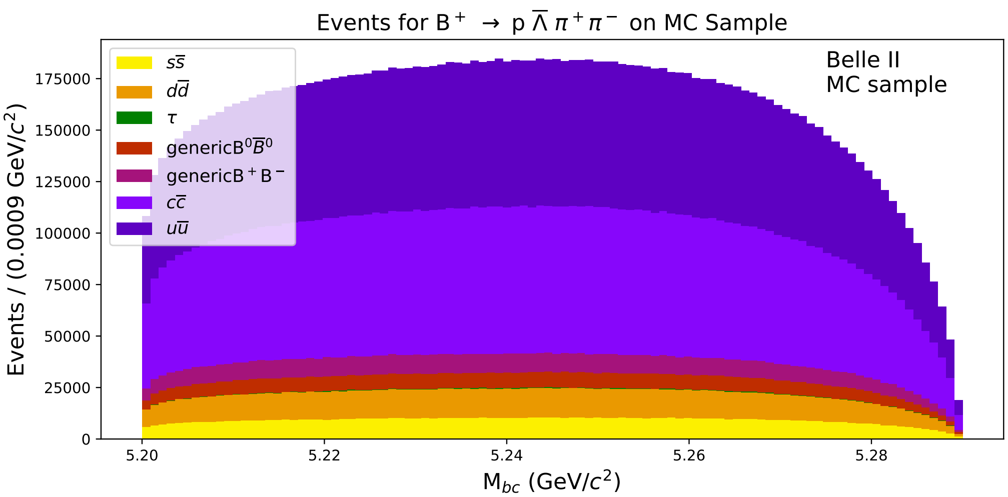

Figure 5.6: This figure, which was produced with an integrated luminosity of $\int \mathcal{L}dt$=400fb^{-1}, shows the events after the reconstruction of the Standard Model decay channel on the MC sample. The most dominant background appears due to the continuum background, especially the $c\overline{c}$ and $u\overline{u}$ quark-pairs. The correctly reconstructed signal events, which are contained in the MC sample, are included in the genericB^+B^- contribution, but there is no visible peak in the signal region. With genericB^+B^- and generic$B^0\overline{B}^0$ the decays of these $B\overline{B}$ pairs according to the Standard Model are represented.

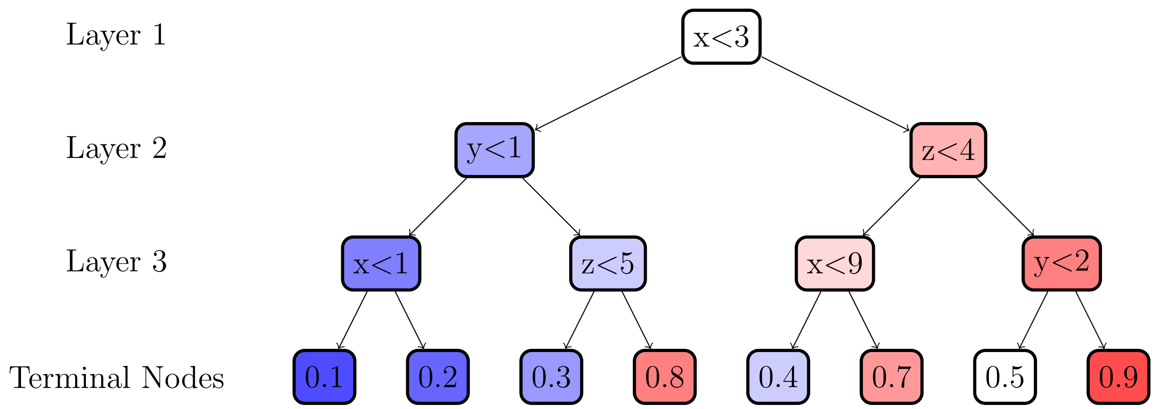

Figure 5.7: This figure is reproduced from ref. [45]. It depicts the functionality of a Decision Tree containing three layers. For each layer, the condition has to be verified or falsified and this decides, which tree branch has to be taken next. The Terminal Nodes state the probability of the data-point to be signal, where the definition of signal has to be adapted to the individual DT.

region. As can be observed from the figure 5.6, the background events dominate over the signal of the MC sample, which is not visible. Especially the continuum background $e^+e^- \to q\overline{q}$ with $q = u, d, s, c$ leads to the dominance over the signal. Here, the $u\overline{u}$ and $c\overline{c}$ quark-pairs produce more background than the $d\overline{d}$ and $s\overline{s}$ quarks. This was expected, since the production is mainly electromagnetic. Thus, the square of the charge is included in the cross section. Consequently, four times more produced $u\overline{u}$ and $c\overline{c}$ over $d\overline{d}$ and $s\overline{s}$ are expected. In comparison to the continuum background, the tau background is small.
To decrease the background and make the signal visible, a Boosted Decision Tree (BDT) was trained. The concept of the BDT is introduced in the following chapter.

5.2.1 Boosted Decision Tree

A Boosted Decision Tree (BDT) is used to reduce the background and extract the signal events for the analysis of the MC sample. There are different BDTs (multivariate classifiers) and two of them are explained now based on ref. [45].

Decision Tree
The functionality of a Decision Tree (DT) is described by figure 5.7. The depth of the tree D, a hyper-parameter, fixes the number of consecutive cuts, which lead to the classification of an event. The training sample includes labels differentiating signal and background. The cuts are optimized during the fitting-phase such that the progress in separating signal from background is locally optimized since at each node every feature is analysed separately. As a critical point of the DT one has to mention the easily resulting over-fitted state of these Decision Trees since statistical fluctuations in the sample used for the training often dominate the predictions of the deep DT. This DT description is based on ref. [45].

	$c\bar{c}$	$u\bar{u}$	$d\bar{d}$	$s\bar{s}$	τ-pair	$B^0\overline{B}^0$	B^+B^-	Signal MC (SM)
BDT training files	3.45	3.12	3.11	3.28	2.62	3.57	3.35	39.95
BDT test files	0.17	0.16	0.15	0.15	0.13	0.18	0.17	2.01
reduced MC	96.42	96.39	96.46	96.38	96.28	96.43	96.60	60.05

Table 5.1: This table provides an overview percentage of particles after the reconstruction included in the individual categories. For Signal MC correctly reconstructed signal events and incorrectly events are included in the numbers. The denominator for the calculation is the corresponding number of events in the full MC sample after the reconstruction.

Boosted Decision Tree

During the fitting-phase, DTs are constructed one after another. Because of this procedure, the separation power of the BDT is usually larger than the one of the DT. In contrast to a DT, the Boosted Decision Tree has two more hyper-parameters, which act anti-correlated to each other: N and η. N represents the number of trees, which is also the number of boosting steps and η is the shrinkage. The presented BDT description is based on ref. [45]. An overview of other possible Decision Trees can be found in ref. [45].

The BDT for this analysis, implemented in the Belle II software [2, 47], was trained on event shape variables. They contain different variables connected with the thrust [33] axis and KSFW variables ([23], Chapter 9) as well as Cleo Cone [17] variables. The KSFW variables are given by the following equation ([23], Chapter 9):

$$KSFW = \sum_{l=0}^{4} R_l^{so} + \sum_{l=0}^{4} R_l^{oo} + \gamma \sum_{n=1}^{N_t} |(P_t)_n| \tag{5.4}$$

Here, the variables for the first two sums are modified Fox-Wolfram moments and the third term is multiplied by γ, which is a free parameter and is summed to the total number of the particles, while the variable inside the sum is the transverse momentum of the corresponding particle ([23], Chapter 9).

The modified Fox-Wolfram moments of equ. 5.4 are explained in more detail in ref. ([23], Chapter 9) as are the Fox-Wolfram moments, which were defined in ref. [36].

The Cleo Cones are defined as nine cones of 10 degree more opening angle than the previous cone each around the thrust axis of the candidate and also covering the backwards direction of the thrust axis with the same definition [17].

The reduced Fox-Wolfram R2 ([23], Chapter 17) variable was excluded for the final BDT, since previous attempts of training a BDT have shown, that the BDT focuses on this variable and basically ignores the other variables. So it was decided to cut on this variable separately and to exclude it from the BDT.

The training sample (overview in table 5.1) was chosen to roughly represent the ratio of the contents of the MC sample and at the same time it should be possible to create a

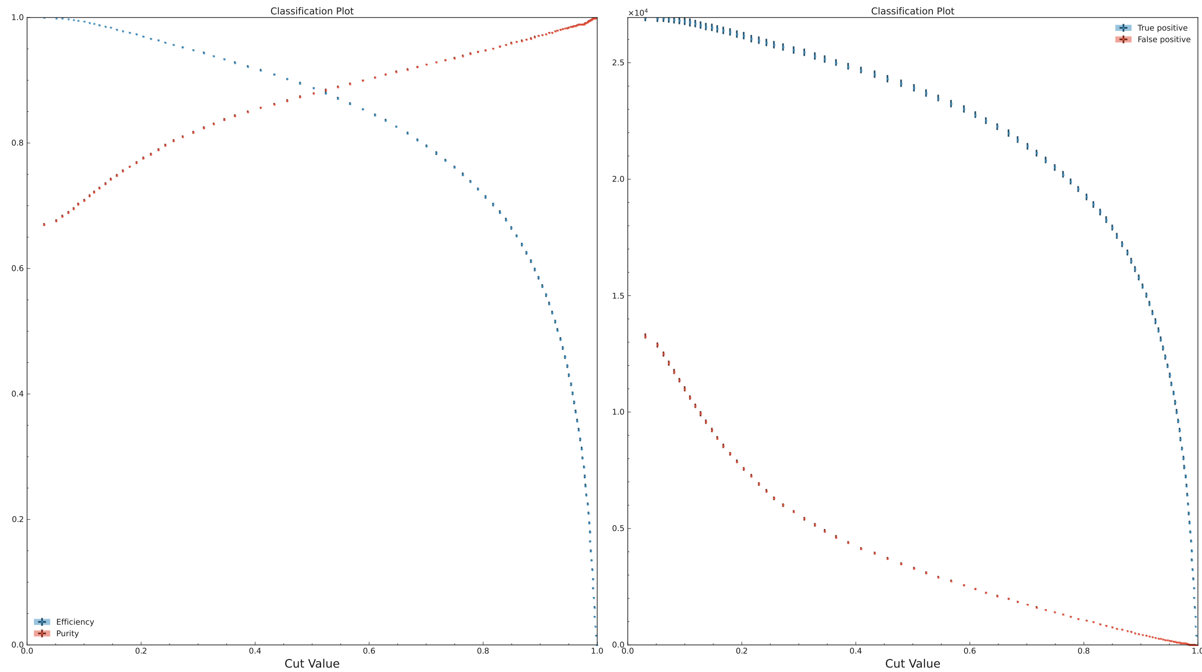

Figure 5.8: This figure depicts the classification plot of the BDT training. On the left side, the horizontal axis is the cut value, while the blue color depicts the efficiency and the red color the purity. The plot on the right side uses the blue color for true positive and the red color for false positive, while the horizontal axis is again the cut value with range (0,1).

smaller test sample for the BDT with exactly the same ratios (see Appendix table B.1). To enhance the signal events, signal MC was added to both the training samples for the BDT and the test samples to check the performance of the BDT. The exact number of files can be found in the Appendix in table B.1, while the percentage of used particles is presented in table 5.1. This table also includes the percentage of files for the decreased MC sample, which excludes the files used for the BDT training and adjusts the number of files such that it matches the ratios in the full MC data sample. The training sample of the BDT has apart from the reconstruction cuts none of the additional cuts explained in the next chapter. The aim of the BDT training is to reduce the background events, therefore the target variable is chosen to be the variable stating whether an event is a continuum event or not.
For the BDT characteristics the default values of the Belle II software implementation [2, 47] are used.
Testing the BDT led to the results depicted in figures 5.8 - 5.10. The classification plot, figure 5.8, depicts the curves for efficiency and purity and furthermore the true positive and false positive events with the cut value as horizontal axis. The second picture, figure 5.9, compares the training sample and the test sample on the signal efficiency and the background rejection. Since both behave equally, there seems to be no bias in the training sample. The last figure 5.10 presents the overtraining plot. Also this plot underlines that

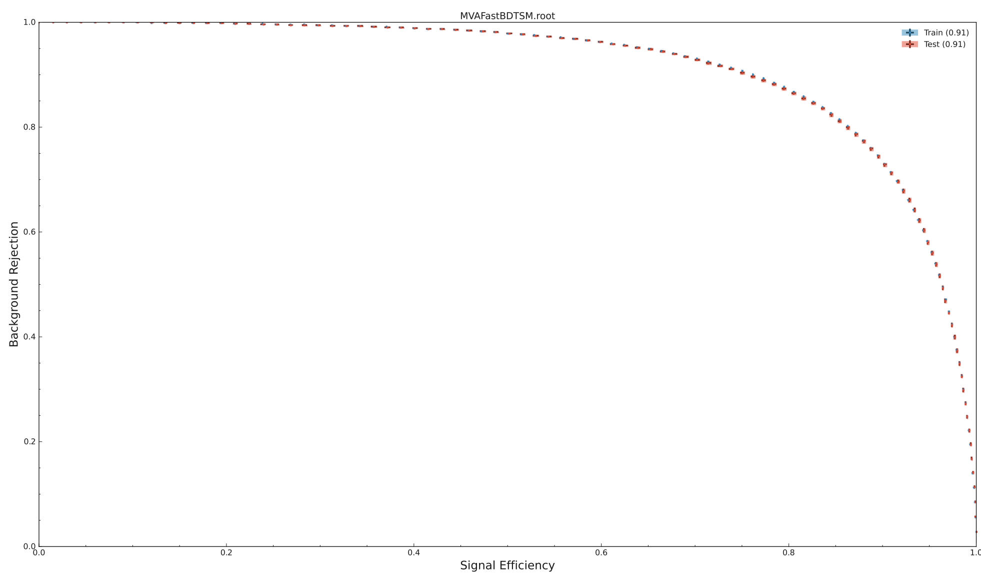

Figure 5.9: This figure shows the signal efficiency of the BDT on the horizontal axis versus the background rejection on the vertical axis both with a range of zero to one. The red colour represents the test sample and the blue colour the training sample. As can be seen in the figure, both samples have a similar distribution.

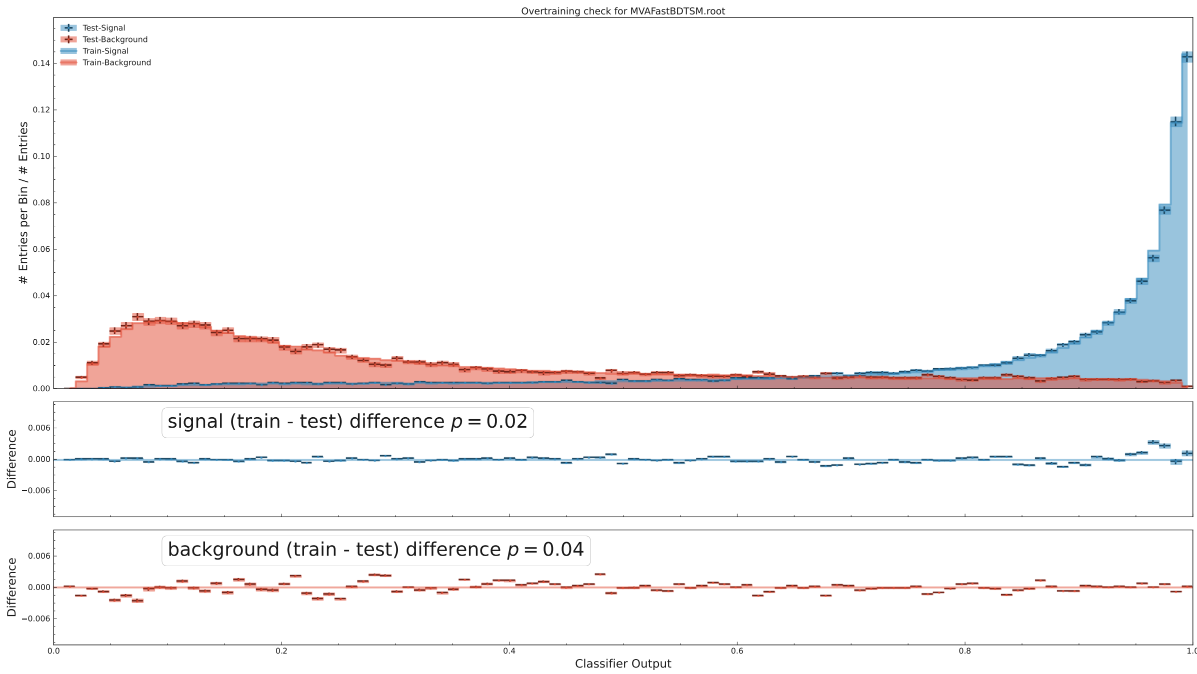

Figure 5.10: This figure visualizes the overtraining test for the BDT. The test sample and the training sample match quite well as can be seen from the overtraining plot. The p-value is also included in the figure. The horizontal axis is the classifier output.

the training sample is not biased.
As a next step, the importance of the input variables is analysed. The variables connected to the thrust axis and three KSFW variables turned out to be the most important ones with an importance of more than 3 out of the range from 0 to 100. The exact numbers can be found in the Appendix in figure A.1 and the used variables in the Appendix in chapter A.1.

5.2.2 The Cut Optimization

As a next step, the Cont.BDT output is combined with other variables to find the optimal cut on the data sample. Therefore, a figure of merit (f.o.m.) is used, whose definition is given in the following [55]:

$$f.o.m. \equiv \frac{\epsilon}{\frac{a}{2} + \sqrt{N_{bkg}}} \tag{5.5}$$

Here, ϵ is the signal efficiency in the signal region and N_{bkg} is the number of background events in the signal region. The parameter a corresponds to the number of sigmas. For this analysis, a is chosen to be three. The MC sample used for the cut optimization is the full data sample. This would lead to a small bias, since roughly 3% of the sample have been used for the BDT training. Thus, the efficiency (table 5.2) of the BDT variable was calculated on the decreased MC sample and its impact is comparable with the numbers

cut	complete MC sample		decreased MC sample	
	ϵ of N_{sig} $\frac{N_{sig,all}}{N_{sig,others}}$	ϵ of N_{bkg} $\frac{N_{bkg,all}}{N_{bkg,others}}$	ϵ of N_{sig} $\frac{N_{sig,all}}{N_{sig,others}}$	ϵ of N_{bkg} $\frac{N_{bkg,all}}{N_{bkg,others}}$
Cont.BDT output<0.44	0.812	0.370	0.810	0.370
χ^2 probability (vertex fit)>0.001	0.789	0.363	0.787	0.363
E(p_Λ) >1.11 [GeV]	0.924	0.765	0.923	0.764
$\lvert\Delta E\rvert$ <0.02 [GeV]	0.930	0.063	0.932	0.063
R2<0.37	1.000	0.998	1.000	0.999
$\frac{p_\Lambda\_protonID}{p_\Lambda\_protonID+p_\Lambda\_pionID}$>0.6	0.949	0.275	0.950	0.275
$\frac{p\_protonID}{p\_protonID+p\_pionID}$>0.6	0.996	0.932	0.996	0.932
cosTBTO<0.9	0.958	0.905	0.958	0.908

Table 5.2: This table summarizes the cuts used on the MC sample. Cont.BDT output is the BDT variable. $N_{sig,all}$ is the number of signal events after all cuts applied, whereas $N_{sig,others}$ is the number of signal events after the application of all cuts except the cut in column 1. The same system is used for the calculation of the background efficiency. The efficiency, which is denoted as ϵ and is calculated for the signal region, for the signal should be bigger than the efficiency for the background. Otherwise, the cut would decrease the signal amount more than the background events. While the complete MC sample has an integrated luminosity of $\int \mathcal{L}dt$=400fb^{-1}, the decreased MC sample is roughly 3% smaller, since the MC data sample used for the training of the BDT, is excluded.

on the full MC data sample. This result is expected, since the figure 5.10 does not exhibit an overtraining. As a result, the cuts optimized on the full MC sample are taken without further maximization on the reduced MC sample.
In order to find the initial cuts, different cut variables are varied to maximize the figure of merit. Every time one variable changes the limit, the other variables are varied again to check for a better combination of cuts.
In the end, eight different variables were used, which are presented in the following. Out of these eight, only six are varied and two cuts connected to the particle identification are adopted from ref. [61]. Their efficiencies are summarized in table 5.2 and visualized in fig. 5.11. In fig. 5.11, the picture in the middle depicts the MC sample for the SM decay channel with all cuts applied. The pictures in the circle around depict the sample with all cuts implemented except the cut specified on the arrow pointing to the middle. Thus, the impact of the individual cuts with all other cuts applied is depicted. In the following, the cuts will be presented in more detail.

Cont.BDT output < 0.44

The BDT variable is the output of the BDT. According to the values of the training variables of the BDT, each event is assigned a probability to be a background event. Thus, signal events should have a low value for the BDT variable, whereas background events are expected to have a high value. Since the BDT output variable is a probability, its output

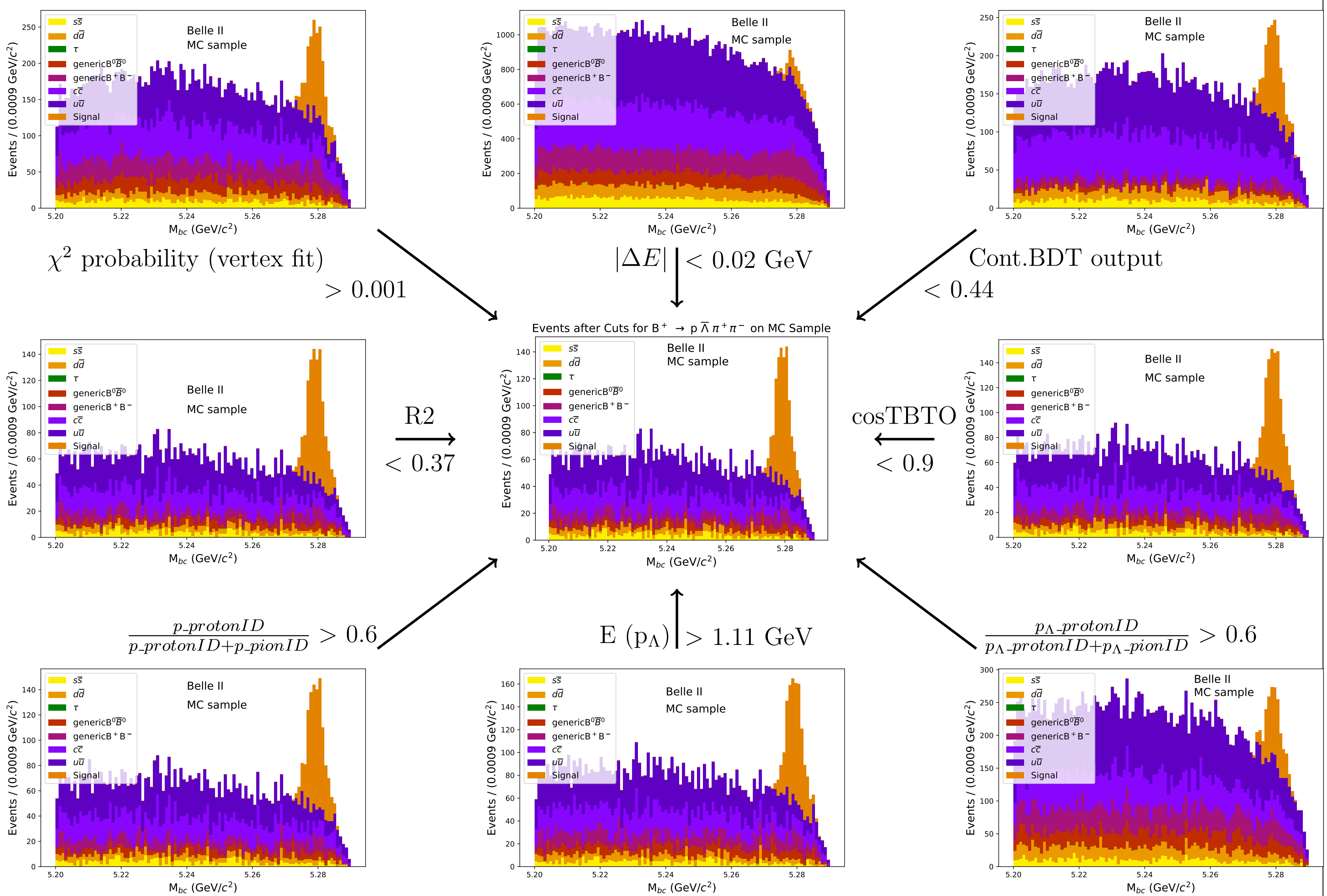

Figure 5.11: These images show the efficiencies for the cuts. They picture the application of one cut, where all others are implemented. This is a visualization of table 5.2. Background (top down): $u\bar{u}$, $c\bar{c}$, genericB^+B^-, generic$B^0\overline{B}^0$, τ, $d\bar{d}$, $s\bar{s}$

can take values in the range of zero to one.

χ^2 probability > 0.001
Another variable used is the χ^2 probability of the vertex fit result from TreeFitter [38]. This is the p-value, which has already been used before (equ. 5.3). The distribution of this variable for the signal and the background is presented in fig. 5.12. Here, both signal and background peak at zero, but it is still reasonable to cut on χ^2 probability > 0.001 as is demonstrated in table 5.2.

E (p_Λ) > 1.11 [GeV]
On top of that, the energy of the proton p of the Lambda Λ is utilized as another cut variable. This was found to be meaningful, since there is a background enhancement beneath this energy (fig. 5.12). Thus, misidentified decays can be excluded.

$|\Delta E| < 0.02$ [GeV]
This variable has already been used for a cut during the reconstruction of the events. Though, a much wider cut of $|\Delta E| < 0.3$ [GeV] has been used. As can be seen in table 5.2, this cut is the most powerful one for the background reduction. But in order to not cut into the steep side of the signal distribution (fig. 5.12) of the $|\Delta E|$, it is not chosen tighter.

R2 < 0.37
This variable is a continuum suppression variable, but as already explained, instead of using it for the BDT, it is a separate cut variable. The calculation of R2 requires the 2nd order Fox-Wolfram moments and the 0-th order Fox-Wolfram moments and takes the ratio of these two ([23], Chapter 17). Table 5.2 reveals the small impact of this cut. Nevertheless, it reduces more background than signal. As a consequence, it is included.

$$\frac{\mathbf{p_\Lambda\_protonID}}{\mathbf{p_\Lambda\_protonID + p_\Lambda\_pionID}} > \mathbf{0.6}$$

In contrast to the previously described cuts, this cut is not a cut on a variable itself, but on the combination of variables. The ratio of the probability of the proton candidate from the Λ decay to be a proton divided by its combined probability to be a proton or a pion has to be greater than 0.6. This can be recalculated to the following: $p_\Lambda\_protonID > \frac{3}{2} p_\Lambda\_pionID$ This cut is adapted from ref. [61]. Therefore, the same limits were used as in the reference, where they also cut on this ratio with kaonID.

$$\frac{\mathbf{p\_protonID}}{\mathbf{p\_protonID + p\_pionID}} > \mathbf{0.6}$$

In analogy to the cut on the protonID of the p_Λ, the same cut was applied on the proton resulting directly out of the B meson decay. As before, this cut is also adapted from ref. [61] and is not varied. The limit is fixed on the likelihood of the particle to be a proton to be greater than 1.5 times the likelihood of the proton to be a pion. As can be seen in table 5.2, the impact of this cut on the background reduction is smaller, than the impact of the cut on the p_Λ. Therefore, the cut on p_Λ is more efficient.

cosTBTO < 0.9

Although this variable was used for the BDT, it was found to be still useful to cut upon. For the calculation of cosTBTO, the thrust axis of the signal B and the thrust axis of all other particles are needed. The variable is the cosine of the angle between these two axes ([1], Chapter 7). The importance of the cosTBTO for the background reduction is also rather small, but it is still kept, since it reduces more background than signal.

At this point, it should be mentioned, that the definition of the f.o.m. (equ. 5.5) is rather used for decay channels, where no prediction is present, e. g. so far unmeasured decay channels. For the cut optimization of the Standard Model decay channel, the significance could have been used, as N_{sig} is known:

$$S = \frac{N_{sig}}{\sqrt{N_{sig} + N_{bkg}}} \tag{5.6}$$

This formula is used for example in ref. [26]. As the cut optimization is done on the Standard Model decay channel, there might be a better composition of the cuts for the beyond Standard Model decay channel. To estimate the impact of other cuts, the previously found cuts were varied on a small scale for the analysis of the beyond Standard Model decay channel using the f.o.m. (equ. 5.5) for the cut optimization. The cut variation is done in the signal region of the reduced MC sample and the efficiency is calculated on the Signal MC sample. Paying attention to not cut into the side of the signal distribution for the cut variables (fig. 5.12, fig. 5.14), it was found, that the biggest impact results out of the cosTBTO parameter, which could have an enhanced accepted interval corresponding to a cut of cosTBTO<0.9. Still, the increase in the f.o.m. (equ. 5.5) is 3% and thus rather negligible. Details can be found in the Appendix in table B.2.
As was already mentioned, the shapes of the Signal MC for the Standard Model decay channel and for the beyond Standard Model decay channel were found to be similar. To underline this, fig. 5.13 depicts the shapes for the M_{bc} variable after the application of the presented cuts and only for correctly reconstructed signal events. The χ^2 value for the comparison is calculated in the range (5.27, 5.288) GeV/c^2 with forty bins and a normalization of the total number of counts of the Standard Model decay channel to match the total amount of counts of the beyond Standard Model decay channel and its p-value (equ. 5.3) is 0.01. Although this value is small, fig. 5.13 depicts the similarity of the distribution of the M_{bc} variable for the two decays. The comparison of the shapes and the calculation of the p-value is also done for the cut variables. The results for the calculated p-values are given in the Appendix in chapter B.3. Although the p-values are rather low especially for R2 and the Cont.Prob output, the distributions (figure 5.14) are found to be similar. Thus, the determined cuts presented in this chapter are not changed. These cuts, developed on the SM decay channel, will be applied to the beyond Standard Model decay channel.

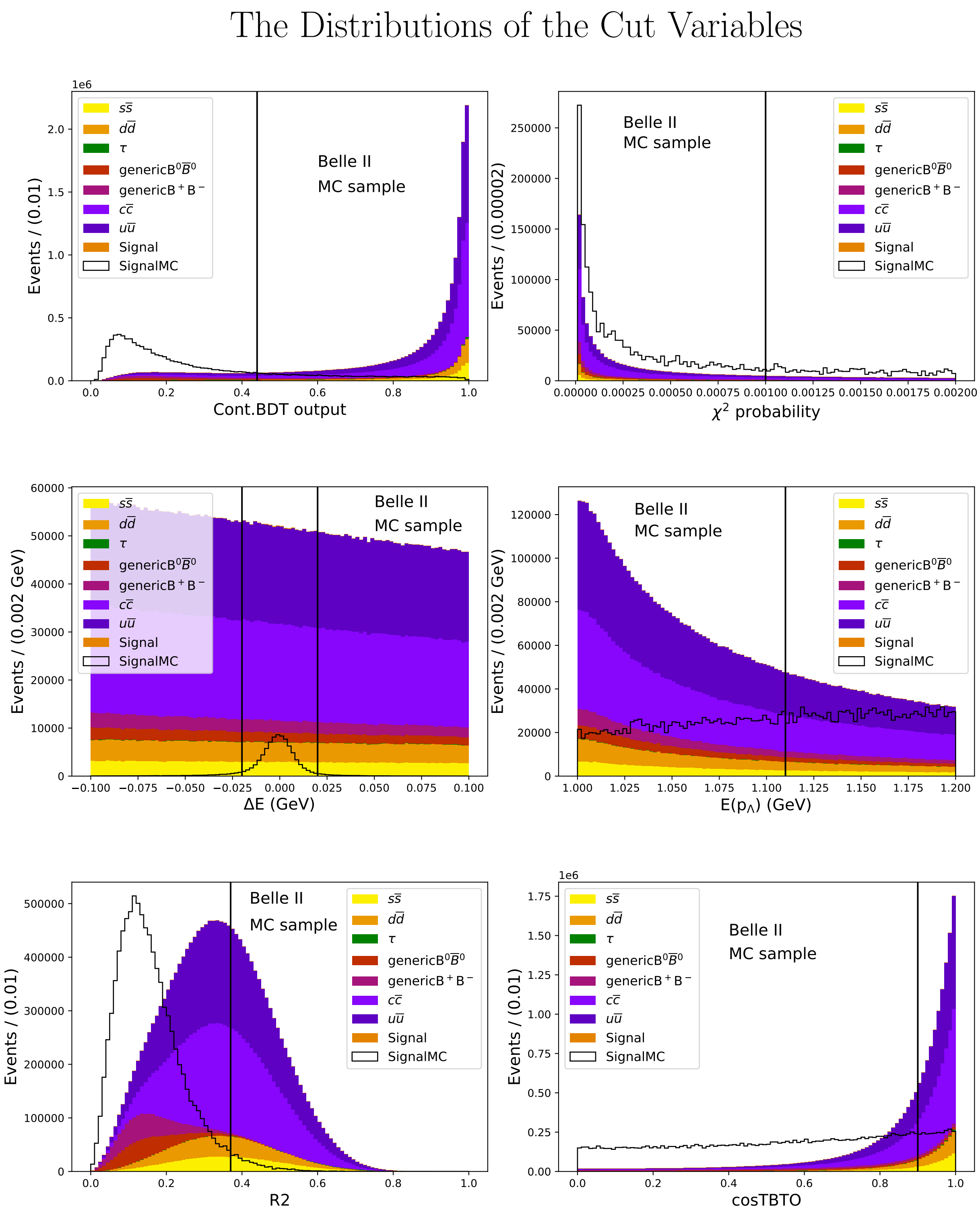

Figure 5.12: This figure presents the distributions of the six cut variables, which are not fixed throughout the optimization. The signal includes only correctly reconstructed decays of the Signal MC, which are weighted in order to enhance them.

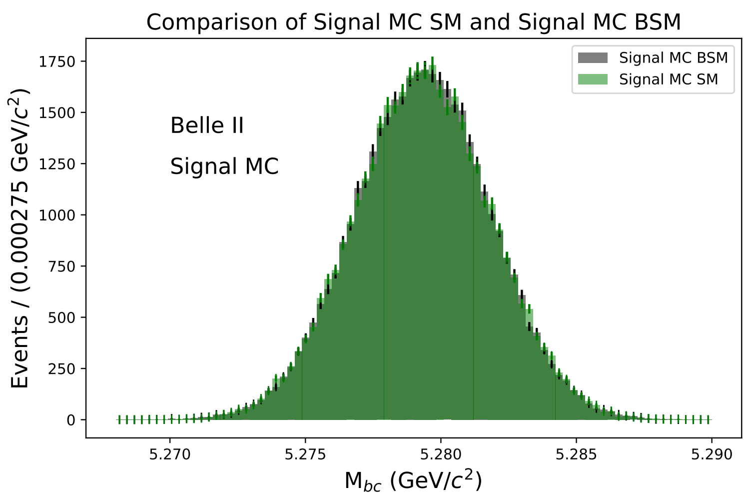

Figure 5.13: This picture shows the comparison of the two decay channels $B^+ \to p\,\Lambda\,\pi^+\,\pi^-$ and $B^+ \to p\,\overline{\Lambda}\,\pi^+\,\pi^-$ on Signal MC with applied cuts, proving the similar shapes and thus the compatibility of the two decay channels. For the beyond Standard Model decay channel, the full Signal MC data sample is taken, while for the Standard Model decay channel, the reduced Signal MC (see Appendix table B.1) was used, hence the beyond Standard Model decay channel was scaled down with a weight computed out of the number of signal events to match the other decay. This plot only depicts correctly reconstructed signal events.

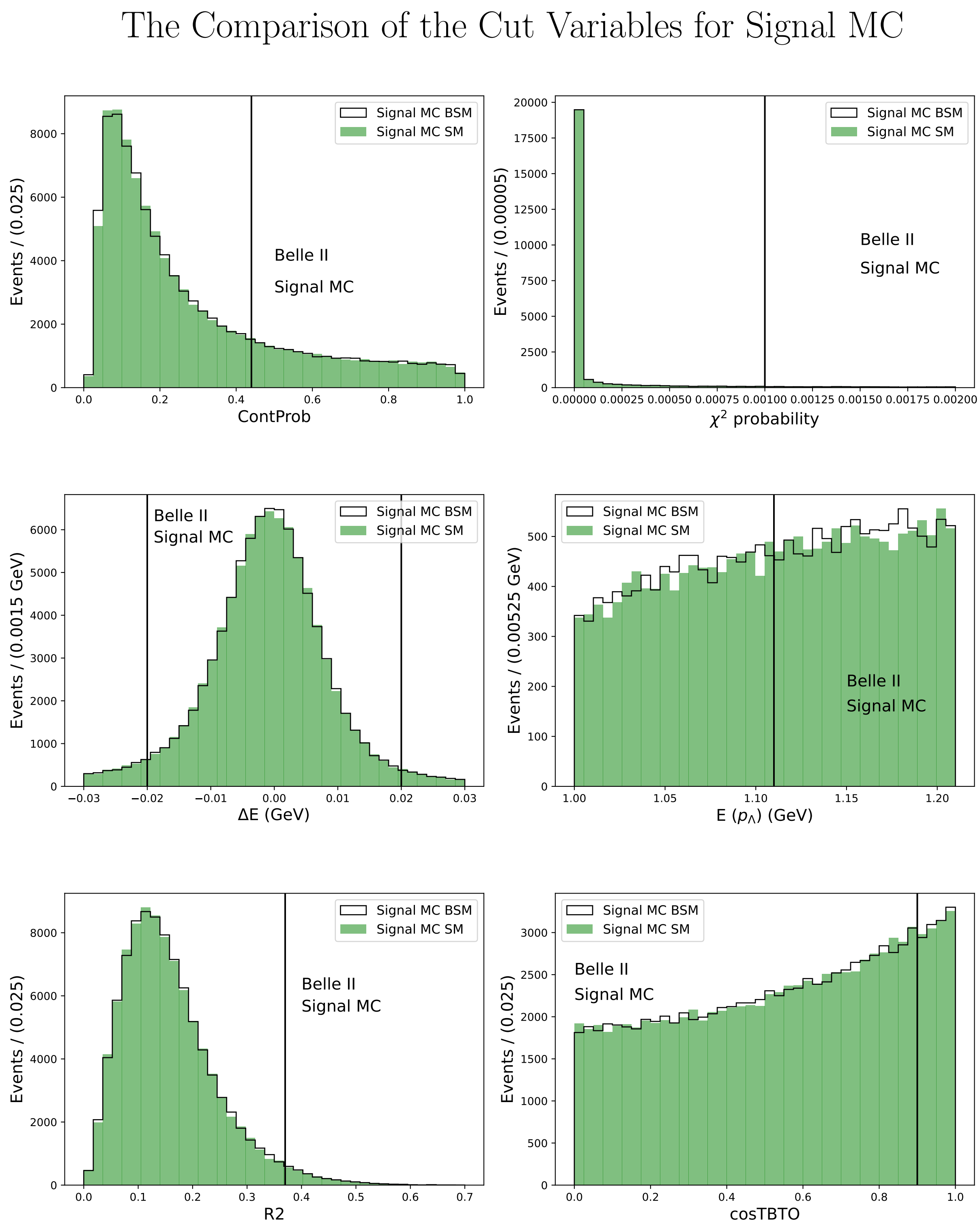

Figure 5.14: This figure presents the distributions of the six cut variables, which are not fixed throughout the optimization. The Signal MCs contain only correctly reconstructed signal events and the BSM decay channel events are normalized to the SM decay channel events.

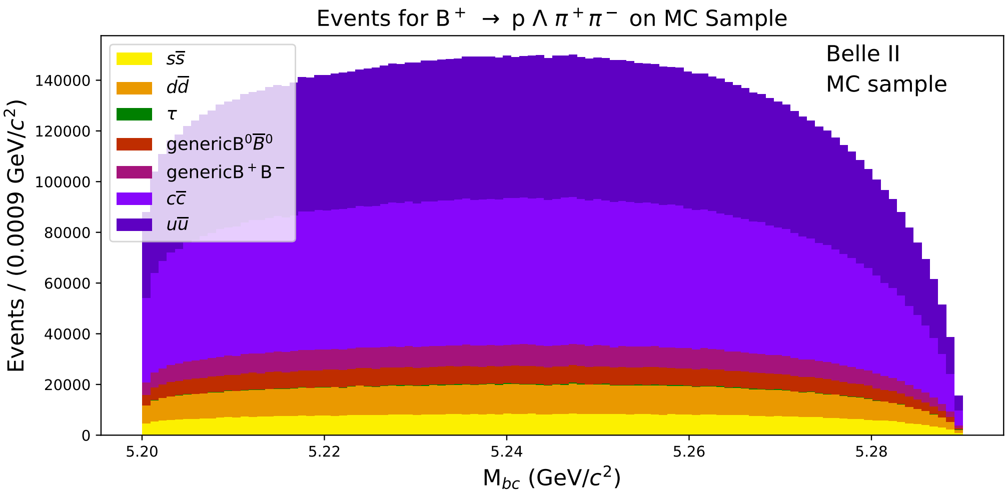

Figure 5.15: This picture illustrates the events after the reconstruction for the beyond Standard Model decay channel. Compared to the figure 5.6 for the Standard Model decay channel, the distribution of the individual components is the same, though the total height is smaller. Again, the continuum background dominates and the τ background is barely visible. This figure is created with the reduced MC sample (see Appendix table B.1).

After reconstructing the beyond Standard Model decay channel on the reduced MC sample, the different components are analysed. As can be seen in figure 5.15, the dominant background is again the continuum background, though the total height of the background components is less than that for the Standard Model decay channel. Again, the τ background is only a small component and is dominated by all other background.
Since this is the result of the beyond Standard Model decay channel, no signal event is expected. However, using the MC variables, two signal events are found. Their origin was determined to be a mistake in the MC simulation, since correctly reconstructed signal events would lead to baryon number violation, which is not included in the Standard Model MC. This mistake was the implementation of the decay channel $B^+ \to p\,\Lambda(1520)$, which has a branching fraction of $\mathcal{BR} = 1.5 \times 10^{-6}$. However, the $\mathcal{BR}$ is outdated as there was a new measurement by ref. [7], which was also adapted from the PDG [62]. These events are ignored since for the beyond Standard Model decay channel and for the Standard Model decay channel they are removed through the cuts after the reconstruction.
To decrease the background, the cuts of the Standard Model decay channel are applied to the beyond Standard Model decay channel. The efficiencies of the cuts are provided in table 5.3. Since there are no signal events in the reduced MC sample (the wrong signal events are excluded), the efficiencies of the cuts are estimated using the Signal MC for the signal efficiency and the reduced MC sample for the background efficiency. The efficiency of the Signal MC for the beyond Standard Model decay channel is:

$$\epsilon_{BSM,SigMC} = 0.0652 \pm 0.0003 \tag{5.7}$$

cut	ϵ of N_{sig} $\frac{N_{sig,all}}{N_{sig,others}}$	ϵ of N_{bkg} $\frac{N_{bkg,all}}{N_{bkg,others}}$
Cont.BDT output<0.44	0.856	0.305
χ^2 probability (vertex fit)>0.001	0.790	0.345
E(p_Λ) >1.11 [GeV]	0.892	0.627
$\lvert\Delta E\rvert$ <0.02 [GeV]	0.905	0.059
R2<0.37	0.999	0.997
$\frac{p_\Lambda\_protonID}{p_\Lambda\_protonID+p_\Lambda\_pionID}$>0.6	0.953	0.103
$\frac{p\_protonID}{p\_protonID+p\_pionID}$>0.6	0.994	0.750
cosTBTO<0.9	0.935	0.931

Table 5.3: This table depicts the cut efficiency ϵ analysis for the beyond Standard Model decay channel. The efficiency of N_{sig} has been calculated on the full Signal MC for the beyond Standard Model decay channel, whereas the ϵ of the background has been determined on the reduced MC sample. Since the ϵ of N_{sig} is always higher than the ϵ of N_{bkg}, the cuts are reducing more background than signal events. The nomenclature used in this table is the same as in the text.

Comparing the cut efficiencies of the beyond Standard Model decay channel (table 5.3) with the Standard Model decay channel (table 5.2), the background reduction is almost for all variables better for the beyond Standard Model decay channel, while the signal efficiency roughly remains the same.
Comparing now the two decays with the cuts applied, which is visualized in figure 5.16, the reduced background for the beyond Standard Model decay channel has to be noted. For both decay channels, the τ background vanishes and the continuum background is dominant. Because of the application of the cuts, the signal peak for the Standard Model decay channel is clearly visible. To determine the quality of the status, the efficiency ϵ and the significance (equ. 5.6) are calculated for the Standard Model decay channel. The efficiency for the MC sample is defined as [27]:

$$\epsilon = \frac{N_{signal}}{N_{B^+B^-} * 2 * \mathcal{BR}} \tag{5.8}$$

At this point of the analysis, the intermediate decay channels contributing to the correctly reconstructed signal events were not known, thus the following numbers hinted at the decay structure in the MC sample.
Using the $\mathcal{BR}$ for the direct decay channel from the MC simulation, the efficiency for the SM decay channel on the reduced MC sample is $\epsilon = 0.144 \pm 0.006$, where the error is always rounded up in order to not underestimate it. The value of the significance is calculated to be $S = 17.09$. Comparing the efficiency to the Signal MC, where the efficiency of the reduced Signal MC for the SM decay channel after the application of the cuts is $\epsilon_{SM,SignMC} = 0.0651 \pm 0.0004$, the values do not agree.
To find the reason for the different efficiencies, different analyses have been carried out.

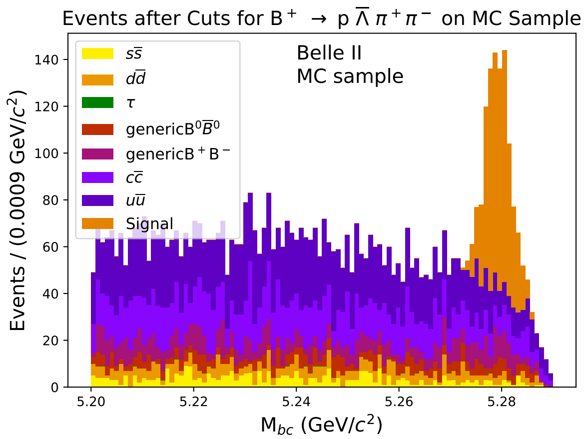

(a) Standard Model

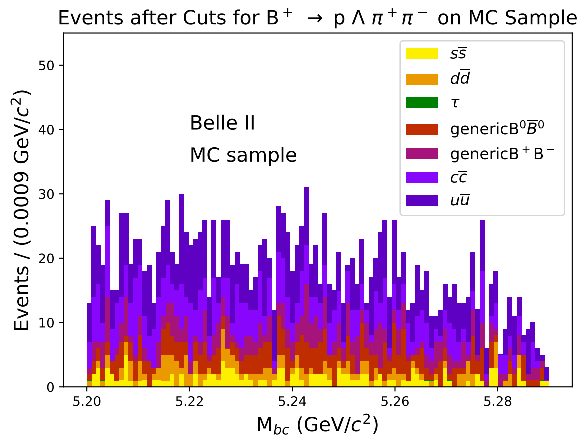

(b) Beyond Standard Model

Figure 5.16: These two figures show the events for the corresponding decays after the reconstruction and application of cuts. Both figures have been produced with the reduced MC sample (see Appendix table B.1). For the Standard Model decay channel, the signal peak is clearly visible, while the background for the beyond Standard Model decay channel is even more reduced. Also for both decay channels, the tau background vanishes and the continuum background still dominates over the background from B meson decays.

	MC sample 1	MC sample 2	Signal MC 1	Signal MC 2
correctly reconstructed	64.7 %	64.6 %	60.9 %	61.4 %
misidentified	30.4 %	30.4 %	33.9%	33.4 %
others	4.9 %	5.1 %	5.2 %	5.1 %

Table 5.4: This table depicts the analysis of the charged pions. Due to rounding, two columns do not add up to 100 %. The percentages for the MC sample and the Signal MC sample are comparable to each other, especially for the row 'others'.

At first, the consistency of the amount of beam background is tested, since this influences the reconstruction efficiency. Therefore, two random files have been chosen out of the Signal MC and the MC sample each. The analysis applied to those consists just of the charged pion reconstruction without cuts and the MC truth matching. Afterwards, the percentage of the correctly reconstructed particles, the incorrectly reconstructed particles and the others is compared. The results are shown in table 5.4. Huge discrepancies are not obviously seen, especially not in the row 'others', which is the important one in this case, because it usually contains the beam background, which has no MC information and is thus neither classified as signal or not signal. Thus, another approach is tried to explain the differences of the efficiencies.
This is the distribution of the signal in the signal MC, which might influence the efficiencies of the cuts. Here, the full Signal MC sample with $1{\times}10^6$ events is used. For each file, the number of correctly reconstructed signal events is determined. Out of these numbers, the mean value and the standard deviation are calculated. Thereupon, the files are grouped according to their distance to the mean value in terms of standard deviations, where the 2σ interval also contains the 1σ results and the same applies to the 3σ interval. The results are presented in the following:

$$1\sigma\text{: } 67.2\ \% \qquad 2\sigma\text{: } 96.0\ \% \qquad 3\sigma\text{: } 99.6\ \%$$

These results are consistent with a Gaussian distribution ([28], Chapter 9). Thus, they match the expectations and it is unlikely to find the reason for the different efficiencies here.
The next attempt is to analyse the signal events of the MC sample. Therefore, the MC information is used, to find the mother particle of the p, $\overline{\Lambda}$, π^+, π^-, p_Λ and π_Λ. Sixteen different decay channels were found to contribute to the correctly reconstructed signal events in the MC sample. The results of the decay channels found in the MC simulation and defined in the decay file are presented in table 5.5 including the efficiencies. More details on the intermediate decays can be found in chapter 3. As can be seen in the table 5.5, some decay channels are removed through the application of the cuts after the reconstruction. An overview over the structure of the correctly reconstructed signal events after the additional cuts is given in fig. 5.17.
Thus, the naive expectation of having reconstructed only the direct decay is the origin of the differences between the efficiencies of the Signal MC and the MC sample. Therefore, the efficiency and significance are now calculated for the MC sample and only the direct decay channel.
Comparing the efficiencies of the direct decay $B^+ \to p\,\overline{\Lambda}\,\pi^+\,\pi^-$ of the reduced MC sample (Appendix B.1) with the Signal MC, the discrepancies are vanishing and the different efficiencies are comparable. The value for the efficiency ϵ (equ. 5.8) and the significance S (equ. 5.6) are presented in the following:

$$S = 9.47$$

$$\epsilon = 0.073 \pm 0.004$$

decay	product $\mathcal{BR}$	ϵ_{rec}	ϵ
$B^+ \longrightarrow p\overline{\Lambda}\pi^+\pi^-$	1.13×10^{-5}	0.163	0.073
$B^+ \longrightarrow p\overline{\Lambda}\rho^0(\rightarrow \pi^+\pi^-)$	4.80×10^{-6}	0.143	0.066
$B^+ \longrightarrow p\overline{\Lambda}f_2(\rightarrow \pi^+\pi^-)$	1.13×10^{-6}	0.155	0.081
$B^+ \longrightarrow \Lambda(\rightarrow p\pi^-)\overline{\Xi}^+(\rightarrow \overline{\Lambda}\pi^+)$	3.19×10^{-7}	0.023	0.000
$B^+ \longrightarrow \Lambda(\rightarrow p\pi^-)\overline{\Lambda}\pi^+$	1.79×10^{-6}	0.031	0.000
$B^+ \longrightarrow \pi^+$ J/ψ $(\rightarrow \overline{\Lambda}\Lambda(\rightarrow p\pi^-))$	3.98×10^{-8}	0.121	0.000
$B^+ \longrightarrow \Delta^{++}(\rightarrow p\pi^+)\overline{\Lambda}\pi^-$	2.00×10^{-6}	0.144	0.053
$B^+ \longrightarrow p\overline{\Sigma}_c^0(\rightarrow \pi^+\overline{\Lambda}_c^-(\rightarrow \overline{\Lambda}\pi^-))$	3.15×10^{-7}	0.168	0.084
$B^+ \longrightarrow p\pi^+\overline{\Lambda}_c^-(\rightarrow \overline{\Lambda}\pi^-)$	2.41×10^{-6}	0.146	0.055
$B^- \longrightarrow \overline{p}\ \Lambda(1520)\ (\rightarrow \Lambda\pi^+\pi^-)$	1.00×10^{-7}	0.096	0.000

Table 5.5: This table summarizes the decays contributing to the correctly reconstructed signal for the reduced (see Appendix table B.1) MC sample. For each decay, the product branching ratio $\mathcal{BR}$ is given as well as the efficiency ϵ_{rec} after the reconstruction and the efficiency ϵ after the application of the cuts. The decays are subdivided into four groups. The structure is the same as in table 3.1. The first one is the direct Standard Model decay channel without intermediate resonances. The second group consists the two decays included in the total $\mathcal{BR}$ (ref [26]). The third category contains other intermediate decays resulting in the same final state, while the fourth one is a mistake in the MC simulation. The zero efficiency fields are due to no remaining events after the cuts. The last category is given as a B^- decay, since this is the wrongly implemented decay channel.

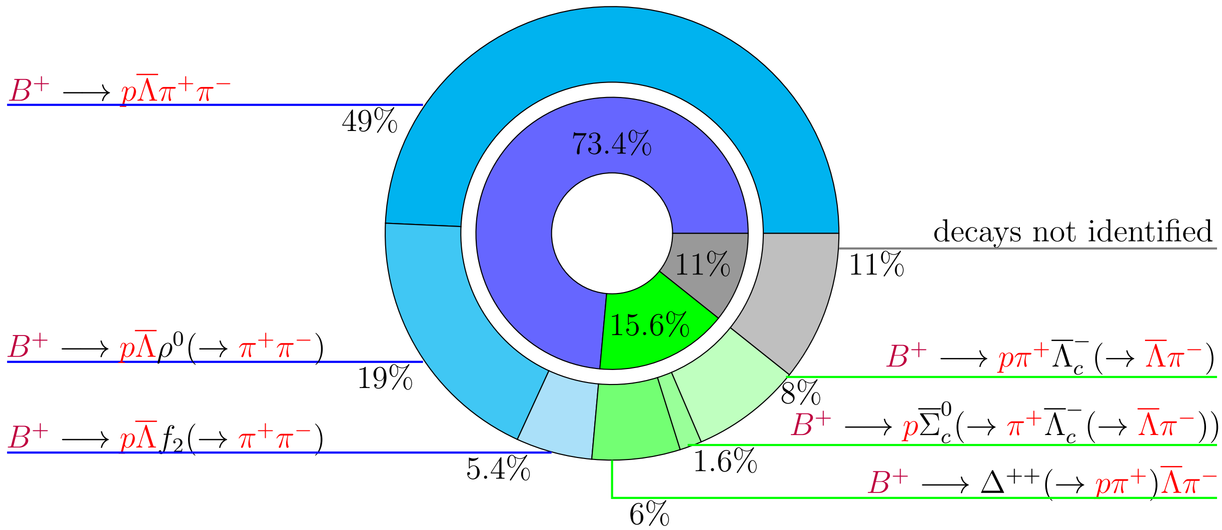

Figure 5.17: This diagram visualizes the shares of the individual decays on the correctly reconstructed signal events. It is divided into three groups, where the blue ones represent the decays measured in ref. [26], the green ones represent other intermediate decays and the gray slice could not be identified as specific B meson decay. The coloured particles denote the particles reconstructed in the Standard Model decay channel. More details are presented in the text and in table 5.5.

These values are now compared to the values from ref. [26], where the significance is given by $S = 9.1$ and the efficiency is $\epsilon = 4.32\%$ for the decay $B^+ \to p\,\overline{\Lambda}\,\pi^+\,\pi^-$. It has to be noted, that the definition of the significance is based on the likelihood values of the fit (details in ref. [26]) and thus it differs from the definition used here. The integrated luminosity of ref. [26] is 605fb^{-1}, whereas the integrated luminosity used for this analysis is roughly 386fb^{-1} for the reduced MC sample. However, the significance and the efficiency are better than the values presented in the paper. A possible reason for the huge difference in ϵ could be their different analysis approach in separating three decay channels from the beginning and trying to exclude some of the intermediate decays (ref [26]).
Since later on the three decays of ref. [26] are used, also the efficiency and significance of the intermediate decays via the ρ^0 and the f_2 are calculated for the MC sample:

$$S_{p\overline{\Lambda}\rho^0} = 3.95$$

$$S_{p\overline{\Lambda}f_2} = 1.19$$

$$\epsilon_{p\overline{\Lambda}\rho^0} = 0.066 \pm 0.006$$

$$\epsilon_{p\overline{\Lambda}f_2} = 0.081 \pm 0.013$$

Comparing these results with the results in the paper (ref. [26]), the efficiencies of this analysis are higher, but the significance in the paper is higher. As is already mentioned, their definition of the significance is different, thus it is hard to directly compare them. As a last step, the efficiencies are compared to the efficiencies of the Signal MC, which are summarizes here:

$$\epsilon_{p\overline{\Lambda}\pi^+\pi^-,SigMC} = 0.065145 \pm 0.000319 \tag{5.9}$$

$$\epsilon_{p\overline{\Lambda}\rho^0,SigMC} = 0.063757 \pm 0.000245 \tag{5.10}$$

$$\epsilon_{p\overline{\Lambda}f_2,SigMC} = 0.067565 \pm 0.000251 \tag{5.11}$$

$$\epsilon_{p\Lambda\pi^+\pi^-,SigMC} = 0.065230 \pm 0.000247 \tag{5.12}$$

The values are the exact Signal MC values and the digits of the errors are chosen to match them, since the rounding for the final results will be done later. In order to not underestimate the uncertainty, the errors are rounded up. First of all, the efficiencies for the three Standard Model decay channels are higher for the MC sample than for the Signal MC. However, they are still comparable within two standard deviations for the direct decay and the intermediate decay via the f_2 and within one standard deviation for the intermediate decay via the ρ^0. Furthermore, the efficiencies for the direct decay of the Standard Model and the beyond Standard Model decay on the Signal MC are roughly the same.

5.3 The Fit and Its Validation

After reconstructing signal candidates out of the whole reconstructed events of the MC sample, the number of correctly reconstructed signal events has to be determined. For the simulation, this can be done with the MC variables, though on data, another method is required. Thus, a fit of the MC sample is implemented to identify the signal yield. Different fits and their validation are presented in the next subchapters. First of all, a one-dimensional fit is implemented to extract the amount of signal and background. This fit was created, when the structure of the MC sample with the intermediate decays was not known. Here, the branching ratio is hard to calculate out of the number of signal events, since the overall efficiency relies on sixteen decays with some unknown efficiencies for single decay channels. In order to cancel systematic uncertainties, a second fitting method is implemented, where the Standard Model and the beyond Standard Model are fitted simultaneously using the ratio of the branching fractions. Here, the MC sample is reduced to exclude some of the intermediate decays of the correctly reconstructed signal events. Also, the fitting variables are adjusted such that the fit can return the branching fraction. Before presenting the fits and their results in detail, the preparations are presented as the used probability density functions and the correlations.

5.3.1 Search for Correlations between M_{bc} and $|\Delta E|$

At first, a 2-dimensional fit in M_{bc} and ΔE was considered. Therefore, the correlations between the two variables M_{bc} and ΔE are analysed. In case of a simultaneous fit of these

	all no range		only signal events signal region		all events signal region	
variable	M_{bc}	ΔE	M_{bc}	ΔE	M_{bc}	ΔE
M_{bc}	1.0000	0.0034	1.0000	-0.2720	1.0000	-0.0374
ΔE	0.0034	1.0000	-0.2720	1.0000	-0.0374	1.0000

Table 5.6: This table depicts the correlations for the two variables M_{bc} and $|\Delta E|$. It is structured in three different domains. The first one depicts the correlation for the whole range of the reconstructed events, while the second and third focuses on the signal region defined as $M_{bc} > 5.268$ GeV/c^2. The difference between two and three is the analysed event type being all events for domain three and only correctly reconstructed signal events in domain two. For all three domains, only the remaining events after the application of the cuts are analysed.

two variables, possible correlations complicate the fitting function. Since such a fitting method is not used for this analysis, the results are presented briefly in table 5.6. In order to interpret the results, the values have to be contextualized. The numbers 1 and -1 stand for 100% positive and negative correlation respectively and the number 0 for no correlation. Possible correlations between the two variables are analysed for three different conditions and only for the reduced MC sample for the Standard Model decay channel reconstruction with cuts applied. First of all, the whole MC sample is used and only small correlations have been found between M_{bc} and ΔE. Thereupon, the range is decreased to the signal region, which increases the correlation by roughly a factor of 10 to -4%. Thirdly, only correctly reconstructed events are used for the correlation test. This leads to -27% correlation between the variables M_{bc} and ΔE. Consequently, a two dimensional fit in both variables would be more complicated as the pdf cannot be written as the pdf of $M_{bc} \times \Delta E$, but this was discarded for the present. However, the fit has to be verified. Therefore, different methods are used, which will be presented later. As a variable for the fit, the variable M_{bc} is used and consequently ΔE is implemented as a cut variable.
As the MC sample should not contain signal events for the beyond Standard Model decay channel, the correlation analysis would need to be done using Signal MC. This step was omitted, since it was already certain, that the pdf of $M_{bc} \times \Delta E$ would not be fitted.

5.3.2 Probability Density Functions

First of all, the procedure and the results of the one-dimensional fit will be presented in the following.
The fitting function consists of different probability density functions for the signal and for the background. For the latter one, the Argus function is used:

Argus Function
The Argus function or also called Argus distribution is useful to describe combinatorial

background in particle physics, where the total beam energy sets a limit for the measured beam constrained mass. This function is given by ([51], Chapter 3):

$$f_{Argus}\,(x,\Theta,\xi) = N\,x\,\sqrt{1-\left(\frac{x}{\Theta}\right)^2}\;e^{-\xi^2\,\left[1-\left(\frac{x}{\Theta}\right)^2\right]/2} \tag{5.13}$$

Here, the normalization coefficient is N and Θ is the maximal allowed value. In particle physics using colliders, the maximal value of Θ is half of the center of mass energy.
The function was used by the Argus collaboration in 1990 for modelling of the background of their analysis of B-Mesons decaying into different combinations of pions [16].
The Argus function used for the fitting in this analysis is defined as follows:

$$f_{Argus}\,(x,\Theta,\xi) = N\,x\,\sqrt{1-\left(\tfrac{x}{\Theta}\right)^2}\;e^{\xi\,\left[1-\left(\frac{x}{\Theta}\right)^2\right]}$$

This is basically a redefinition of the parameter ξ. It is implemented as RooArgusBG in ref. [3].

While the Argus function is often used to model the background for example in ref. [26, 58, 61], the signal distributions can be varied. Here, the signal has the shape of a peak with one-sided tail. Therefore, two different functions modelling a Gaussian with a tail are utilised and compared. These two functions are presented in the following:

Crystal Ball Function
The Crystal Ball function depends on the four parameters $\alpha, n, \overline{x}, \sigma$ and is given either by a power-law distribution or by a Gaussian function ([51], Chapter 3):

$$f_{cb}(x,\alpha,n,\overline{x},\sigma) = \begin{cases} N\,e^{-\frac{(x-\overline{x})^2}{2\sigma^2}} & \frac{x-\overline{x}}{\sigma} > -\alpha \\ N\,A\,\left[B-\left(\frac{x-\overline{x}}{\sigma}\right)\right]^{-n} & \frac{x-\overline{x}}{\sigma} \leq -\alpha \end{cases} \tag{5.14}$$

Here, α indicates the point of transition between the two different functions and n is the exponent of the power-law distribution. $\overline{x}$ is the mean value of the Gaussian and σ is its standard deviation. The function is normalized by the coefficient N. The parameters A and B can be derived by demanding the Crystal Ball function to be continuous ([51], Chapter 3). This also applies for the first derivative ([51], Chapter 3):

$$f'_{cb}(x,\alpha,n,\overline{x},\sigma) = \begin{cases} N\,\frac{x-\overline{x}}{\sigma^2}\,e^{-\frac{(x-\overline{x})^2}{2\sigma^2}} & \frac{x-\overline{x}}{\sigma} > -\alpha \\ -\frac{n}{\sigma}\,N\,A\,\left[B-\left(\frac{x-\overline{x}}{\sigma}\right)\right]^{-n-1} & \frac{x-\overline{x}}{\sigma} \leq -\alpha \end{cases}$$

This gives two conditions for A and B that must be fulfilled and the resulting values are ([51], Chapter 3):

$$A = \left(\frac{n}{|\alpha|}\right)^n\,e^{-\frac{\alpha^2}{2}} \tag{5.15}$$

$$B = \frac{n}{|\alpha|} - |\alpha| \tag{5.16}$$

In particle physics this function can be used to model the signal. The implementation used is named RooCBShape and is described in ref. [3].

Novosibirsk Function

Another function to model the signal peak is to use the Novosibirsk function. Based on ref. [40], this function is defined as:

$$f_{Nov}\left(x,\sigma,m,\alpha\right) = exp\left[-\tfrac{1}{2}\left(\left(\tfrac{\sqrt{ln4}}{sinh^{-1}\left(\alpha\sqrt{ln4}\right)}\right)^2 ln^2\left(1-\tfrac{x-m}{\sigma}\alpha\right)+\left(\tfrac{sinh^{-1}\left(\alpha\sqrt{ln4}\right)}{\sqrt{ln4}}\right)^2\right)\right]$$

Here, σ is the width of the peak and m is the peak position, while α is related to the tail of the function [3]. RooNovosibirsk of ref. [3] is used for the fitting.
Thus, the Novosibirsk function has one parameter less than the Crystal Ball function.

The fitting itself is done with Roofit [59]. This includes MINUIT [43] and for this analysis its methods migrad and hesse. The basis for the fitting method is an extended maximum likelihood fit for all performed fits. The extended likelihood function $L(\nu,\boldsymbol{\Theta})$ is given by ([28], Chapter 6):

$$L(\nu,\boldsymbol{\Theta}) = \frac{e^{-\nu}}{n!}\prod_{i=1}^{n}\nu f(x_i;\boldsymbol{\Theta}) \tag{5.17}$$

Here, $\boldsymbol{\Theta}$ represents unknown parameters, n is the number of observations and ν is the mean value of the Poisson variable n ([28], Chapter 6). The assumption, that ν and $\boldsymbol{\Theta}$ are functional unrelated and that the pdf is given by equ. 5.18 leads to the expression for the loglikelihood function given in equ. 5.19 ([28], Chapter 6):

$$f(x;\boldsymbol{\Theta}) = \sum_{i=1}^{m}\Theta_i f_i(x) \tag{5.18}$$

$$logL(\boldsymbol{\mu}) = -\sum_{j=1}^{m}\mu_j + \sum_{i=1}^{n} log\left(\sum_{j=1}^{m}\mu_j f_j(x_i)\right) \tag{5.19}$$

The parameter μ_i is given by $\mu_i = \Theta_i\nu$ and represents for type i the number of events, which are expected ([28], Chapter 6).
Although it is called maximum likelihood fit, the negative loglikelihood is taken and minimized.

5.3.3 Separate Fit on SM and BSM Decay Channel

The aim is to fit the beyond Standard Model (BSM) decay channel. It is chosen to develop the fitting function on the Standard Model (SM) decay channel on the MC sample. Then, the fitting function including the signal function will be applied to the MC sample of the beyond Standard Model decay channel.

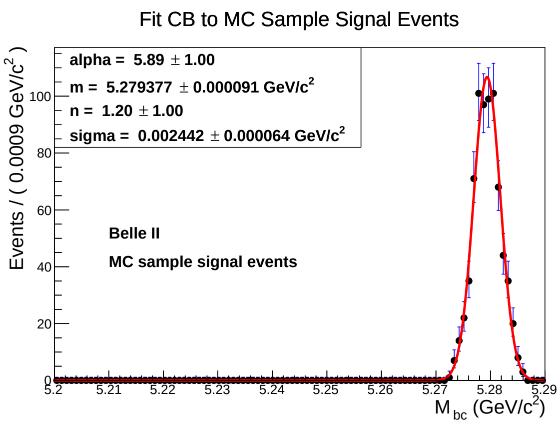

(a) Crystal Ball function

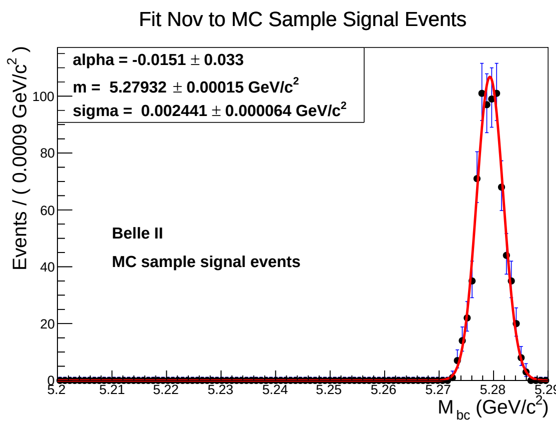

(b) Novosibirsk function

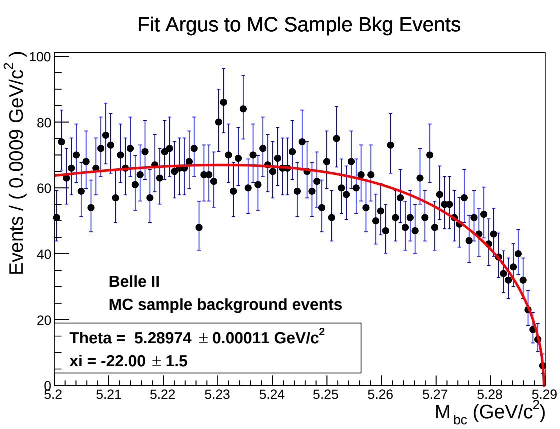

(c) Argus function fitted to events of SM decay channel

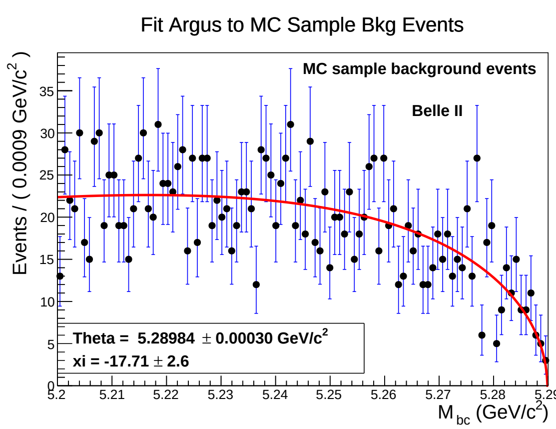

(d) Argus function fitted to events of BSM decay channel

Figure 5.18: This figure presents the shape values for the different functions. The two pictures on the top show the signal functions Crystal Ball and Novosibirsk fitted to the signal events of the MC sample, whereas the pictures on the bottom depict the Argus function fitted to the background events of the MC sample for the Standard Model decay channel on the left and for the beyond Standard Model decay channel on the right. The used abbreviation Bkg means background and CB stands for Crystal Ball. The parameters for the Crystal Ball function correspond to the defined parameters in a way that alpha and sigma are the written out Greek letters. The parameters of the Novosibirsk function and the Argus function are written out Greek letters and m is the peak position.

Fit Strategy

In order to get a converging fit, a strategy is elaborated. First of all, the MC sample is divided into correctly reconstructed signal events and the remaining events. Hereupon, the Argus function is fitted to the background only sample and both the Novosibirsk function and the Crystal Ball function are fitted separately to the signal sample in order to fix the shape variables or alternatively establish them as initial values with their uncertainties for the implementation of the nuisance parameters. During these fits, all function parameters are kept floating. The results are depicted in figure 5.18 for the Novosibirsk function and the Crystal Ball function. The values for the Argus function for the SM decay channel and the BSM decay channel can also be found in figure 5.18. It should be noted, that the full MC sample is used in this step. But since the aim is to determine the function shape, the impact is expected to be small as the bias accounts for only 3% of the MC sample and thus would have a small impact. Furthermore, the BDT training results do not show an overtraining (fig. 5.10).

As a next step, the different signal functions are compared. Therefore, the Crystal Ball function was combined with the Argus function and the shape parameters are fixed to the determined values. The combination was realized by addition of the functions with coefficients describing the number of signals as is stated in equ. 5.18:

$$f_{ges} = N_{sig} \times f_{Nov} + N_{bkg} \times f_{Argus}$$

Then, an extended maximum likelihood fit of the function to the full MC sample is done to estimate the number of signal events and the number of background events. The same procedure was repeated with the Novosibirsk function combined with the Argus function. To the results, a χ^2 test was applied (equ. 5.2), to determine which function models the MC sample better. The number of floating parameters was included in the calculation. The χ^2 test p-value (equ. 5.3) for the first function combination is 0.751 and for the second one it is 0.746. As the results are roughly the same, the number of variables is compared. Since the Novosibirsk function has one fit parameter less than the Crystal Ball function, it is supposed to be more stable. Thus, it was decided to use the Novosibirsk function over the Crystal Ball function.

For the previous step, again the full MC sample was used. The fit results and their validation of the full MC sample can be found in the Appendix (A.3 - A.6). These also include the nuisance parameters, which are not implemented in the previous steps, and follow the procedure described in the next steps. From now on, the results focus on the reduced MC sample.

The Fit

As a next step, the Novosibirsk function parameters and the Argus function parameters are fixed to the determined values. Then, the fitting function was fitted to the MC sample for the reconstructed SM decay channel and the reconstructed BSM decay channel separately.

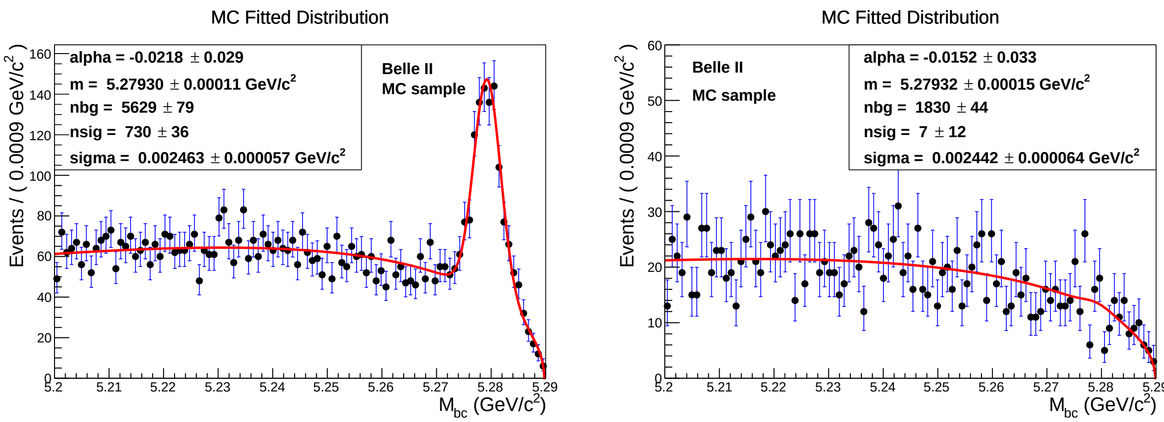

Figure 5.19: This figure depicts the fit to the SM decay channel events on the left and to the BSM decay channel on the right.

The results were further improved with the following: to take into account systematic uncertainties, the shape parameters of only f_{Nov} are included as nuisance parameters. This is done by defining a Gaussian function with the value of the shape parameter as mean value of the Gaussian and taking the uncertainty of the parameter as width of the Gaussian function. The thus defined Gaussians are all multiplied to the fitting function. This procedure assumes that the variables are uncorrelated. Otherwise one Gaussian function for all of them including the correlation matrix would need to be used as is explained in ref. [44]. The probability density function (pdf) and their components are depicted in the Appendix in table A.2. The composed model includes the Gaussian functions for the nuisance parameters.
Now, the fit to the MC sample is performed using an unbinned extended maximum likelihood fit including the shape parameters of the signal pdf as nuisance parameters. The fit results for the full MC sample are in the Appendix in figure A.3. The results for the reduced MC sample are shown in figure 5.19 with nsig=N_{sig} and nbg=N_{bkg}. A first test of the fit quality is the comparison of N_{sig} and N_{bkg} with the true MC values. For the Standard Model decay channel, the true values and the fit results are:

$$N_{sig,MC} = 700 \qquad N_{bkg,MC} = 5686$$

$$N_{sig,fit} = 730 \pm 36 \qquad N_{bkg,fit} = 5629 \pm 79$$

Thus, the fit values for N_{sig} are higher than the true values, but they still agree within one standard deviation. The numbers for N_{bkg} also agree within one standard deviation. As the signal events from the fit are enhanced compared to the MC values, the N_{bkg} events are decreased. The comparison for the BSM decay channel is similar:

$$N_{sig,MC} = 0 \qquad N_{bkg,MC} = 1841$$

$$N_{sig,fit} = 7 \pm 12 \qquad N_{bkg,fit} = 1830 \pm 44$$

	SM					BSM				
	α	m	σ	N_{sig}	N_{bkg}	α	m	σ	N_{sig}	N_{bkg}
α	100	32.1	2.6	0.6	-0.3	100	0.0	-0.1	-0.5	0.1
m	32.1	100	0.3	-2.9	1.3	0.0	100	0.1	-3.8	1.0
σ	2.6	0.3	100	17.7	-8.0	-0.1	0.1	100	3.7	-1.0
N_{sig}	0.6	-2.9	17.7	100	-19.3	-0.5	-3.8	3.7	100	-25.5
N_{bkg}	-0.3	1.3	-8.0	-19.3	100	0.1	1.0	-1.0	-25.5	100

Table 5.7: This table summarizes the correlation matrix of the fit parameters in %.

Again, the number of N_{bkg} events from the fit is smaller than the true MC value, but they are compatible within one standard deviation. The N_{sig} variable for the fit is positive and thus higher as expected, but it agrees with zero within one standard deviation. For both decay channels, the shape variables of the Novosibirsk function are similar to the variables calculated in figure 5.18 and therefore behaving as expected since they are constrained.
Furthermore, the correlations of the fit variables are analysed. The values for both fits are given in table 5.7. For both decay channels, the correlation between N_{sig} and N_{bkg} is negative with nearly -20% or even more. A difference between the correlations for the two fits are the shape parameters of the Novosibirsk function. For the SM decay channel, where signal events are present, α and m show a correlation of more than 30%, whereas the correlation between the shape parameters are nearly zero for the BSM decay channel.

Toy Studies

To validate the fit results, the toy study provided by RooFit [59] is used. For the implementation RooMCStudy of ref.[3] is used. 1000 data sets are generated from the pdf and fitted for both decay channels separately. The starting values for N_{sig} and N_{bkg} are set to the MC expectation. Unfortunately, the toy studies did not produce converging fits with a constrained function, unless some ranges were implemented on the yield and constrained shape parameters. Thus, the results for the fitting function without constraints are shown here.
The results for the fit to the SM decay channel are depicted in figure 5.20. This figure consists of three different subpictures. In the picture on the left, the number of signal events N_{sig} for the 1000 performed fits is depicted. In the picture in the middle, the uncertainty on the N_{sig} of the 1000 fits is plotted and in the picture on the right, the pull distribution is shown, which is defined as follows:

$$N_{sig,pull} = \frac{N_{sig,fit} - N_{sig,gen}}{\sigma_{N_{sig,fit}}} \tag{5.20}$$

The definition and the expected values are given in [44]. Furthermore, the mean value and the standard deviation of the 1000 N_{sig} and uncertainties of N_{sig} are calculated and added in the plot on the left and the plot in the middle as the blue lines. For the calculation each fit result for N_{sig} of the 1000 toy studies is extracted. Out of the resulting 1000 values for

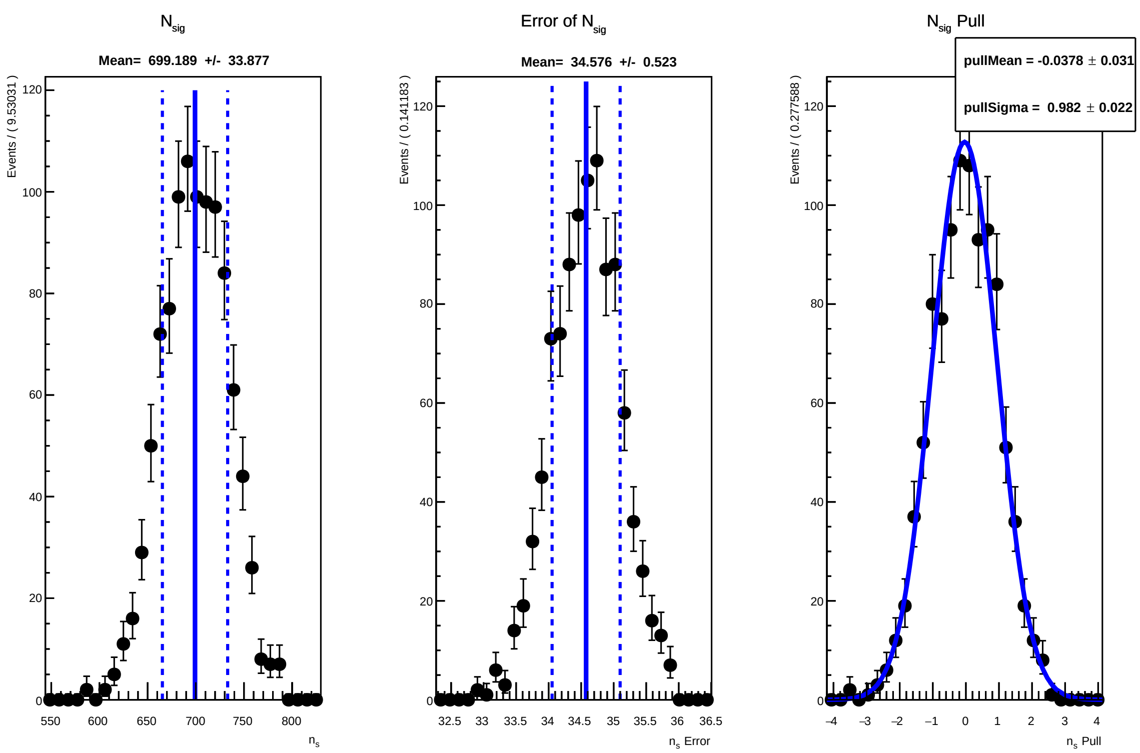

Figure 5.20: This picture presents the results for the toy studies of the fit to the SM decay channel events. The description of the subplots and the blue lines is given in the text.

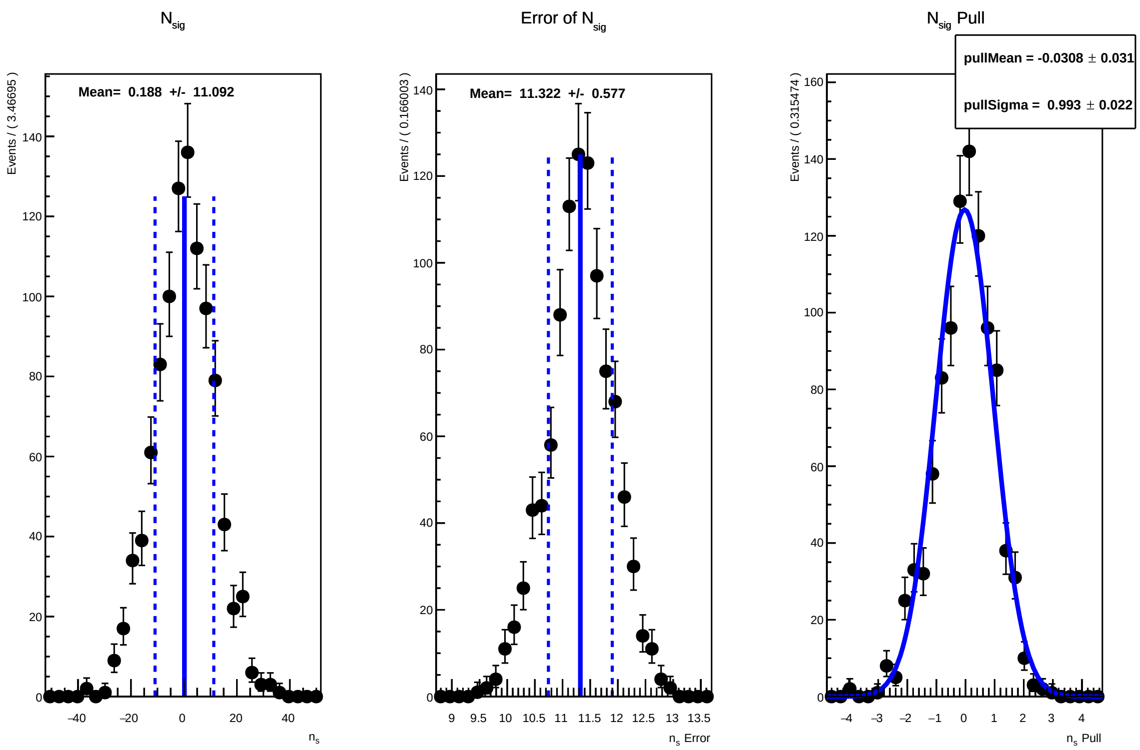

Figure 5.21: This picture depicts the results of the toy studies of the fit to the BSM decay channel events. As for fig. 5.20, the explanation and discussion is given in the text.

N_{sig}, the mean value and its error are calculated. Also the mean value and its error of the uncertainties of N_{sig} are determined out of the 1000 toy results.
Comparing now the results of the toys for the fit to the SM decay channel events with the expectations, the plot of N_{sig} resembles a Gaussian distribution with the mean value nearly at the MC expectation. The same applies to the plot of the uncertainties. Furthermore, the calculated mean values are printed in the figure. Thus, the good agreement to the MC value is pointed out, since the mean value of N_{sig} reflects the 700 signal events, which were also used as starting value of the MC Study. On top of that, the mean of the error of N_{sig}, which is the peak of the Gaussian, and the calculated error of N_{sig} given as the text in fig. 5.20 are similar. The pull plot should represent a Gaussian with a mean value of zero and a width of one. Figure 5.20 depicts a Gaussian shape with a width comparable to one within one standard deviation and a mean value agreeing with zero within 1.3 standard deviations.
In analogy to toys for the fit to the SM decay channel events, also 1000 samples were generated and fitted using the fit to the BSM decay channel. The procedure is the same, but the starting value for N_{bkg} is adjusted to the MC value for the BSM decay channel. The starting value of N_{sig} is chosen to be zero. Again, the plot of the 1000 fitted N_{sig} shows a Gaussian shape with the mean value at the MC value. As for the toys for the

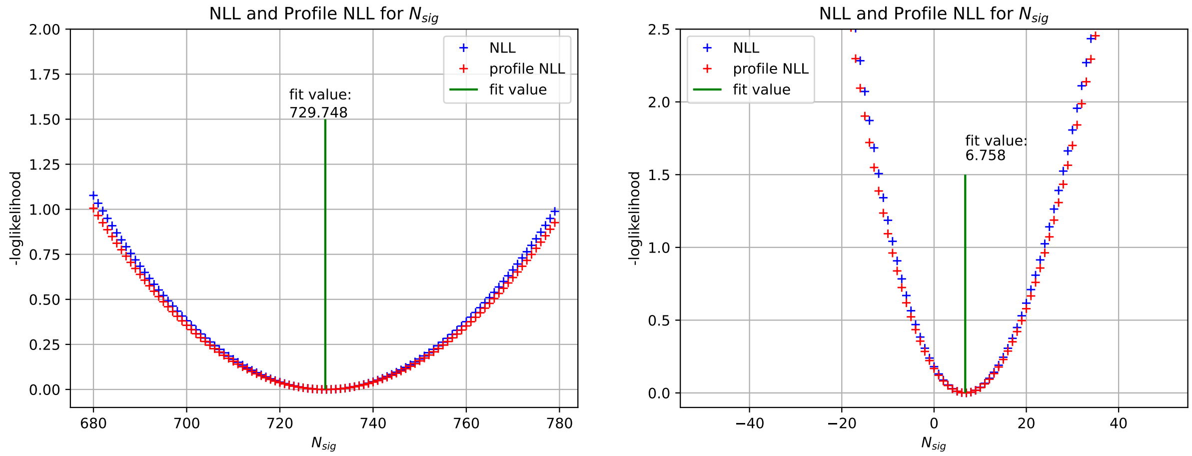

Figure 5.22: This figure visualizes the NLL and the profile NLL for the fit to the SM channel on the left and to the BSM channel on the right. Furthermore, the fit value is included for comparison. Additionally, the function value at the minima is chosen to be zero.

Standard Model decay channel, the 1000 results for N_{sig} of the toys are extracted and their mean value, which agrees with the MC expectation, and its error is calculated. The same procedure is applied to the uncertainties of the 1000 results of the toys for N_{sig}. The calculated error of the mean 1000 fit results agrees with the mean error of the fit results, which are depicted in the plot in the middle of figure 5.21. The pull plot does not only exhibit a Gaussian shape, but also the values for the mean and the width are better than for the previously presented toy studies. Both the mean and the width agree with the expected values within one standard deviation. The width meets with a value of 0.993 nearly perfectly the expectation.
The toy studies for the pdf validation fitted to the full MC sample are included in the Appendix in figure A.4 and in figure A.5. The mean of the Gaussian fitted to the pull plot for the SM decay channel is slightly better than for the reduced MC sample, but the width is further away from the expectation and smaller than the expected value. This would mean, that the uncertainties are overestimated. For the BSM decay channel events on the full MC sample, the mean value of the Gaussian fitted to the pull plot is worse than for the reduced MC sample, but it is still compatible to zero within one standard deviation. In contrast, the width is even closer to one.
As a result, the toy studies are taken as a validation of the fitting procedure.

Negative Loglikelihood (NLL) and Profile NLL

A second method to check the consistency of the fit is the negative loglikelihood. The loglikelihood is explained in equ. 5.19 and the command of [3] is createNLL for this analysis. This method is completed by the profile likelihood implemented as createProfile of [3]. These methods are also implemented, since they are used for the upper limit estima-

tion later on. Unfortunately, the root implementation of the profile loglikelihood failed sometimes for pdfs including the constraints and returned illogical results. Thus, the profile NLL provided by RooFit is not used, but the procedure is implemented step by step. Certain values for N_{sig} were fixed and for each of them the fit including the nuisance parameters was performed before calculating the NLL and calling the minimizer. Between each calculation for the different numbers of N_{sig}, the values for the shape parameters of the Novosibirsk function are reset. However, this is not supposed to make a difference, since the first step of each iteration for different values of N_{sig} is the fit and a slight difference in the starting values should not influence the results significantly. The results of the calculation by hand were compared with the in Root implemented code for the fitting function without nuisance parameters and the values were found to be similar. For that reason, the calculation by hand is verified.
The results for the two fits to both SM and BSM decay channel are depicted in figure 5.22. The minimum of the negative loglikelihood and of the profile NLL is expected to represent the minimum of the fit. This is the case for both images. Thus, the consistency check is performed successfully and the profile NLL can be used to estimate the upper limit.

Branching Ratio
To sum it up, the one-dimensional fit was tested with different methods and though sometimes exhibiting problems, the overall procedure is confirmed. Thus, the resulting signal yields are 730±36 events for the SM decay channel and 7±12 for the BSM decay channel. As the aim is to determine the $\mathcal{BR}$, the $\mathcal{BR}$ has to be calculated [27]:

$$\mathcal{BR} = \frac{N_{sig,fit}}{\epsilon \times N_{B\overline{B}} \times f_{\pm} \times 2} \tag{5.21}$$

For the MC calculation, equ. 5.21 is adapted as $N_{B^+B^-}$ is known and does not have to be calculated via $N_{B\overline{B}}$ and $f_{\pm}$. However, since equ. 5.21 includes the efficiency, the $\mathcal{BR}$ can not be calculated, since the efficiency of the not identified intermediate decays is not known. Therefore, the MC sample is edited such that only the direct decay is included for the correctly reconstructed signal events. The results of the fit can be seen in figure 5.23. Here, N_{sig}= 371±29 and this can be used to calculate the branching ration, since the efficiency is known from the Signal MC (equ. 5.9). Thus, the $\mathcal{BR}$ is equal to $(1.37 \pm 0.11)\times 10^{-5}$ which is consistent with the value of the MC simulation within 2.2 standard deviations. Therefore, the fit is again validated.

5.3.4 Simultaneous Fit

The second fitting method is the simultaneous fit of the MC sample for the beyond Standard Model decay channel and the Standard Model decay channel. This method provides some advantages, as parameters of the pdf are shared. Furthermore, for the beyond Standard Model decay channel the ratio of the branching ratios can be used as a fit variable. Thus, some systematic uncertainties are expected to cancel.

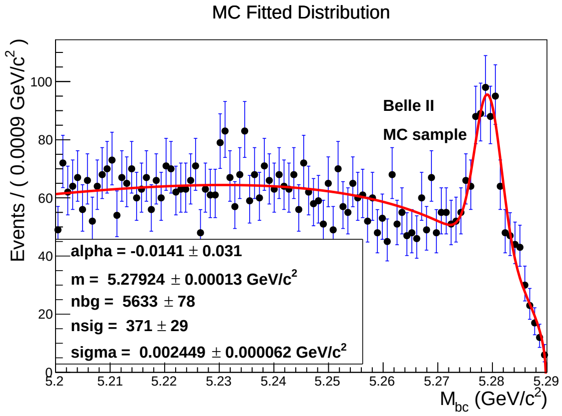

Figure 5.23: This figure depicts the fit for the reduced MC sample for the SM decay reconstruction. The correctly reconstructed signal events consist only of direct decay events ($B^+ \to p\,\overline{\Lambda}\,\pi^+\,\pi^-$) excluding any intermediate decays.

Fit Strategy

Now, the reduced MC sample for the SM decay channel and for the BSM decay channel are fitted at the same time. The shape variable of the Argus function is defined for both samples separately, while the Novosibirsk function parameters and the cut-off value of the Argus function are shared. The initial values for the shape parameters are chosen such that they are close to the from previous fits expected minimum. An advantage of the simultaneous fit is the cancellation of some systematic uncertainties like tracking efficiencies. Further improvements were made on the fitting procedure, which are explained in the following.

First of all, the fitting variable for the beyond Standard Model decay channel is no longer N_{sig}, but the ratio $\mathcal{R}$

$$\mathcal{R} \equiv \frac{\mathcal{BR}_{BSM}}{\mathcal{BR}_{SM}} \tag{5.22}$$

Secondly, the fitting variable of the Standard Model decay channel can be chosen between N_{sig} and $\mathcal{BR}_{SM}$. The variable $\mathcal{BR}_{SM}$ provides the advantage of calculating the upper limit on the $\mathcal{BR}$ for the BSM decay channel out of the fit results without using further variables. Thirdly, the MC sample provides difficulties for the calculation of the branching fraction (equ. 5.21) if N_{sig} is chosen as the fit variable, since some decays are not directly defined in the decay file and therefore their reconstruction efficiency is not determined. Consequently, the MC sample was edited by excluding the other decays such that only the three decays contribute to the correctly reconstructed signal events, which are measured in ref. [26]. In particular, the decay channels are $B^+ \longrightarrow p\overline{\Lambda}\pi^+\pi^-$, $B^+ \longrightarrow p\overline{\Lambda}\rho^0(\rightarrow \pi^+\pi^-)$ and $B^+ \longrightarrow p\overline{\Lambda}f_2(\rightarrow \pi^+\pi^-)$.

The shapes for the fit variable and the cut variables are compared and the results are presented in figure 5.24. Since the reduced Signal MC sample was used for the direct decay, the other two decay channels were scaled down. Some of the variables, especially $\mathrm{E}(p_\Lambda)$, R2 and χ^2 probability are not plotted for the full range. While the shapes for the fit

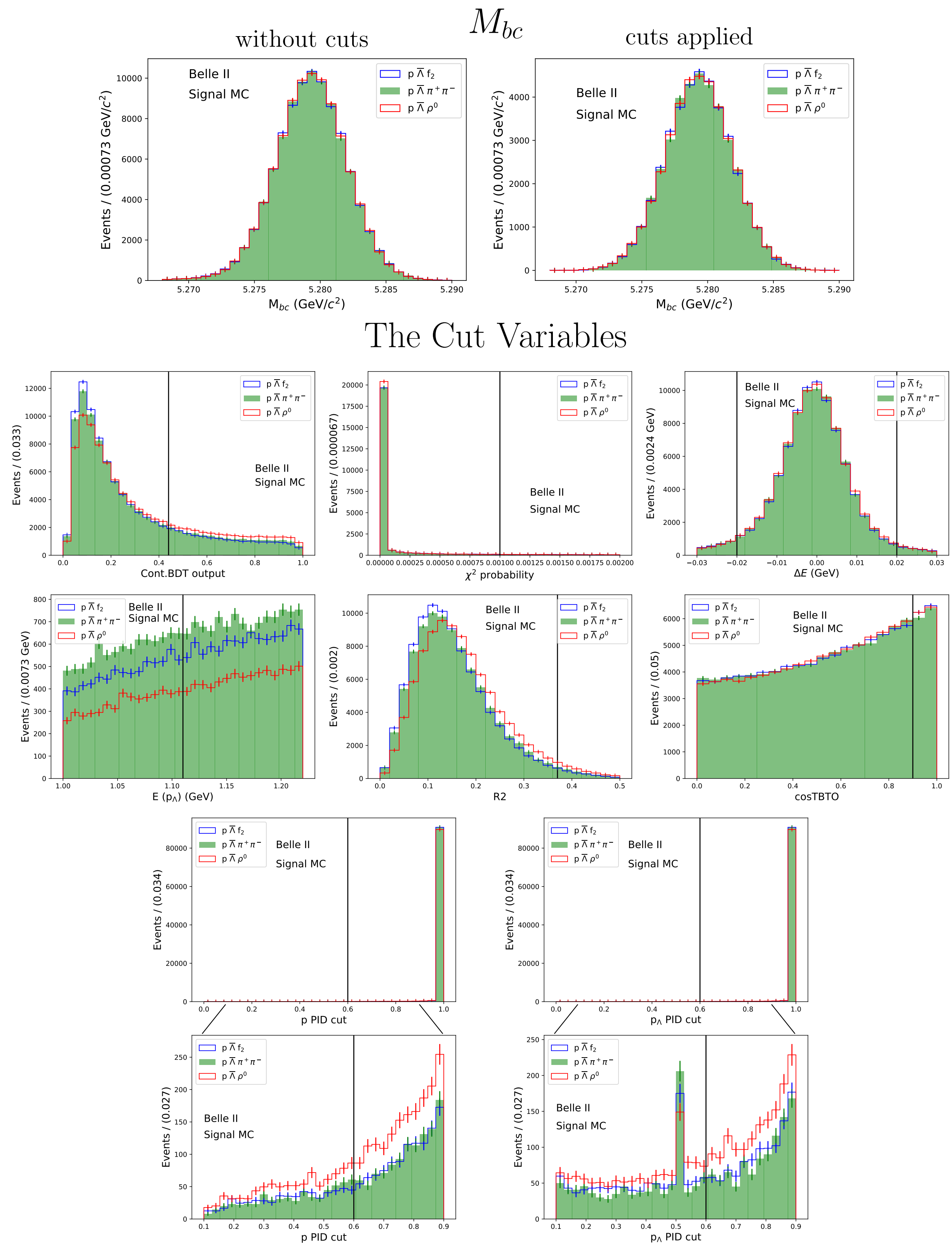

Figure 5.24: This figure compares the distributions of the three decays $B^+ \rightarrow p\overline{\Lambda}\pi^+\pi^-$ (green), $B^+ \rightarrow p\overline{\Lambda}\rho^0$ (red) and $B^+ \rightarrow p\overline{\Lambda}f_2$ (blue) for the M_{bc} variable and the cut variables. The black line indicates the cut value.

variable are similar, differences can be seen for E(p_Λ) and R2. This is expected, since the different decays consist of different kinematics. The peak for the p_Λ pid cut at 0.5 might be a result of technical issues, since it is a sharp peak and not spread and it appears for all three decays. Since it is removed by the cut and its height is not comparable to the peak at one, it is ignored in the following.
As is discussed in the previous chapters, the $\mathcal{BR}$s for the three decays have wrong values in the simulation. Thus, correction weights have to be applied. The weights are calculated the following way using $\mathcal{BR}_{paper}$ from [26] from equ. 2.1 - equ. 2.3 :

$$\omega_{p\overline{\Lambda}\pi^+\pi^-} \equiv \frac{\mathcal{BR}_{paper,B^+\to p\overline{\Lambda}\pi^+\pi^-}}{\mathcal{BR}_{MC,B^+\to p\overline{\Lambda}\pi^+\pi^-}} = 0.525 \tag{5.23}$$

$$\omega_{p\overline{\Lambda}\rho^0} \equiv \frac{\mathcal{BR}_{paper,B^+\longrightarrow p\overline{\Lambda}\rho^0(\to\pi^+\pi^-)}}{\mathcal{BR}_{MC,B^+\to p\overline{\Lambda}\rho^0} \times \mathcal{BR}_{MC,\rho^0\to\pi^+\pi^-}} = 0.997 \tag{5.24}$$

$$\omega_{p\overline{\Lambda}f_2} \equiv \frac{\mathcal{BR}_{paper,B^+\longrightarrow p\overline{\Lambda}f_2(\to\pi^+\pi^-)}}{\mathcal{BR}_{MC,B^+\to p\overline{\Lambda}f_2} \times \mathcal{BR}_{f_2\to\pi^+\pi^-}} = 1.796 \tag{5.25}$$

Each correctly reconstructed signal event is weighted with the corresponding value. The efficiency for the combination of the three decays is calculated as follows:

$$\epsilon = \frac{\mathcal{BR}_{p\overline{\Lambda}\pi^+\pi^-} \times \epsilon_{p\overline{\Lambda}\pi^+\pi^-} + \mathcal{BR}_{p\overline{\Lambda}\rho^0} \times \epsilon_{p\overline{\Lambda}\rho^0} + \mathcal{BR}_{p\overline{\Lambda}f_2} \times \epsilon_{p\overline{\Lambda}f_2}}{\mathcal{BR}_{p\overline{\Lambda}\pi^+\pi^-} + \mathcal{BR}_{p\overline{\Lambda}\rho^0} + \mathcal{BR}_{p\overline{\Lambda}f_2}} \tag{5.26}$$

The branching ratios for the intermediate decays via ρ^0 and f_2 include their decays into the two charged pions. The values for the branching ratios are taken from ref. [26]. The efficiencies for the decays are calculated using the corresponding Signal MC and the events in the signal region after the application of the cuts. These results are presented in equ. 5.9 - equ. 5.12. Thus, the efficiency of equ. 5.26 is 0.0650 ± 0.0002.
In order to decrease the number of fit variables, the denominator of the equation of the branching fraction (equ. 5.21) is combined into one variable η_{SM}, where $\eta_{SM} = \epsilon_{SM} \times N_{B^+B^-} \times 2$. In analogy, the variable η_{BSM} is defined as $\eta_{BSM} = \epsilon_{p\Lambda\pi^+\pi^-} \times N_{B^+B^-} \times 2$. This is an adjustment of the denominator to the MC conditions, where the number of B^+B^- events can be determined. If the fit for the SM is chosen to focus on the $\mathcal{BR}_{SM}$, the formula $N_{sig} = \mathcal{BR}_{SM} \times \eta_{SM}$ is used, where $\mathcal{BR}_{SM}$ is the sum over the branching fraction of all three decays given in ref. [26]. As a consequence, the fit variable for the BSM is the formula $N_{sig,BSM} = \mathcal{BR}_{BSM} \times \eta_{BSM} = \mathcal{R} \times \mathcal{BR}_{SM} \times \eta_{BSM}$. If the SM fit reproduces the N_{sig} variable, the formula for the BSM is adjusted to $N_{sig,BSM} = \mathcal{R} \times N_{sig} \times \mathcal{R}_\eta$ with $\mathcal{R}_\eta = \eta_{BSM}/\eta_{SM}$. For the fit, either η_{SM} and η_{BSM} are included as nuisance parameters or $\mathcal{R}_\eta$. Taking into account the nuisance parameters follows another procedure than for the definition for the one-dimensional fit since they are included as external constraints. Thus, they are taken into account for the fit, but they are not directly part of the pdf. The function is still a Gaussian. For the calculation of the uncertainty of $\mathcal{R}_\eta$, Gaussian error propagation (equ. 5.33) is used. Thus, the uncertainties are overestimated as they are

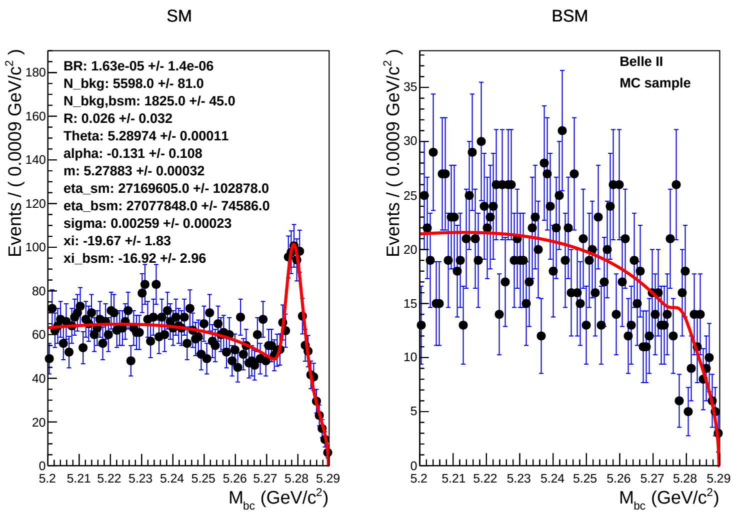

Figure 5.25: This fit shows the results for the simultaneous fit focusing on $\mathcal{BR}_{SM}$ and $\mathcal{R}$. BR represents $\mathcal{BR}_{SM}$ and the greek letters are written out.

taken to be uncorrelated. So far, only the statistical error of the efficiencies is considered as an uncertainty.

The Fit

At this point, the fit can be performed. As for the one-dimensional fit, the method is the unbinned extended maximum likelihood fit. No ranges are defined for any of the parameters. The only nuisance parameters are connected to the efficiencies. At first, the fit focusing on $\mathcal{BR}_{SM}$ and $\mathcal{R}$ is analysed. The results are presented in figure 5.25. The $N_{bkg,BSM}$ variable is consistent within one standard deviation with the true value, whereas the variable $N_{bkg,SM}$ is slightly above one standard deviation. Now, the value for $\mathcal{BR}_{SM}$ is compared to the expectations. Adding up the three branching ratios and adding the uncertainties up quadratically, the theoretical value is $(1.27 \pm 0.18)\times 10^{-5}$. This is consistent with the fit value of $\mathcal{BR}_{SM}$=$(1.63 \pm 0.14)\times 10^{-5}$ within two standard deviations. The ratio is obtained by the fit as $\mathcal{R} = 0.026 \pm 0.032$. Thus, the resulting branching ratio for the BSM decay channel is compatible with zero as it should be for the fit to the MC sample.

As a next step, the highest correlations are named. The full correlation matrix can be found in the Appendix in table B.4. For the $\mathcal{BR}_{SM}$, the most correlated variables are σ and ξ with around 50% each and $N_{bkg,SM}$ with -33%. For $N_{bkg,SM}$, whose correlation to $\mathcal{BR}_{SM}$ was already given, further variables are again σ and ξ with around -23% each. In contrast to the SM channel, for the BSM channel ξ_{BSM} is correlated to $\mathcal{R}$ (45%) and to $N_{bkg,BSM}$ (-14%). The last mentioned variables are correlated to each other with around 30%. Also σ and ξ exhibit 34% correlation.

The other fit option is analysed now. This is the fit focusing on N_{sig} and the ratio. The results are presented in figure 5.26. Comparing the results for the number of background

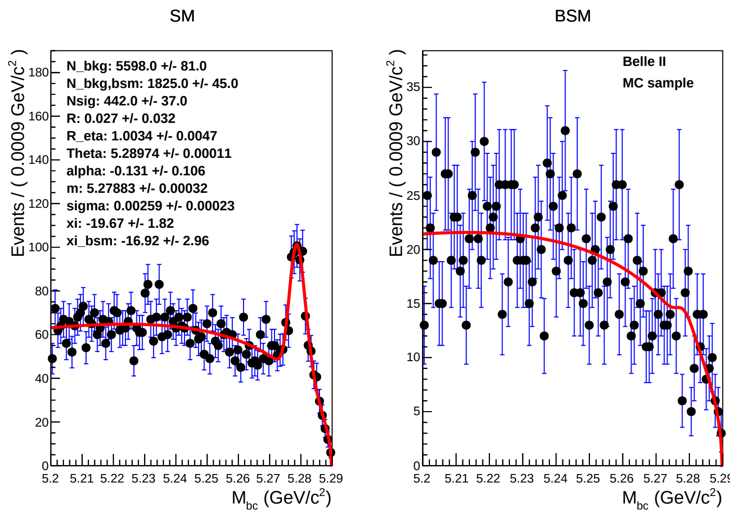

Figure 5.26: This fit shows the results for the simultaneous fit focusing on N_{sig} and $\mathcal{R}$. The variable R_eta represents $\mathcal{R}_\eta$. The greek letters are written out and correspond to the defined variables.

events to the previous fit, they are found to be exactly the same. However, the ratio $\mathcal{R} = 0.027 \pm 0.032$ is slightly higher than for the first fit, but still agrees with zero within one standard deviation. By adding up the weighted correctly reconstructed signal events of the reduced MC sample for only the direct decay and the intermediate decays via the ρ^0 and the f_2, the theoretical value is calculated to be 381 signal events. Thus, the fit value for N_{sig}, which is N_{sig}= 442±37, agrees within two standard deviations with the expectation. Like the fit value for the $\mathcal{BR}_{SM}$ from the previous simultaneous fit (figure 5.25), it is overestimating the signal events.
An overview over the correlations between the parameters is given in the Appendix in table B.5. The ratio $\mathcal{R}$ turns out to be mostly correlated to ξ_{BSM} (45%) and to the number of background events for the BSM decay channel (-30%). In contrast to that, the N_{sig} is correlated to N_{bkg} (-33%), σ and ξ and thus only to variables used for the fit of the SM decay channel.

Toy Studies

In analogy to the one-dimensional fit, toy studies are used to test the fit quality. At first the toy studies for the first fitting method focusing on $\mathcal{BR}_{SM}$ and $\mathcal{R}$ are presented. The results can be seen in figure 5.27. In contrast to the one-dimensional fit, the nuisance parameters are included in the toy studies as external constraints. More details on the procedure can be found in ref. [44]. However, the range (0,1) had to be set on the $\mathcal{BR}_{SM}$, since the toys failed for negative $\mathcal{BR}$s. $N_{bkg,SM}$, $N_{bkg,BSM}$ and $\mathcal{R}$ are set to the MC values. Also the total branching ratio is set to the weighted sum of the three decays in the MC (see table 5.5) simulation based on ref. [26]. Furthermore, Θ and m had to be set constant. The figure 5.27 depicts the results of the toy studies for the $\mathcal{BR}_{SM}$ and the $\mathcal{R}$. The structure of the

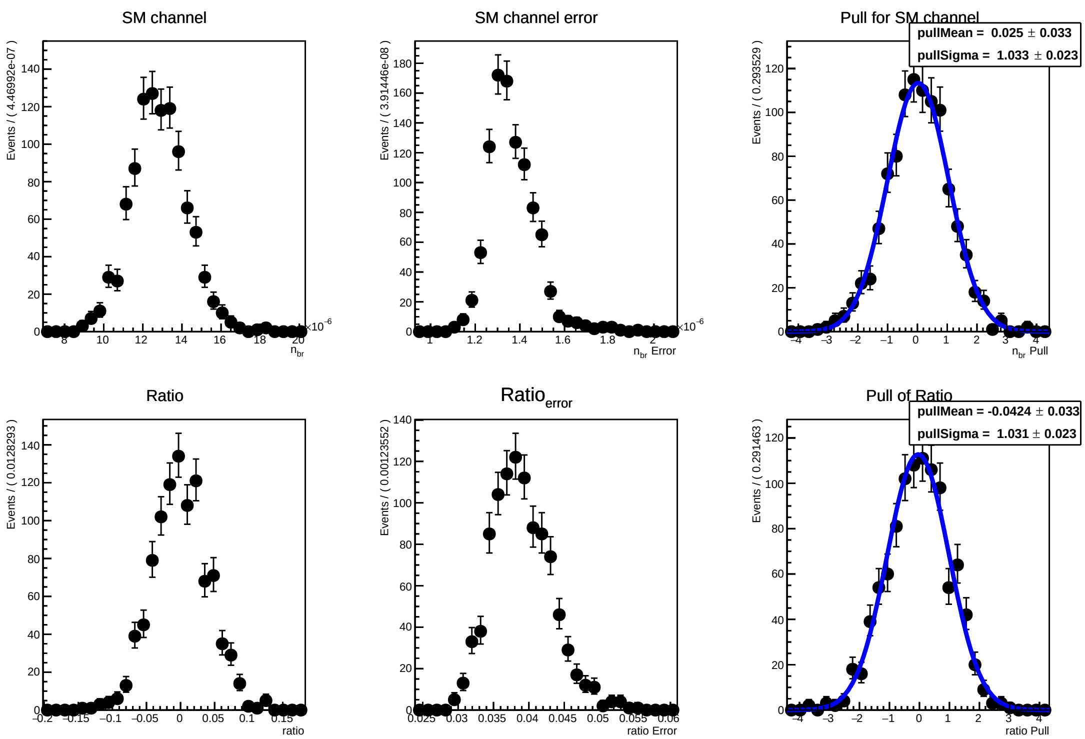

Figure 5.27: This figure presents the results of the toy studies for the simultaneous fit focusing on $\mathcal{BR}_{SM}$ and $\mathcal{R}$. As a consequence, these two variables are presented in the two rows. Here, n_{br} in the first row represents $\mathcal{BR}_{SM}$.

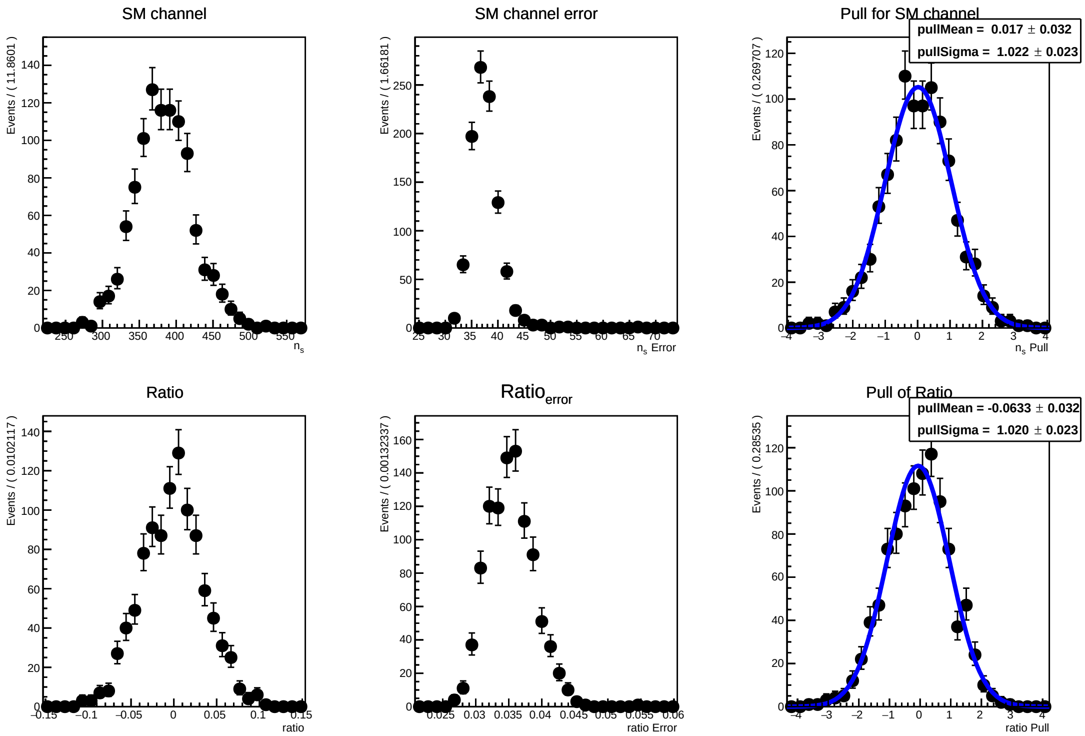

Figure 5.28: This figure represents the toy study results for the simultaneous fit focusing on N_{sig} and $\mathcal{R}$. As for the first method (fig. 5.27), the results for the two variables are presented in each row separately. The variable n_s in the first row represents N_{sig}.

plots is the same as for the one-dimensional fit. Both the pull plots of the $\mathcal{BR}_{SM}$ and the $\mathcal{R}$ can be modeled by Gaussian functions. For $\mathcal{BR}_{SM}$, the mean value is compatible to zero within one standard deviation and the width is higher than one, but still agrees to the expected value in two standard deviations. The pull plot of $\mathcal{R}$ exhibits a bigger deviation to the expected values. However, the mean value of the Gaussian fitted to the pull plot is compatible with zero within 1.5 standard deviations and the width agrees with one within two standard deviations. The first column of figure 5.27 depicts the 1000 results for $\mathcal{BR}_{SM}$ and $\mathcal{R}$, which agree with the expectation through the input variables. Thus, the results underline the fit quality.

The results of the toys for the second fitting function focusing on N_{sig} and $\mathcal{R}$ are presented in fig. 5.28. The initial value for Nsig=381 is chosen to match the weighted number of signals. The pull plot of N_{sig} is fitted with a Gaussian distribution and both the mean and the sigma agree with the expected value within one standard deviation. In contrast to this result, the fit to the pull distribution of $\mathcal{R}$ exhibits a mean value in the two standard deviation range around the expected value. Once again, the sigma is consistent with one within one standard deviation. Also the distributions of the 1000 values for N_{sig} and $\mathcal{R}$ resemble Gaussian distributions with the mean value located at the from the input value expected number, which is zero for $\mathcal{R}$ and 381 for the variable N_{sig}.

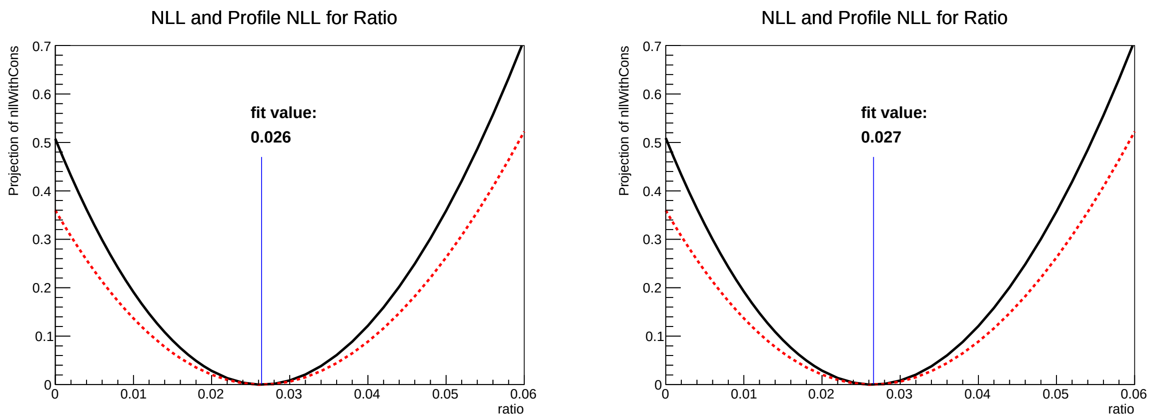

Figure 5.29: These two figures show the NLL (black) and the profile NLL (red dashed) for the simultaneous fit via the $\mathcal{BR}_{SM}$ (left) and the variable N_{sig} (right). The plotted variable is for both figures the ratio $\mathcal{R}$ and the fit value is indicated via the blue line.

Comparing now the pull distributions of the two methods, the mean value of the Gaussian fit is better for fitting $\mathcal{BR}_{SM}$ instead of N_{sig}. However, both show sufficiently good results for the toy studies.

NLL and Profile NLL

As before, the NLL and the profile NLL are used as a consistency check for the fit quality and as a preparation for the upper limit estimation. The method of the NLL and the profile NLL is described in the previous chapter (equ. 5.19) and the results for the simultaneous fit are presented in figure 5.29. Just as it was implemented for the simultaneous fit, the constraints are included as external constraints. Both the NLL and the profile NLL match the expected minimum. Therefore, the fit quality is confirmed.

Test Simultaneous Fit on $B^+ \to p\,\overline{\Lambda}\,\pi^+\,\pi^-$

In order to test the fit on weighted data, the simultaneous fit is performed on the unweighted dataset, where the correctly reconstructed signal events include only the direct decay events as this should produce similar results. The results are shown in fig. 5.30 for $\mathcal{BR}_{SM}$ and $\mathcal{R}$ and in fig. 5.31 for N_{sig} and $\mathcal{R}$. The corresponding toy studies validating the fits are in the Appendix in figure A.7 and figure A.8. All Gaussian fits to the different pull plots show results agreeing within two standard deviations with the expected values. The results of the weighted MC sample should correspond to the sum of the branching ratios of the three decays of ref. [26]. The $\mathcal{BR}_{SM}$ for the direct decay in the MC simulation is not equal to the sum of the three decays of the paper [26], but roughly to the PDG value including all these three decays ([62]). Since it is decreased in comparison to the sum of the three decays, also the fit results are expected to be smaller than for the weighted MC sample including the three decay channels as signal events. For this fit, the shape parameters are not changed, but the efficiency is now the Signal MC efficiency of the direct decay

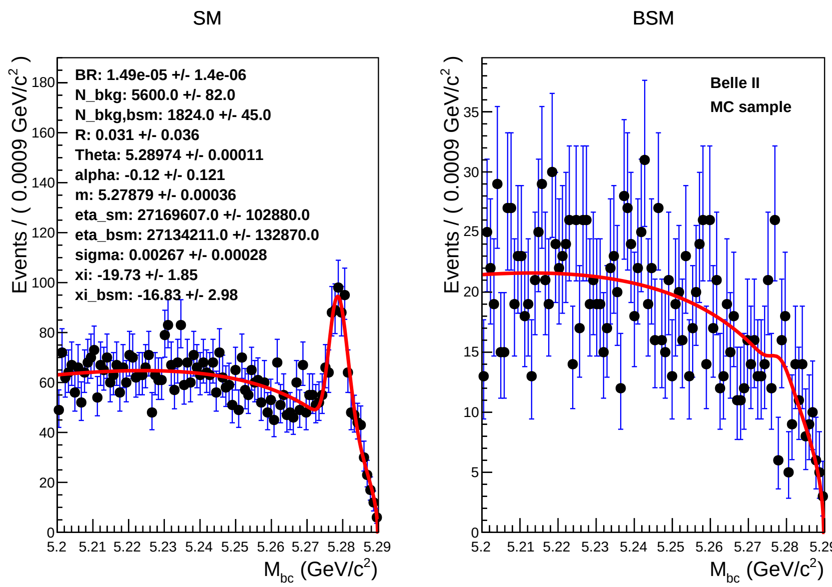

Figure 5.30: This figure depicts the results for the simultaneous fit on the unweighted reduced MC dataset. The correctly reconstructed signal events include just the direct decay. The fit variable for the SM decay channel is $\mathcal{BR}_{SM}$.

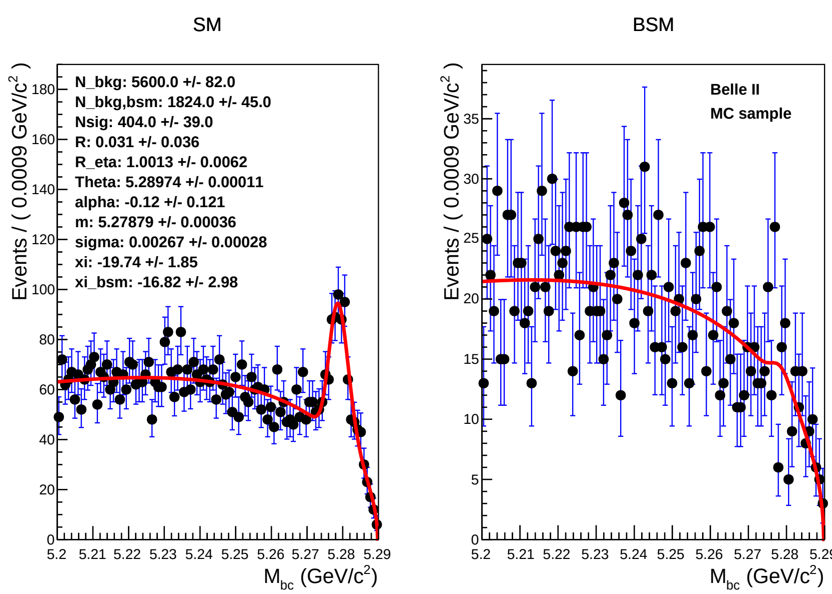

Figure 5.31: This figure depicts the results for the simultaneous fit on the unweighted reduced MC dataset. As in figure 5.30, the correctly reconstructed signal events include just the direct decay. The fit variable for the SM decay channel is N_{sig}.

only and the initial value for the $\mathcal{BR}_{SM}$ is the MC value for the direct decay. The results are summarized in the table 5.8.

	only direct decay		three decays	
	N_{sig}	$\mathcal{BR}_{SM}$	N_{sig}	$\mathcal{BR}_{SM}$
fit value	404 ± 39	$(1.49 \pm 0.14)\times10^{-5}$	442 ± 37	$(1.63 \pm 0.14)\times10^{-5}$
expected value	345	1.128×10^{-5}	381	1.273×10^{-5}
difference	59 ± 39	$(0.36 \pm 0.14)\times10^{-5}$	61 ± 37	$(0.36 \pm 0.14)\times10^{-5}$

Table 5.8: This table presents the different values for N_{sig} and $\mathcal{BR}_{SM}$. It also depicts the differences (by subtraction) between fit results and expectations. The expected value for the direct decay is the MC value, while the expected value for the three decays is calculated out of the weighted MC values.

The results for the number of background events is roughly the same, but the number of signal events shows the expected deviations between the two data samples. This results in different ratios $\mathcal{R}$. As can be seen in table 5.8, the differences between expectation and fit results are roughly the same for the direct decay and the three decays. Thus, this could be a small fit bias maybe resulting out of the background peak in the signal region, which is mentioned in the discussion of the Signal MC and will be discussed later. To sum it up, the results of this fit meet the expectations and thus confirm the results of the fit on the weighted MC sample.

5.3.5 Comparison of the Fitting Strategies

Comparing now the simultaneous fit with the results of the one-dimensional fit, the N_{sig} and N_{bkg} of the one-d fit tend to be closer to the true value than for the simultaneous fit. This is also true for the reduced MC sample modified such that the correctly reconstructed signal events include just the direct decay channel. Yet it has to be taken into account, that the one-d fit does not include the Argus function parameters as nuisance parameters and that the calculation of the corresponding $\mathcal{BR}$ (equ. 5.21) might lead to huge uncertainties, since this formula requires the knowledge of the efficiency and this quantity can only be estimated for the decay channels contributing to the correctly reconstructed signal events and not directly included in the decay table. For the toy studies, both fitting methods include fixed parameters, but the one-d fit could not take into account nuisance parameters without setting ranges. These ranges were set to all floating parameters. In contrast to the one-d fit, the simultaneous fit requires just a range on the branching ratio. Also the NLL and the profile NLL provide reasonable results for the simultaneous fit, while they sometimes failed for the nuisance parameters of the first fitting method.
Overall, the simultaneous fit is preferred over the one-dimensional fit, since it provides similar or even better results and the uncertainties can be included in the fit. Furthermore, systematic uncertainties are expected to cancel since the ratio is used as a fitting variable. Before continuing with the calculation of the uncertainties, the first upper limits

1-γ	Q_γ				
	n=1	n=2	n=3	n=4	n=5
0.683	1.00	2.30	3.53	4.72	5.89
0.90	2.71	4.61	6.25	7.78	9.24
0.95	3.84	5.99	7.82	9.49	11.1
0.99	6.63	9.21	11.3	13.3	15.1

Table 5.9: This table describes the numbers used for the upper limit estimation. It is taken from ref. ([28], Chapter 9). 1-γ is the confidence level and n is equivalent to the number of parameters. For this analysis the numbers of Q_γ are taken from the n=1 column.

are presented in the next chapter.

5.4 Upper Limit

Different approaches to calculate an upper limit through the profile likelihood are explained for example in ref. ([51], Chapter 12).
The method for the upper limit estimation used in this analysis and described briefly in the following is based on ref. ([28], Chapter 9). After choosing a confidence level 1-γ, one can calculate the corresponding Q_γ, which defines the confidence region ([28], Chapter 9).

$$\int_0^{Q_\gamma} f(z;n)dz = 1 - \gamma \tag{5.27}$$

Here, $f(z;n)$ is the χ^2 distribution (equ. 5.1) and n is the number of degrees of freedom. In the case of the likelihood function (equ. 5.19), this translates to $logL(\mathbf{\Theta}) = logL_{max} - \frac{Q_\gamma}{2}$. This equation assumes the likelihood function to be Gaussian. $\mathbf{\Theta}$ represents n parameters, which should be contained in the confidence interval. Some examples for Q_γ and 1-γ can be found in table 5.9. This summarized the upper limit estimation method based on chapter 9 of ref. [28].
In this analysis, the negative loglikelihood is used and the minimum is shifted to zero. Thus, the equation can be rewritten as:

$$-logL(\mathbf{\Theta}) = \frac{Q_\gamma}{2} \tag{5.28}$$

Instead of the NLL, the profile NLL can be used ([51], Chapter 12)([35], Chapter 5). The profile negative loglikelihood is calculated for the ratio $\mathcal{R}$ and thus $\mathbf{\Theta} = \mathcal{R}$. As a result of equ. 5.28, a horizontal line is implemented for the required value of $\frac{Q_\gamma}{2}$ and the intersection point with the profile NLL function is the upper limit for the corresponding confidence interval. The results are visualized in figure 5.32.
All results are obtained at 90% confidence level ($\mathcal{CL}$). The results have to be recalculated to upper limits on the branching ratio for the BSM decay channel. For the plot on the

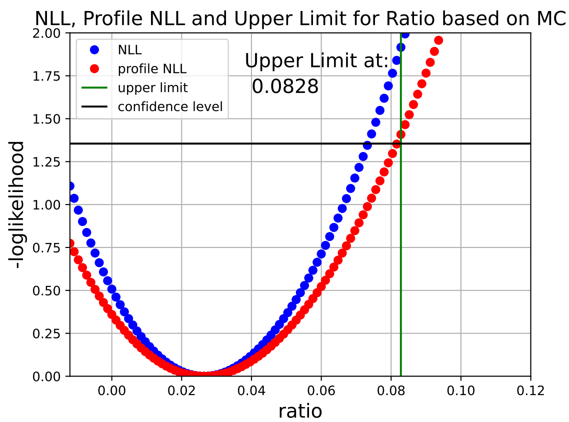

(a) Fit method: simultaneous fit on $\mathcal{BR}_{SM}$ and $\mathcal{R}$. This figure presents the upper limit on $\mathcal{R}$ at 90% $\mathcal{CL}$.

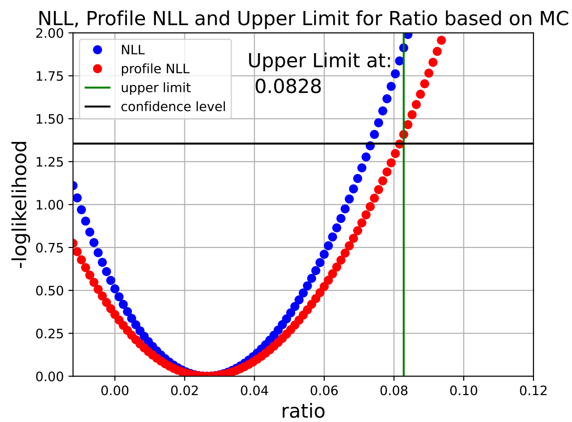

(b) Fit method: simultaneous fit on N_{sig} and $\mathcal{R}$. This figure also shows the upper limit on $\mathcal{R}$ at 90% $\mathcal{CL}$.

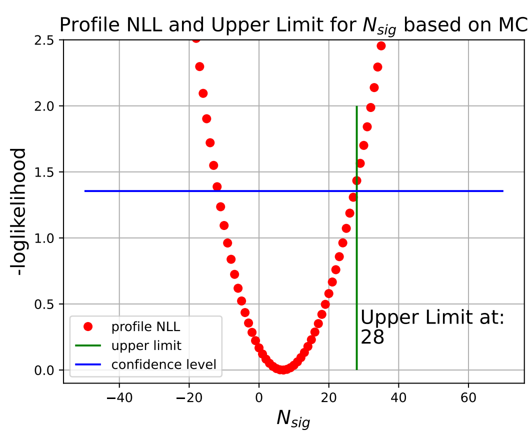

(c) Fit method: one-dimensional fit of the BSM decay channel events with N_{sig} as fit variable. Thus, the figure depicts the upper limit on N_{sig} at 90% $\mathcal{CL}$.

Figure 5.32: This figure represents the upper limits for the different fitting procedures.

upper left, this is simply done by multiplying the $\mathcal{R}$ with the $\mathcal{BR}_{SM}$. Thus, the upper limit would be 1.35×10^{-6}. This corresponds to 37 signal events. The plot on the upper right corresponds to the fit of N_{sig} for the SM decay channel. Therefore, the $\mathcal{BR}_{SM}$ is calculated using the weighted sum of the efficiencies. This results in an upper limit of also 1.35×10^{-6} for the branching ratio of the BSM decay channel. Thus, the simultaneous fits result in the same upper limit.
For the one-dimensional fit, the upper limit on the branching ratio of the beyond Standard Model decay channel can not be estimated as was already explained. The upper limit for the full MC sample is given in the Appendix in figure A.11.
Comparing the upper limit on the number of events, the one-dimensional fit is with 28 signal events below the simultaneous fits with 37 signal events, but as already mentioned, this fitting function does not include all nuisance parameters. Therefore, the results are expected to get worse. Also the recalculation of the branching ratio has large errors due to the different efficiencies. Another problem is the uncorrected number of events for the SM decay, which does not include weights for the false implemented branching ratios in the simulation.
As a result, the upper limit for the simultaneous fit is more reliable. Therefore, the calculation of the systematic uncertainties will focus on the simultaneous fit and thus the three decays of ref. [26].

5.5 Systematic Uncertainties

The last step consists of the determination of the systematic uncertainties. Due to time constraints, the corrections could not be applied to the MC samples to be included in the fit. However, the systematic uncertainties can not only change the shape of the distribution and thus need an adjustment of the pdf, but they also change the norm and thus the efficiency. Therefore, the efficiency correction is calculated and the individual corrections are applied to the MC sample in order to prove that the shape does not change. Since the three decays of the ref. [26] $B^+ \longrightarrow p\overline{\Lambda}\pi^+\pi^-$, $B^+ \longrightarrow p\overline{\Lambda}\rho^0(\rightarrow \pi^+\pi^-)$ and $B^+ \longrightarrow p\overline{\Lambda}f_2(\rightarrow \pi^+\pi^-)$ are used for the simultaneous fit as correctly reconstructed signal events, also the efficiency corrections will be calculated for all of them separately and combined in the end. For the efficiency corrections, the Signal MC sample for the three individual decays mentioned above is used and for the direct decay included in the three decays, the decreased Signal MC sample (see Appendix table B.1) is used. The efficiency correction of the BSM decay channel is estimated by taking the maximum of the SM decay channel correction. It is not calculated on the Signal MC for the beyond Standard Model decay channel, since the properties of this decay channel can only be estimated as it is not found so far. In order to not underestimate the efficiency correction, the maximum of the Standard Model decay channel correction is taken. In principal, the beyond Standard Model decay channel could have additional systematic uncertainties for example out of the signal modelling, but due to time constraints these are not covered.

5.5.1 PID Corrections

During the reconstruction and the cut optimization, different cuts on the pid variables are performed. This results in uncertainties, which have to be estimated. Therefore, data and Monte Carlo samples are compared for high purity decay channels to determine the correction weights. For this analysis, the decay channels $\Lambda^0 \to p\pi^-$, $D^{*+} \longrightarrow D^0(\to K^-\pi^+)\pi^+$ and $K_S^0 \to \pi^+\pi^-$ are relevant, since the first one is used for the corrections of the proton and all three are used for the corrections of the pion [4]. The code, which was used in this analysis was taken from [5].
The pid correction has to be applied to all final state particles with a pid cut. For this analysis, this incorporates the p and the p_Λ, as there is a cut implemented on these particles after the reconstruction. But also for the reconstruction itself, pid cuts have been applied as can be seen in table 4.1. The reconstruction pid cut for the p is included in the pid correction for the implemented cut after the reconstruction, but the cut on the pion pid has to be treated separately. However, the reconstruction pid cuts were not found to be applied to the p_Λ and the π_Λ. Thus, pid corrections are calculated for the p, π^+, π^- and p_Λ. For each particle, three correction tables are created. The first one is the correction for the correctly identified particle. The second and third one are the corrections for the incorrectly identified particles. For the p and p_Λ, the π and K were included as fake rate particles. Whereas for the π, the p and K were used as fake rate particle types. The percentage of incorrectly identified particles to whom a correction is assigned, is 96% for the p, 95% for the p_Λ, 81% for the π^+ and 80% for the π^- for the MC sample and the SM decay channel reconstruction. The missing percentage results out of for example electrons or muons as fake rate particles, for which no correction is calculated. At the first sight, the results for the pions seem to be low, but the missing 20% are both less than one percent of the total number of events. Thus, they are assigned the correction weight one. The percentages for the MC sample and the BSM decay channel are 93% for the p, 95% for the p_Λ, 65% for the π^+ and 72% for the π^-. Again, the missing percentages of the pion account for only less than 2% of the total number of events and are thus negligible. As a result, no more fake rate particles additional to the ones already presented are included.
The actual calculation is done following the sysscorrf documentation [4], where for example different procedures for the weight table creation, the addition of new pid studies and the pid fitting are described. Due to the application of cuts during the reconstruction, these have to be implemented as precuts for the table creation for every table individually and are summarized in table 5.10. The same cuts were applied to the efficiency correction table for the true particle and the fake rate correction table of the wrong particles for the same particle type (p, p_Λ and π). The correction tables are produced in momentum bins and $\cos\Theta$ bins. The exact binning is [0.3, 0.6, 0.9, 1.2, 1.5, 1.8, 2.1, 2.4, 2.7, 3.0, 3.3, 3.5, 4, 4.5] GeV/c for the momentum and [-0.866, -0.682, -0.4226, -0.1045, 0.225, 0.5, 0.766, 0.8829, 0.9563] for the variable $\cos\Theta$. These bin ranges are chosen as was proposed in the tutorial in order to not violate detector ranges. As input data samples, external data samples have been used. For the MC, the MC15ri (400 fb^{-1} run independent MC15) is used, since this matches the MC sample used for this analysis. For the data representation,

particle	implemented precuts	pid cut
p	nCDCHits>20, Θ >0.297 rad, Θ <2.618 rad , dr < 0.5 cm, |dz| <2 cm, p_protonID>0.1	$\frac{p\_protonID}{p\_protonID+p\_pionID} > 0.6$
p_Λ	no precuts	$\frac{p_\Lambda\_protonID}{p_\Lambda\_protonID+p_\Lambda\_pionID} > 0.6$
π	nCDCHits>20, Θ >0.297 rad , Θ <2.618 rad, dr < 0.5 cm, |dz| < 2 cm	$\pi\_pionID > 0.1$

Table 5.10: This table shows the setup for the pid correction table calculation. The implemented precuts are described in detail elsewhere (table 4.1). The values for the Θ had to be converted from degree to rad.

the proc13+prompt is used, which consists of the Belle II data until the run period 2022c and includes 404fb^{-1} data taken at the energy of the $\Upsilon(4S)$ resonance, $\Upsilon(4S)$ off resonance data and the scan of $\Upsilon(5S)$ energies. After the creation of the tables, the weights can be applied.
At first, the variation of the shapes is analysed. This is done for both the SM decay channel and the BSM decay channel on the reduced MC sample. For the SM decay channel, the MC sample is prepared in such a way, that only the three decays $B^+ \longrightarrow p\overline{\Lambda}\pi^+\pi^-$, $B^+ \longrightarrow p\overline{\Lambda}\rho^0(\rightarrow \pi^+\pi^-)$ and $B^+ \longrightarrow p\overline{\Lambda}f_2(\rightarrow \pi^+\pi^-)$ are included as correctly reconstructed signal events. Both efficiency correction and fake rate correction are used. The percentage of particles with missing correction is given in the Appendix in table B.6. Missing particles here means, that the weight could not be determined though the particle type would be included in the tables. This can happen for example if the momentum or the cosΘ of the event is not covered by the defined range. The bigger part of the values is fine, but for the pion efficiency, roughly 7.4% for the SM decay and roughly 10% for the BSM decay are not covered. This accounts for 7.1% of all events for the SM decay channel and for 10% of events for the BSM decay channel. If the pid corrections are applied to the MC sample, a solution would need to be found for this. Due to time constraints, the topic is not completely explored. For the fake rate particles, the p_Λ has the most particles with missing correction for the pion fake rate, but this accounts for only 3.2% of the total number of events for the BSM decay channel and 0.9% for the SM decay channel. Thus, it is negligible.
Comparing the shape of the unweighted MC sample for the SM decay to the weighted MC sample events (figure 5.33 left), the shape basically does not change. There is one enhancement of the weighted events around 5.24 GeV/c^2. A closer analysis of this region revealed, that the cause of the enhancement are two data points with a weight of more than 14, since they are located in the bin 0.9 GeV/c > p > 0.6 GeV/c and -0.1045 > cosΘ > -0.4226. Both events include an as a p_Λ misidentified pion. Overall, the weights

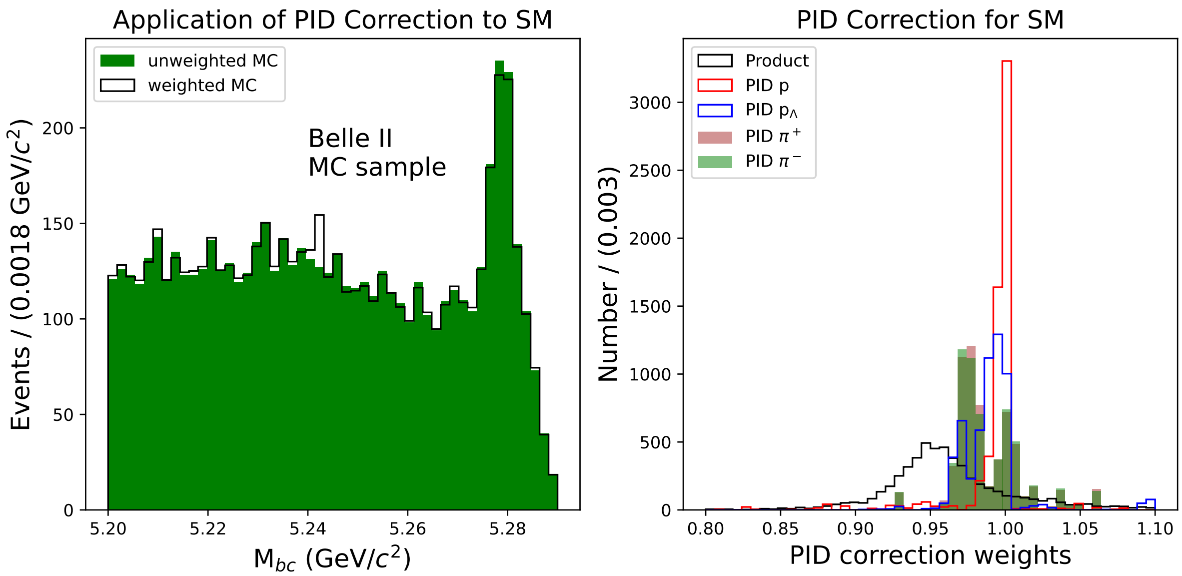

Figure 5.33: The left figure compares the weighted events to the unweighted events for the SM decay channel on the reduced MC sample. On the right, the weights for the four particles are shown completed by the multiplied event weight in black.

just reduce the height of the reduced MC sample events in the plot. This is expected by the results of the right figure 5.33. There, the weights for all individual particles are plotted as is the product of the weights for each event. The average event weight is influenced by the two high weights mentioned before. Thus, the number is not representative. The pid corrections for the two pions are similar and the pid correction of the p basically peaks at one.

After the presentation of the SM decay channel pid corrections, the BSM decay channel is analysed. The results are visualized in figure 5.34. The picture on the right shows the weights for the four particles and the black histogram depicts the multiplied event weight. In contrast to the multiplied event weight of the SM decay channel (figure 5.33), the multiplied event weight here is spread more widely. Again, the shapes of the pion weights are similar and the p peaks at one.

The average weight of the pid corrections for the BSM decay channel is roughly 1.04. In figure 5.34, there is a small enhancement of the multiplied event weight below one, but not the total range is covered by the plot, since it focuses on the individual particle corrections. However, the average multiplied weight leads to an enhancement of four percent, which is pictured in the left image of figure 5.34.

In summary, the shapes of the events reconstructed on the MC sample do not exhibit big changes. As a next step, the systematic uncertainty on the efficiency correction is estimated.

Therefore, 200 variations of the event weights are calculated the following way [5]: The systematic error is taken to be 100% correlated and the statistical error is defined as

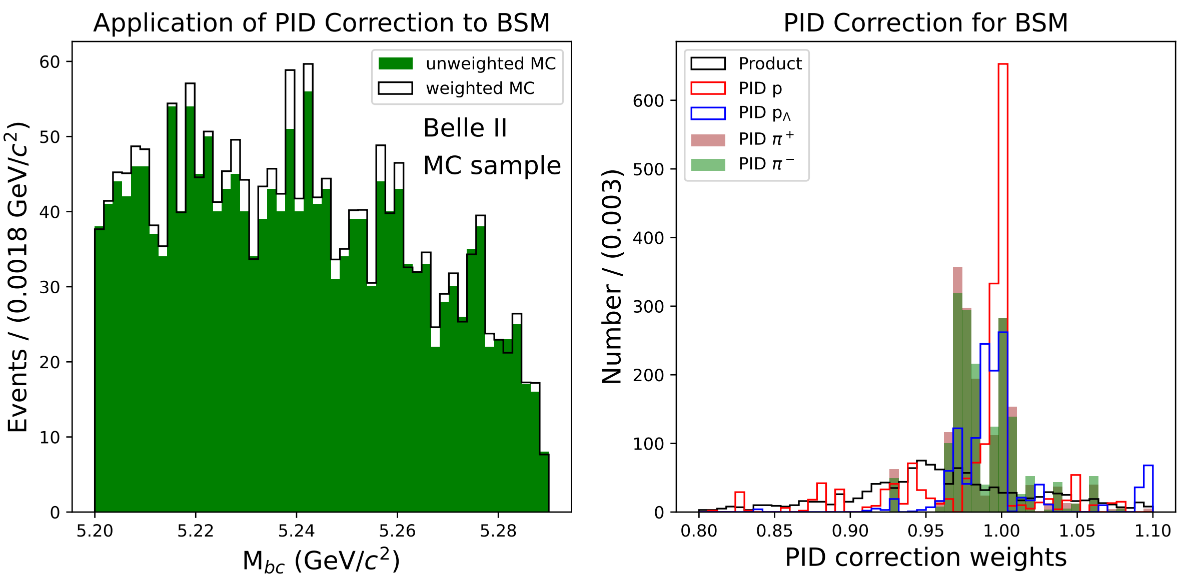

Figure 5.34: The picture on the right depicts the event weights for the individual particles and the multiplied event weight for the pid corrections. The image on the left shows the histogram for the weighted and unweighted events of the BSM decay channel on the reduced MC sample.

uncorrelated. Both systematic and statistical variations are calculated using Gaussian functions and taking the correlations into account. The variations are computed within the pid framework.

In order to calculate the efficiency corrections, the same requirements are made as for the calculation of the efficiency. Thus, only correctly reconstructed events are used remaining after the application of the cuts. As has already been mentioned, the three Signal MC samples are used for the SM decays. For each of the three decays $B^+ \longrightarrow p\overline{\Lambda}\pi^+\pi^-$, $B^+ \longrightarrow p\overline{\Lambda}\rho^0(\rightarrow \pi^+\pi^-)$ and $B^+ \longrightarrow p\overline{\Lambda}f_2(\rightarrow \pi^+\pi^-)$, individual pid corrections have to be applied to the p, p_Λ, π^+ and π^-. For the corrections of all four particles, 200 variations are performed. Then, for each one of the 200 variations separately, the following procedure is done:

$$(\sum_{i}^{N_{events}} \prod_{k} pid_{k,i})/(N_{events}) \qquad k \in \{p, p_\Lambda, \pi^+, \pi^-\}$$

For each of the events, the individual pid corrections (pid) for all four particles are multiplied. Afterwards, the results are added up and divided by the number of events N_{events}. As also for the Signal MC sample some events are outside of the variable range for the pid corrections, the percentage of missed events can be found in the Appendix in table B.7. The weight one is assigned to these events and the variation is again calculated from a Gaussian [5]. For the direct decay, the percentage of missed events is for each particle below five percent as is the case for the intermediate decay via the f_2. In contrast to that,

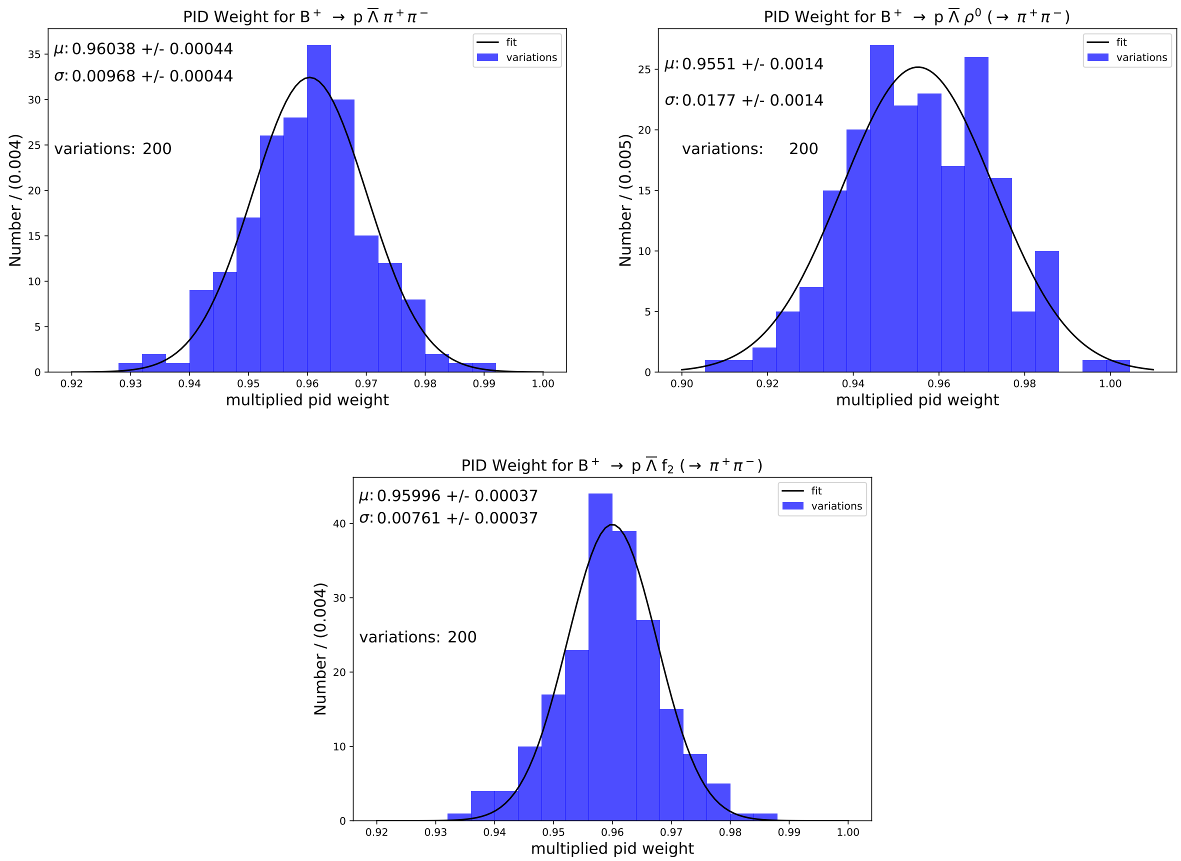

Figure 5.35: This figure depicts the results of the variations of the pid corrections and the gaussian function fitted to them. On the horizontal axis, the sum over all events of the multiplied pid corrections for all four particles divided by the number of events is presented. All three decay channels are shown. The results of the fit can be seen in the individual pictures including the fit values.

the pions of the intermediate decay via the ρ^0 are missed to 10%. Probably, the different kinematics lead to more particles being located in the excluded regions for the weight corrections of the momentum p and the $\cos\Theta$. Due to time constraints, these particles are not treated separately.
After performing this 200 times, a Gaussian distribution is used to fit the histogram of the 200 results:

$$f(x, A, \overline{x}, \sigma) = A\, e^{(-\frac{(x-\overline{x})^2}{2\sigma^2})} \tag{5.29}$$

The results are presented in figure 5.35. As can be seen, the Gaussian functions match the distributions.
The efficiency corrections result out of the fit to the distributions of mean weights, because the mean value is the correction number and the uncertainty is the width. Thus, the re-

momentum range [GeV/c]	correction	stat_uncorr	stat_corr	sys
0.05 <p< 0.12	0.996	0.020	0.013	0.003
0.12-0.16	0.990	0.015	0.013	0.003
0.16-0.2	0.987	0.017	0.013	0.003

Table 5.11: This table provides an overview over the efficiency corrections for low momentum tracks [32]. The highest momentum bin of (0.2-0.35) GeV/c is used as a reference for the normalization ref. [32] in order to achieve the correction presented in this table.

sulting efficiency corrections for the pid corrections ϵ_{pid} are:

$$\epsilon_{pid} \text{ of } B^+ \to p\overline{\Lambda}\pi^+\pi^-: \qquad 0.9604 \pm 0.0097$$

$$\epsilon_{pid} \text{ of } B^+ \to p\overline{\Lambda}\rho^0(\to \pi^+\pi^-): \qquad 0.9551 \pm 0.0177$$

$$\epsilon_{pid} \text{ of } B^+ \to p\overline{\Lambda}f_2(\to \pi^+\pi^-): \qquad 0.9600 \pm 0.0077$$

Again the errors are rounded up in order to not underestimate them.

5.5.2 Slow Momentum Corrections

Another source for systematic uncertainties are the different tracking efficiencies for data and Monte Carlo. Therefore, in ref. [32] the relative tracking efficiency is measured. In order to do this, the charged low momentum pions π_s of the decay $B^0 \longrightarrow D^{*-}(\to \overline{D}^0\pi_s^-)\pi^+$ are analysed. In contrast to the analysis of the run dependent MC, they use here three out of the four decay channels for the $\overline{D}^0$ namely $K^+\pi^-$, $K^+\pi^-\pi^+\pi^-$ and $K_s^0\pi^+\pi^-$. The results of ref. [32] are used for the calculation of the slow momentum corrections for the momentum in the lab frame.
The slow momentum region is divided into three bins. Each bin has a correction number, an uncorrelated statistical uncertainty, a correlated statistical uncertainty and a systematic uncertainty. The numbers are given in table 5.11. Since the systematic uncertainty is also correlated, it is added quadratically to the correlated statistical uncertainty and the squareroot is taken. Thus, the used corrections are:

$$\text{bin 1: } (0.05, 0.12) \text{ GeV/c} \qquad 0.996 \pm 0.020 \pm 0.0134$$

$$\text{bin 2: } (0.12, 0.16) \text{ GeV/c} \qquad 0.990 \pm 0.015 \pm 0.0134$$

$$\text{bin 3: } (0.16, 0.20) \text{ GeV/c} \qquad 0.987 \pm 0.017 \pm 0.0134$$

Here, the first uncertainty is the uncorrelated uncertainty and the second uncertainty is the correlated uncertainty.
First of all, the number of charged final particle states with p< 0.2 GeV/c is investigated.

	p<0.2 GeV/c				
	p [%]	π^+ [%]	π^- [%]	p_Λ [%]	π_Λ [%]
SM decay channel all events	0.05	2.55	2.68	0.00	42.59
SM decay channel signal events	0.00	2.14	1.36	0.00	27.38
BSM decay channel all events	0.00	4.13	3.97	0.00	43.56

Table 5.12: This table presents the percentage of final state particles with low momentum p<0.2 GeV/c. The first row describes the events of the MC sample for the SM decay channel. The second row states the percentage of the correctly reconstructed signal events in the signal region of the MC sample for the SM decay channel reconstruction for slow momentum and the last row presents the events of the BSM decay channel on the MC sample.

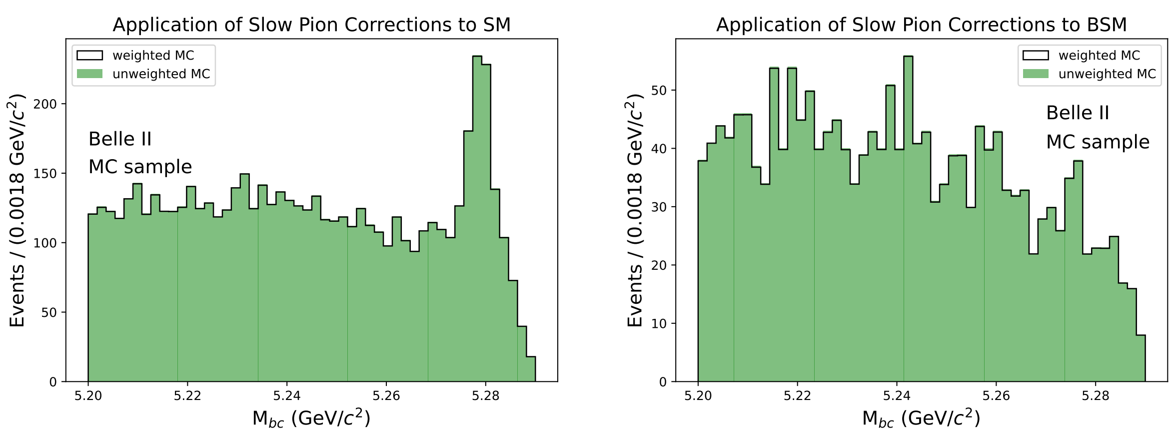

Figure 5.36: These images display the influence of the slow pion momentum corrections to the shape of the histograms. In the picture on the left, the SM decay channel on the reduced MC sample is shown and on the right the BSM decay channel.

The results are presented in table 5.12. For the SM MC sample, only the three decays used for the fit are included. As especially the percentage of the π_Λ nearly corresponds to half of the particles and to a quarter for signal events, the slow momentum correction is taken into account and calculated.
Consistently with the pid corrections, the shape variation is analysed first. The results are depicted in figure 5.36. The used reduced MC sample for the SM decay channel contains as signal events just the three main decay channels. Out of the picture, it is demonstrated, that the shapes of the histograms stay the same. This is expected, since only a few particles need to be corrected (table 5.12) and the average correction for the SM decay channel is 99.6% and 99.5% for the BSM decay channel. This leads to the expected decrease, because the slow pion corrections (table 5.11) only decrease the event weight. However, as the corrections are very small, they are barely visible in figure 5.36. As a next step, the uncertainty on the efficiency correction is calculated.
At first, two covariance matrices are calculated: one out of the uncorrelated uncertainty and one out of the correlated uncertainties. Then, they are added up and rotated to the parameter space, where the parameters are uncorrelated, to determine the variations. Afterwards, it is rotated back. The mathematical expression for the procedure follows [52]:

$$\hat{\vec{\rho}}_{\pi_s} = \vec{\rho}_{\pi_s} \times P^{-1} \tag{5.30}$$

Here, $\vec{\rho}_{\pi_s}$, which is the vector of correction factors for the 3 bins, is rotated to the parameter space using P, which is a matrix with columns given by the eigenvectors of the covariance matrix [52]. As a next step, the up and down variations are calculated by adding or subtracting the corresponding eigenvalue of the correction factor in the parameter space [52].

$$\tilde{\hat{\vec{\rho}}}_{\pi_s,\pm k} = \hat{\vec{\rho}}_{\pi_s} \pm \sqrt{\lambda_k} \tag{5.31}$$

Finally, the determined up and down variations are rotated back.

$$\vec{\rho}^{\,\prime}_{\pi_s,\pm k} = \tilde{\hat{\vec{\rho}}}_{\pi_s,\pm k} \times P \tag{5.32}$$

A more detailed description of the method can be found in ref([52], Chapter 4.3.2.). Now, the uncertainties on the efficiency correction can be calculated. As a next step, the corrections and the obtained variations are applied to the Signal MC samples for the three decays.
If the momentum of a particle is p>0.2 GeV/c, no correction is applied and if the momentum is p<0.05 GeV/c, the correction of the lowest momentum bin is used. The application of the corrections leads to a correction value for each event, where the corrections for the individual particles are multiplied, and a maximal and minimal number for each bin variation. The code for the analysis steps of the slow pion analysis presented above is provided by Dr. Nathalie Eberlein. These numbers are summed up over all events and divided by the number of events. Thus, a sum as the correction value is obtained and six more values for the maximal and minimal variations of the bin variations. Thereupon, the difference between the maximal value and the correction value is calculated as well as the difference

between the correction value and the minimal value. For each bin variation, the larger difference is taken and they are summed up quadratically before taking the squareroot of the result. Thus, the efficiency correction for the slow pion momentum ϵ_{sp} and its error is calculated.
This procedure is repeated for all three decay channels. As for the PID correction, the Signal MC is used and only events, which are correctly reconstructed and not outside of the cut values and the signal region, are taken into account.
The results are given here, the numbers of the individual bins and of the correction can be found in the Appendix in table B.8.

$$\epsilon_{sp} \text{ of } B^+ \to p\overline{\Lambda}\pi^+\pi^-: \qquad 0.99666 \pm 0.00584$$

$$\epsilon_{sp} \text{ of } B^+ \to p\overline{\Lambda}\rho^0(\to \pi^+\pi^-): \qquad 0.99667 \pm 0.00562$$

$$\epsilon_{sp} \text{ of } B^+ \to p\overline{\Lambda}f_2(\to \pi^+\pi^-): \qquad 0.99699 \pm 0.00524$$

The uncertainty in the above results is the one estimated here.

5.5.3 High Momentum Corrections

As can be seen in the previous chapter and particularly in table 5.12, only the minor part of the particles can be categorized as a low momentum particle. Thus, also a correction for the high momentum particles needs to be applied. This is done by estimating the maximal correction. Ref. [56] finds that for high momentum particles, no correction is needed, but the uncertainty on this result is assigned as systematic uncertainty with 1±0.24%. Hence, the efficiency correction for one particle is $(1^{+0.0024}_{-0.0024})$. Since the aim is to estimate the maximum, the efficiency correction has to be taken to the power of five, because five final state particles are used to reconstruct the decay namely p, π^+, π^-, p_Λ and π_Λ. This results in the following efficiency correction ϵ_{hp}:

$$\text{high momentum efficiency correction } \epsilon_{hp}\text{: } 1.000^{+0.01206}_{-0.01195}$$

As before, the errors are rounded up in order to not underestimate them. This correction can be used for all three decays, due to their equal final state particle types. Since no individual corrections to final state particles are applied, the study of the shape variation of the reconstructed events of the MC sample is skipped. To simplify the result, only the bigger uncertainty is used in the following chapter.

5.5.4 Intermediate Results

To summarize the efficiency corrections, the previously presented results are multiplied to the efficiency for each decay channel. Here, ϵ_{cut} is the efficiency after the reconstruction and the application of the cuts. The names for the other efficiencies are equal to the ones used in the last chapters.

	$p\overline{\Lambda}\pi^+\pi^-$ rel [%]	$p\overline{\Lambda}\rho^0$ rel [%]	$p\overline{\Lambda}f_2$ rel [%]
cut	0.49	0.39	0.38
pid	1.01	1.86	0.80
slow momentum (sp)	0.59	0.57	0.53
high momentum (hp)	1.21	1.21	1.21
total	1.76	2.33	1.60

Table 5.13: These are the relative uncertainties on the efficiencies. Here, cut refers to the uncertainty on the efficiency after the reconstruction and application of cuts. The calculation is done by σ_i/ϵ_i with $i \in \{cut, pid, sp, hp\}$.

$$\epsilon_{decay} = \epsilon_{cut} \times \epsilon_{pid} \times \epsilon_{sp} \times \epsilon_{hp}$$

The error is calculated using Gaussian error propagation ([28], Chapter 1):

$$\sigma_f = \sqrt{\sum_{i=1}^{N} \left(\frac{\partial f}{\partial x_i}\sigma_i\right)^2 + \sum_{i\neq j}^{N} \left(\frac{\partial f}{\partial x_i}\right)\left(\frac{\partial f}{\partial x_j}\right) Cov(x_i, x_j)} \tag{5.33}$$

In the following, the correlations are neglected. Thus, the results are:

$$\epsilon_{p\overline{\Lambda}\pi^+\pi^-} = 0.06236 \pm 0.00110 \tag{5.34}$$

$$\epsilon_{p\overline{\Lambda}\rho^0} = 0.06069 \pm 0.00141 \tag{5.35}$$

$$\epsilon_{p\overline{\Lambda}f_2} = 0.06467 \pm 0.00103 \tag{5.36}$$

The results for the relative errors for all three decay channels can be found in table 5.13. Afterwards, the efficiencies for the three decay channels are added up weighted by the corresponding $\mathcal{BR}$ to get the total efficiency and its correction. Thus the efficiency can be calculated using equ. 5.26 :

$$\epsilon = \frac{\mathcal{BR}_{p\overline{\Lambda}\pi^+\pi^-} \times \epsilon_{p\overline{\Lambda}\pi^+\pi^-} + \mathcal{BR}_{p\overline{\Lambda}\rho^0} \times \epsilon_{p\overline{\Lambda}\rho^0} + \mathcal{BR}_{p\overline{\Lambda}f_2} \times \epsilon_{p\overline{\Lambda}f_2}}{\mathcal{BR}_{p\overline{\Lambda}\pi^+\pi^-} + \mathcal{BR}_{p\overline{\Lambda}\rho^0} + \mathcal{BR}_{p\overline{\Lambda}f_2}}$$

It has to be noted, that the uncertainties for the $\mathcal{BR}_i$ are taken from ref. [26], where both the statistical and the systematic uncertainty are given. These two are added up quadratically, before taking the square root and choosing the bigger, rounded up uncertainty. As a result, the following $\mathcal{BR}$s are used:

$$\mathcal{BR}_{p\overline{\Lambda}\pi^+\pi^-} = (5.92 \pm 1.12) \times 10^{-6} \tag{5.37}$$

$$\mathcal{BR}_{p\overline{\Lambda}\rho^0} = (4.78 \pm 0.90) \times 10^{-6} \tag{5.38}$$

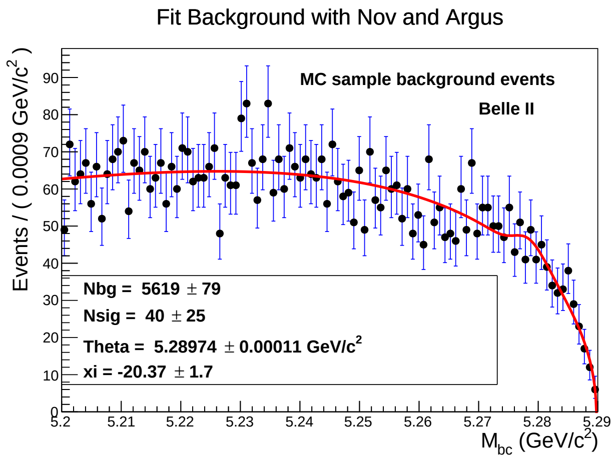

Figure 5.37: This picture depicts the results for the combined fit of Novosibirsk and Argus function to the MC sample background events only.

$$\mathcal{BR}_{p\bar{\Lambda}f_2} = (2.03 \pm 0.82) \times 10^{-6} \tag{5.39}$$

Using now the values of equ. 5.34 - equ. 5.36 and equ. 5.37 - equ. 5.39 for the calculation of the efficiency ϵ and using Gaussian error propagation (equ. 5.33) to calculate the uncertainty, the result for the efficiency is:

$$\epsilon = 0.0621 \pm 0.0008 \tag{5.40}$$

Thus, the uncertainty corresponds to 1.29% of the efficiency. Comparing now the corrected efficiencies for the individual decays with the results of ref. [26], all three efficiencies of equ. 5.34 - equ. 5.36 are higher for this analysis. However, not all of the uncertainties are included yet. There are a few more uncertainties, which have not been explicitly considered for the calculations. Thus, they are shortly presented now.

Reconstruction of the Λ

So far, the efficiency corrections are applied to the final state particles. However, also the Λ ($\overline{\Lambda}$) require corrections. Due to time constraints, this is not implemented for this analysis.

Background Peak

Since all fits result in an increased signal yield, a possible reason for this phenomenon is investigated. Therefore, the background of the MC sample excluding the correctly reconstructed signal events is fitted with a one dimensional fitting function including the Novosibirsk function with fixed shape parameters and the background function. This is performed in order to find out, whether the background exhibits a peak in the signal region. It is also shown in fig. 5.1 and in fig. 5.3, that the background events peak in the signal region. The results of the fit are presented in fig. 5.37. Although the determined signal yield is forty, this still agrees with zero within two standard deviations. Thus, it might be a possible source for the signal enhancement, but there can still exist other reasons.

Decay Channels
Another source for systematic uncertainties are the neglected decay channels contributing to the correctly reconstructed signal events. With the simultaneous fit on the reweighted three decays of ref. [26], roughly 75% of the signal events are covered (see fig. 5.17). However, a quarter is still excluded, which can result in different efficiencies and larger efficiency corrections. On top of that, the three decays have similar shapes for the M_{bc} variable, but differ slightly for the distributions of some cut variables (see fig. 5.24) due to different kinematics. This contributes to the different efficiencies.

Fit
The MC sample used for the fit is weighted with numbers calculated based on one measurement [26]. So far, the weights are not varied to test their impact on the fit result. Furthermore, the uncertainties of the fit results are not included in the calculation of the results.

In order to apply this analysis to data, more corrections would be needed to be taken into account. These are basically two variables, which are used to calculate the branching ratio $\mathcal{BR}$.

$\mathbf{N_{BB}}$
Next to the efficiency, the number of $B\overline{B}$ events is not exact. The absolute number of $N_{B\overline{B}}$ is given as [24]:

$$N_{B\overline{B}} = (387.1 \pm 5.6) \times 10^6$$

This value covers the $B^0\overline{B}^0$ events and the B^+B^- events. Though the number of events does not match the number of events used in the MC sample, the relation of the error to the value is supposed to be the same. Thus, the percentage value of 1.45% will be used as the uncertainty.

$\mathbf{f_\pm}$
Since the number of events includes both $B^0\overline{B}^0$ events and the B^+B^- events, the ratio $R^{+/0} \equiv f_\pm/f_{00}$ between these two has to be taken into account. This value has been measured by ref. [27].
Therefore, they use the decay channels $B^0 \to J/\psi K^0$ and $B^+ \to J/\psi K^+$, where the J/ψ is reconstructed through either e^+e^- or $\mu^+\mu^-$ [27]. Overall, their result for $R^{+/0}$ is [27]:

$$R^{+/0} = 1.065 \pm 0.012 \pm 0.019 \pm 0.047$$

Here, the first uncertainty is statistical and the second one is the systematic uncertainty, while they assign a third uncertainty due to their assumption of isospin symmetry [27].
Thus, $R^{+/0} = 1.065 \pm 0.052$ is the final value. This corresponds to a percentage of 4.89% for the uncertainty, which will be used as a correction factor.

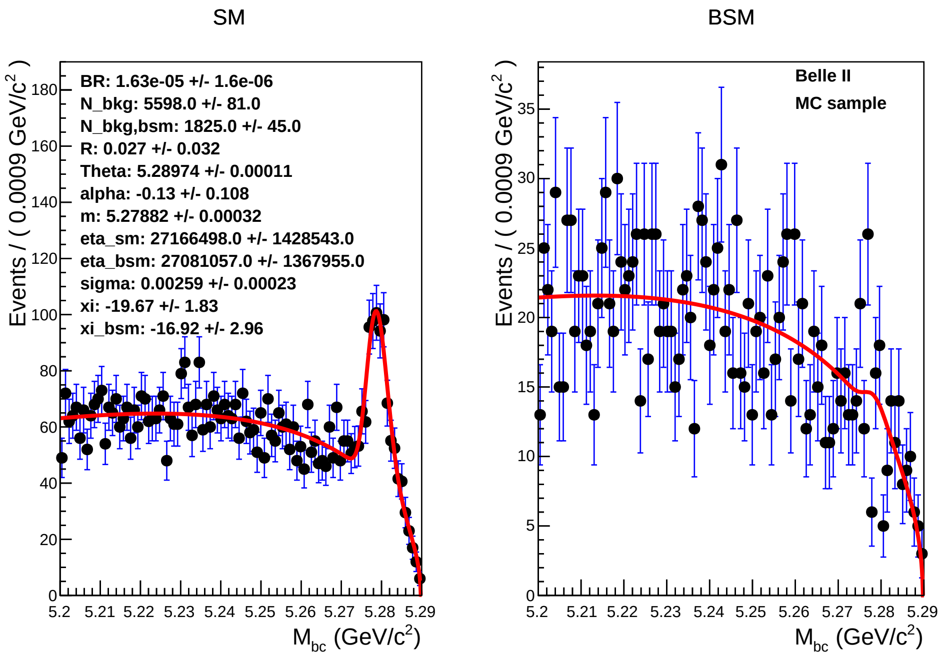

Figure 5.38: This figure presents the fit focusing on $\mathcal{BR}_{SM}$ and on $\mathcal{R}$ on the reduced MC sample including the systematic uncertainties.

5.6 Results

Now, the systematic uncertainties are included for the upper limit calculation. Therefore, the simultaneous fit is used on the weighted data sample including only the three in ref. [26] analysed decays as correctly reconstructed signal events. Thus, the efficiency for the SM channel is unchanged to the efficiency of the one used for the simultaneous fit and the uncertainty is set to the result of the systematic uncertainties chapter. For the efficiency of the BSM decay channel, again the efficiency determined on the Signal MC is used, but the uncertainty is taken to be the same percentage of the efficiency value as for the SM decay channel efficiency. Furthermore, the uncertainties for $N_{B^+B^-}$ and $f_\pm$ are taken to be the same percentage of the value used in the fit as the uncertainties presented in the systematic uncertainties chapter. As a result, the systematic uncertainties are highly overestimated, since the defined ratio $\mathcal{R}_\eta$ would cancel $N_{B^+B^-}$ and $f_\pm$. Thus, the real upper limit would be better and this is an estimation of the upper bound.
In addition to the calculation of the upper limit, the fit (fig. 5.38 and fig. 5.39) is also performed and is validated with toy studies, which can be found in the Appendix in fig. A.9 and in fig. A.10. The results for the fit focusing on $\mathcal{R}$ and $\mathcal{BR}_{SM}$ differ from the previously presented results for the uncertainty of $\mathcal{BR}_{SM}$ and the variable $\mathcal{R}$. For the results of the second fit focusing on N_{sig} and $\mathcal{R}$ only the uncertainty on $\mathcal{R}_\eta$ changed.
The branching ratio for the Standard Model decay channel is given by $\mathcal{BR}_{SM} = (1.63 \pm 0.16) \times 10^{-5}$. Comparing this to the expected value of 1.273×10^{-5} (see table 5.8), they are

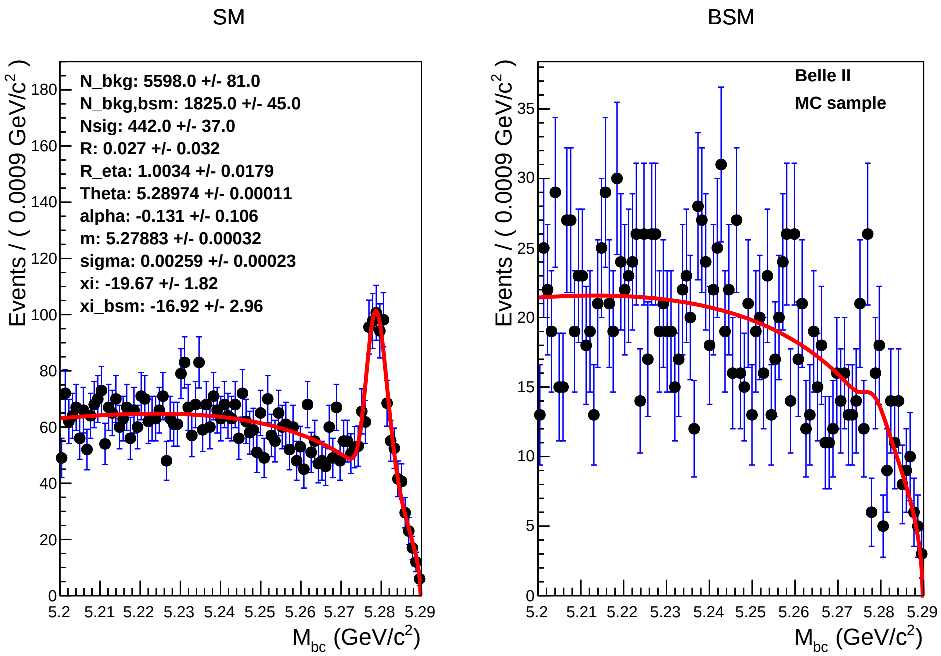

Figure 5.39: This figure presents the fit on the reduced MC sample including the systematic uncertainties and focusing on N_{sig} and $\mathcal{R}$.

compatible within 2.3 standard deviations. In ref. [26], the uncertainty is calculated for each of the three decay channels separately. Thus, the uncertainty stated in the PDG [62] is used as it utilizes ref. [26] only and states an uncertainty for all three decays combined. As the calculation is based on ref. [26], the used integrated luminosity is 605fb^{-1} and the uncertainty is $0.13{\times}10^{-5}$. For this analysis the integrated luminosity is roughly 386fb^{-1}. Thus, the uncertainty on $\mathcal{BR}_{SM}$ calculated in this analysis is higher than the uncertainty given in the PDG. However, the dimension is still the same.
The results for the upper limit at 90% confidence level are presented in fig. 5.40. First of all, the upper limit on the ratio is the same as the results presented in the upper limit chapter. This is not anticipated, since a broader uncertainty should result in a broader profile NLL and thus a larger upper limit. In order to check this, the width due to the uncertainties was increased much more by hand. Then, the upper limit enlarged as expected. Thus, the increase in the uncertainty due to the systematic uncertainties is probably not big enough to change the results significantly.
As a last step, the upper limit on the $\mathcal{BR}_{BSM}$ is calculated out of the upper limit and the fit result for the $\mathcal{BR}_{SM}$:

$$\mathcal{BR}_{BSM} = \mathcal{BR}_{SM} \times \mathcal{R} = 1.63 \times 10^{-5} \times 0.0828 = 1.35 \times 10^{-6} \quad @\ 90\%\ \mathcal{CL} \tag{5.41}$$

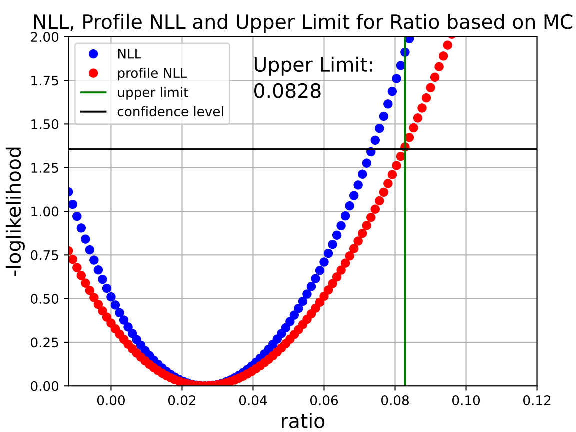

(a) $\mathcal{R}$ and $\mathcal{BR}_{SM}$ in fit

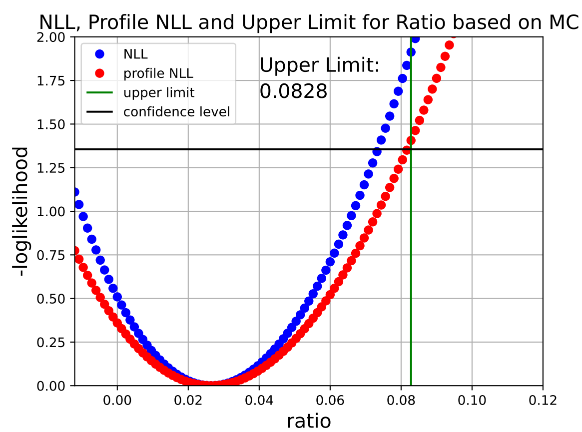

(b) $\mathcal{R}$ and N_{sig} in fit

Figure 5.40: This figure represents the results of the upper limit calculation including the systematic uncertainties for both N_{sig} and $\mathcal{BR}_{SM}$ included in the fit.

Chapter 6

Analysis of the $\mathbf{B^+ \to p\,\Lambda}$ Decay Channel

As a second decay channel for the search for baryon number violation, the decay channel $B^+ \to p\,\Lambda$ is selected for different reasons. First of all, the same reasons as for the first decay channel can be applied: the decay channel violates baryon number, the decay channel has a corresponding SM decay channel $B^+ \to p\,\overline{\Lambda}$, it is a purely hadronic decay and the final state particles including the Λ decay are all charged particles. The main difference between $B^+ \to p\,\Lambda$ and $B^+ \to p\,\Lambda\pi^+\pi^-$ is the absence of the pions. However, this decay channel has another advantage. While the SM decay channel is helicity suppressed, this does not apply to the BSM decay channel. Thus, it might even be enhanced. The helicity h is defined as $h = (\mathbf{s}\cdot\hat{\mathbf{p}})/(s\cdot\hbar)$ with $\mathbf{s}$ as the spin operator and $\hat{\mathbf{p}}$ as the momentum vector as an unit vector ([21], Chapter 7).
Thus, the decay of the B meson in its rest frame can be depicted as either:

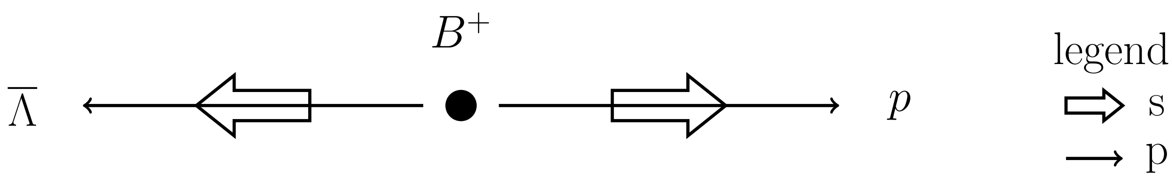

or

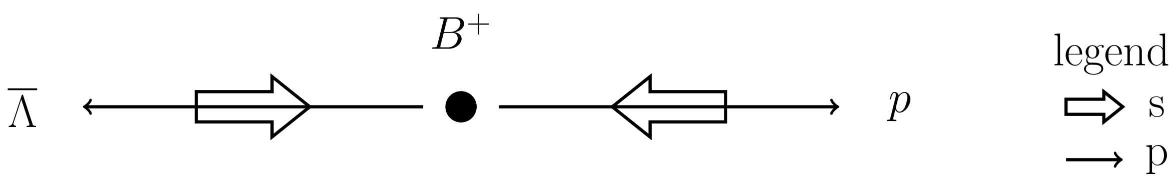

Since the weak interaction preferes left-handed particles and right-handed antiparticles, both options are helicity suppressed with the suppression factor mc^2/E ([21], Chapter 17). For the BSM decay channel, the suppression factor is not applied to the second of the

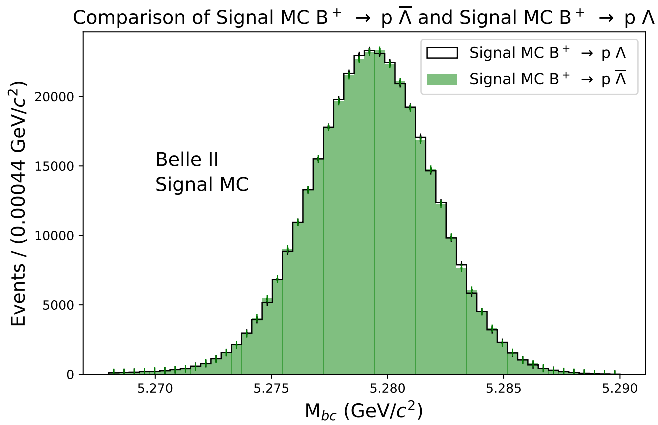

Figure 6.1: This figure depicts the shape comparison of the two Signal MC samples for the SM and the BSM decay channel.

depicted decays and therefore probably leading to the enhancement of signal events.
In the following, some intermediate results are presented. Due to time reasons, the decay channel is not analysed as detailed as the first one.

6.1 Analysis of Signal MC

Now the whole Signal MC for the SM channel and the BSM channel is analysed briefly. Since these are just intermediate results, no detailed study with the decreased sample is performed here.
The signal region is defined as for the first decay channel to be M_{bc} >5.268 GeV/c^2. After the reconstruction, the efficiencies are:

$$\epsilon_{p\overline{\Lambda},rec} = 0.3486 \pm 0.0005$$

$$\epsilon_{p\Lambda,rec} = 0.3481 \pm 0.0005$$

Thus, the efficiencies after the reconstruction are roughly the same for the SM decay channel and the BSM decay channel. This meets the expectations, since the two decay channels differ just in Λ and $\overline{\Lambda}$. In comparison to the first decay channel, the efficiency is twice as big. But since the difference between the decay channels is the presence or absence of $\pi^+\pi^-$, this is also expected.
The shape comparison of the two decays is presented in fig. 6.1. Here, the beyond Standard Model decay channel is weighted down, to match the number of events for the SM decay channel, though the difference between the number of signal events is small since the full Signal MC sample is used for both. Fig. 6.1 shows the shape comparison just for correctly reconstructed signal events. As can be seen, the shapes look similar.

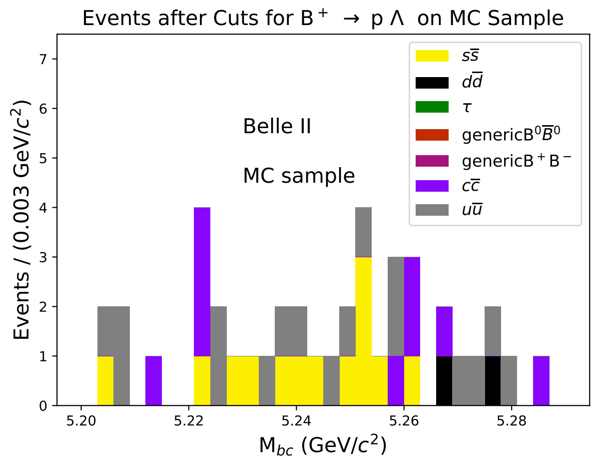

Figure 6.2: This figure presents the results for the reconstruction of the BSM decay channel on the reduced MC sample.

6.2 Analysis of Generic MC

For the analysis of the MC sample, BDTs are trained first. In contrast to the analysis of the first decay channel, two categories are defined and BDTs are trained for each one of them separately.
The first category is the suppression of the continuum events. Here, the training variables for the BDT are similar to the ones used for the BDT in the first analysis, namely CleoCone variables [17], KSFW variables ([23], Chapter 9) and the variables related to the thrust [33] axis. In contrast to the analysis of the first decay channel, the variable R2 is still included. The variable R2 and the variables connected to the thrust axis have importance of more or equal 10 out of 100.
The second category is introduced to focus on the suppression of the background events of the B meson decays. Thus, the BDT is trained on a sample including only Signal MC and generic $B\overline{B}$ events. Therefore, the variable used for the training is the truth-matching MC variable identifying correctly reconstructed decays. Furthermore, the input variables differ from the ones used before. Now, they focus on the distance of the individual particles to the interaction point, the invariant mass of the Λ, which is determined out of the four momentum vector of its decay particles, the flight distance of the B meson and the Λ and the transverse momenta of some particles. These variables are chosen in analogy to the variables used in ref. [6] for the classifier and to the variables cutted on in ref. [58] for the event selection.
Now, the reconstruction of the decay channel $B^+ \rightarrow p\,\Lambda$ on the reduced (see Appendix table B.1) MC sample is analysed. No truth matched signal events are found. As a next step, the background is decreased by maximising the Punzi figure of merit (equ. 5.5) [55]. The full Signal MC sample for the BSM decay was used to determine the efficiency required in the formula.

	$s\bar{s}$	$d\bar{d}$	$c\bar{c}$	$u\bar{u}$
remaining fraction [%]	0.029	0.007	0.009	0.012
remaining fraction in signal region [%]	0.000	0.017	0.006	0.014

Table 6.1: This table provides an overview over the percentage of background events after the application of the cuts for the BSM decay channel.

	$s\bar{s}$	$d\bar{d}$	$c\bar{c}$	$u\bar{u}$	Signal
remaining fraction [%]	0.005	0.003	0.008	0.005	38.636
remaining fraction in signal region [%]	0.002	0.000	0.000	0.008	38.636

Table 6.2: This table gives an overview over the percentage of background events and correctly reconstructed signal events after the application of the cuts for the SM decay channel.

Cuts are applied to both BDT output variables, the ΔE variable, the probability of p and p_Λ to be truly a proton, the χ^2 probability already used in chapter 5 and the decay angle of the π_Λ. The last variable is computed in the center of mass frame of the Λ calculating the angle between the negative center of mass momentum vector and the direction of the π_Λ in the rest frame of the Λ.
The results are presented in fig. 6.2. As can bee seen there, the background events consist only continuum background events. The τ and the B meson decay events are rejected by the cuts. Overall, six events are located in the signal region. An overview over the remaining background events can be found in table 6.1. The fraction is calculated by dividing the events after the application of the cuts by the number of events after the reconstruction. After the application of the cuts, the efficiency of the Signal MC is:

$$\epsilon_{p\Lambda} = 0.1732 \pm 0.0004$$

This is half of the efficiency after the reconstruction.
The SM channel is also analysed on the reduced MC sample. Here, different cuts are varied in order to maximise the significance (equ. 5.6) in the signal region. After the reconstruction, 44 signal events are found. This corresponds to the following reconstruction efficiency:

$$\epsilon_{p\overline{\Lambda},rec} = 0.330 \pm 0.004$$

Thus, the reconstruction efficiency is decreased compared to the Signal MC. Due to time reasons, the origin of this difference is not determined. The variables used for the cuts are similar to the ones for the analysis of the BSM channel. On top, some variables connected with the thrust axis are included, though they are already used for the BDT. The χ^2 probability is excluded and a pid cut on the π_Λ is added as well as another decay angle cut on the Λ.
Using exactly the same cuts as are determined for the BSM decay channel results in a

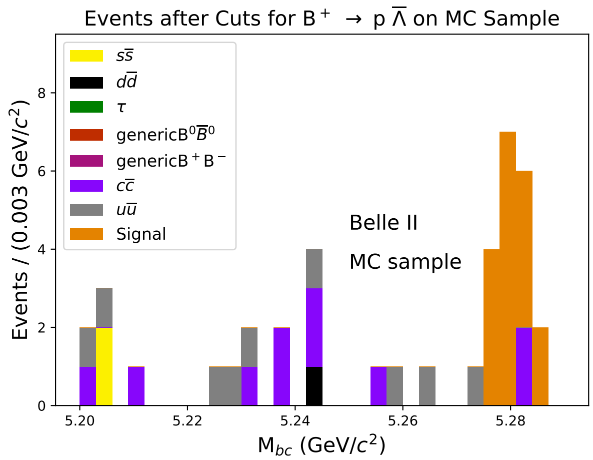

Figure 6.3: In this figure, the results for the SM decay channel after the application of the cuts is presented.

worse significance. However, the assimilation of the cuts could not be done due to time reasons.
The accomplished significance and efficieny after the application of the cuts are:

$$\mathrm{S} = 3.8$$

$$\epsilon_{p\overline{\Lambda}} = 0.13 \pm 0.03$$

The efficiency $\epsilon_{p\overline{\Lambda}}$ differs from the efficiency $\epsilon_{p\Lambda}$, but since the applied cuts are different, they can not be directly compared.
The remaining fractions of both the signal and the background events can be found in table 6.2. The fraction is calculated as for the previously presented table (table 6.1). As for the BSM decay channel, only continuum background events remain.
As the decay $B^+ \to p\,\overline{\Lambda}$ has an enhanced branching ratio in the MC sample, the signal events need to be weighted. The branching ratio in the PDG and the corresponding measurement is 2.4 $\times 10^{-7}$ [62, 6], whereas the branching ratio used in the simulation is 3.2 $\times 10^{-7}$, which is the upper limit determined by ref. [58]. Thus, the correction factor is 0.75 for signal events. This would decrease the significance to:

$$\mathrm{S}_{weight} = 3.2$$

Thus, even the weighted significance has a value of more than three.

Summary

The task of this analysis is to search for baryon number violation by two units. Therefore, an hadronic decay channel of the B meson namely $B^+ \to p\,\Lambda\,\pi^+\,\pi^-$ is chosen, while the corresponding Standard Model decay channel $B^+ \to p\,\overline{\Lambda}\,\pi^+\,\pi^-$ is used as a control channel for the analysis.
This analysis is based on simulation. As the beyond Standard Model decay channel is not included in a simulation based on the Standard Model, the only signal events are obtained using Signal Monte Carlo. Contrarily, the Standard Model decay channel is part of the MC sample, but it provides difficulties, as the collision of the e^+e^- can result in the final state particles not only through the direct decay channel named above, but also through intermediate particles or hadronization of quarks. In order to handle the challenges of unknown efficiencies of some contributing decay channels, for the final fit and systematic uncertainty correction only three decay channels are used, which correspond to nearly three-quarter of the signal events.
For the reconstruction of both the beyond Standard Model and the Standard Model decay channel, loose cuts are applied and the Λ is reconstructed utilizing the decay channel $\Lambda \to p\,\pi^-$. In order to extract the signal events out of the huge background events, additional cuts are implemented after the reconstruction. These cuts are optimized on the Standard Model decay channel using the figure of merit given in equation 5.5. Among them is the variable, which is the output of the classifier (BDT) trained on the Standard Model decay channel to reduce the background.
After the extraction of the signal events, the remaining MC sample is fitted with a pdf consisting of the Novosibirsk function to model the signal shape and the Argus function to shape the background events. At first, a one-dimensional fit is implemented and the beyond Standard Model decay channel and the Standard Model decay channel are fitted separately. Thereupon, a simultaneous fit of these two decay channels is established. The change of the fit variable from signal events to branching ratio for the Standard Model decay channel and to the ratio of the branching ratios for the beyond Standard Model decay channel is one accomplished advantage, since the fit results directly provide the variables required for the upper limit calculation. Furthermore, by fitting the ratio of the branching fractions, systematic uncertainties are expected to cancel.
Before calculating the upper limit, the systematic uncertainties are estimated for the efficiency correction. This includes the pid corrections, the slow momentum corrections and the high momentum corrections. Furthermore, the uncertainties on the number of $B\overline{B}$

events and on the $f_{\pm}$ are taken into account for the final results.
In the end, an upper limit is set on the branching fraction of the $B^+ \to p\,\Lambda\,\pi^+\,\pi^-$ decay channel. Therefore, the profile loglikelihood is used to calculate the upper limit on the ratio at 90% confidence level and including the fit result for the branching ratio of the Standard Model decay channel, this can be transformed to an upper limit on the branching fraction of the beyond Standard Model decay channel.
The final results for the branching fractions are:

$$\mathcal{BR}_{p\,\Lambda\,\pi^+\,\pi^-} = 1.35 \times 10^{-6} \quad @ \ 90\% \ \mathcal{CL} \tag{6.1}$$

$$\mathcal{BR}_{p\,\overline{\Lambda}\,\pi^+\,\pi^-} = (1.63 \pm 0.16) \times 10^{-5} \tag{6.2}$$

No other measurements of $\mathcal{BR}_{p\,\Lambda\,\pi^+\,\pi^-}$ are known to the author at this point. The corresponding PDG uncertainty for $\mathcal{BR}_{p\,\overline{\Lambda}\,\pi^+\,\pi^-}$ is with (1.13 $\pm$ 0.13) $\times 10^{-5}$ [62] below the result of this analysis as is the from weighted events of the MC simulation expected $\mathcal{BR}$ of 1.273×10^{-5}. The calculated uncertainty and the uncertainty of the PDG are still of the same order. A possible explanation for the discrepancy in $\mathcal{BR}$ might be the difference between the efficiencies for the reconstruction on the Signal MC and the MC sample. Due to the usage of the efficiency determined on the Signal MC for the calculation of the $\mathcal{BR}$ on the MC sample, the results are possibly enhanced. It remains a task for the future to investigate the efficiencies further.
More improvements can be implemented during the analysis:

- Boosted Decision Tree: Since the classifier was trained to reduce the continuum background, it might be reasonable to train it only on signal events and continuum background events. Furthermore, the implemented cuts can be optimized without the output variable of the BDT and thus the BDT can be trained on a data sample with these cuts applied. This would probably improve the result further.

- Fit: Another option is to implement the beam constraint mass M_{bc} (equ. 4.1) as a cut variable and fit on ΔE (equ. 4.2) instead. In addition, the cut-off of the Argus distribution used to model the background in the pdf can be set to half of the center-of-mass energy.

- Systematic Uncertainties: Additional uncertainties listed in Chapter 5.5. for completeness can be studied in more detail. Furthermore, the pdf could be fitted to the MC sample implementing not only the efficiency corrections, but also the corrections applied to the MC sample.

- $B^+ \to p\,\Lambda$: A more detailed analysis of this decay channel can be performed. Also the corresponding Standard Model decay channel might be worth to analyse.

To summarize, this analysis contributes an experimental search for baryon number violation as a possible explanation for the matter-antimatter asymmetry in the universe. As no signal events are found in the simulation, an upper limit is estimated for the decay channel. In addition, the branching fraction of $\mathcal{BR}_{p\,\overline{\Lambda}\,\pi^+\,\pi^-}$ is determined. Future analyses might include possible improvements and contain a second decay channel like $B^+ \to p\,\Lambda$.

Appendix A

Diagrams

A.1 BDT

The important variables for the BDT are depicted in the histogram A.1.

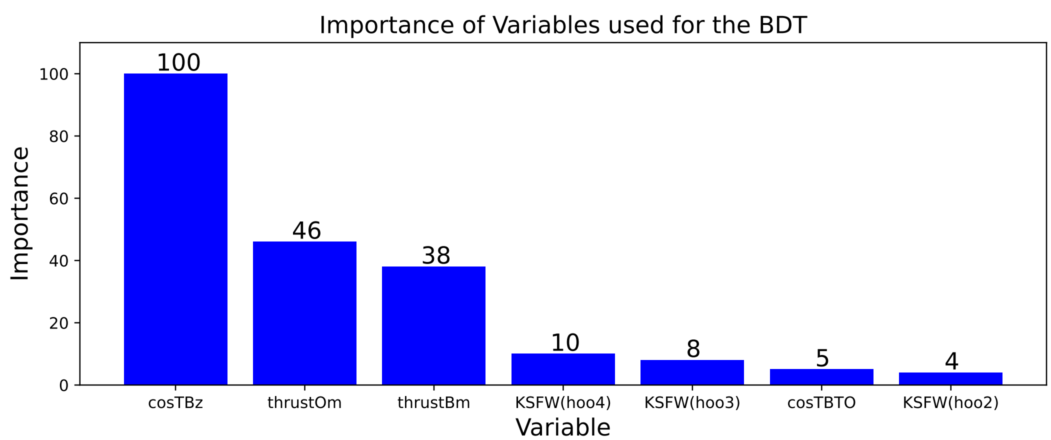

Figure A.1: This diagram visualizes the importance of the BDT training variables. Details are given in the text.

The elements of this diagram are arranged by their importance for the BDT. Only variables with importance > 3 have been listed. The most important variables are connected to the trust axis [33], however also some KSFW variables ([23], Chapter 9) contribute. In contrast to them, the included CleoCone variables [17] are negligible. The variables thrustBm and thrustOm stand for the magnitude of the thrust axis of the signal B and the rest of event respectively, while cosTBTO and cosTBz represent the cosine of the angle between the thrust axis of the signal B meson and the thrust axis of the rest of event or the z-axis ([1], Chapter 7). Furthermore, the variables KSFW(hso10), KSFW(hso12), KSFW(hso14), KSFW(hso20), KSFW(hso22), KSFW(hso24), KSFW(hoo0), KSFW(hoo1) and the last five CleoCones are training variables with importance < 3.

A.2 Fit Addition First Fit

In the following, the fit results for the full MC sample are presented. For the one dimensional fit, no event weights are used. The functions used for the fitting are presented in

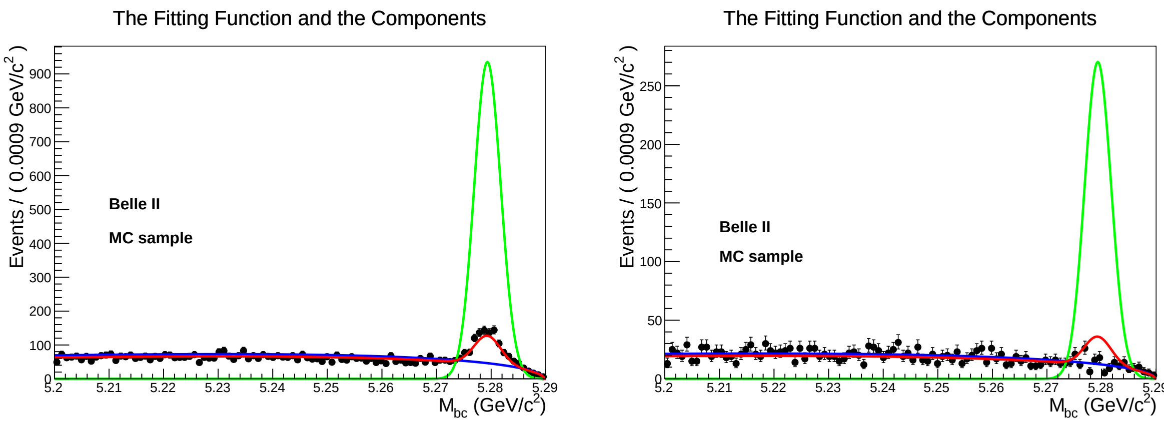

Figure A.2: This figure depicts the functions used for the fit. Green is the Novosibirsk function, blue represents the Argus function and red is the combined function. The black points are the in this case reduced MC sample events. The SM decay channel is depicted on the left and the BSM decay channel events on the right.

figure A.2. The combined function for the BSM decay channel fit still exhibits a peak in the signal region, since the initial value of N_{sig} is chosen unequal to zero. The procedure

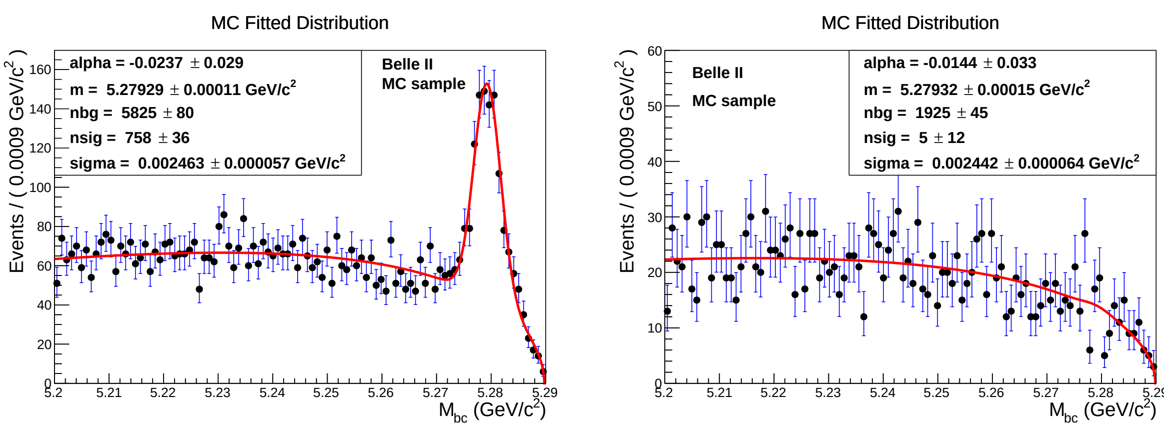

Figure A.3: This figure depicts the fit to the full MC sample for the SM decay reconstruction on the left and for the BSM reconstruction on the right.

and plot style is the same as is described in the text. The functions used for the fit are the same as for the reduced MC sample and include the shape parameters of the Novosibirsk function as nuisance parameters. The fit results are presented in figure A.3. Only the starting points for the N_{sig} and N_{bkg} for the toy studies have been adjusted to the true MC

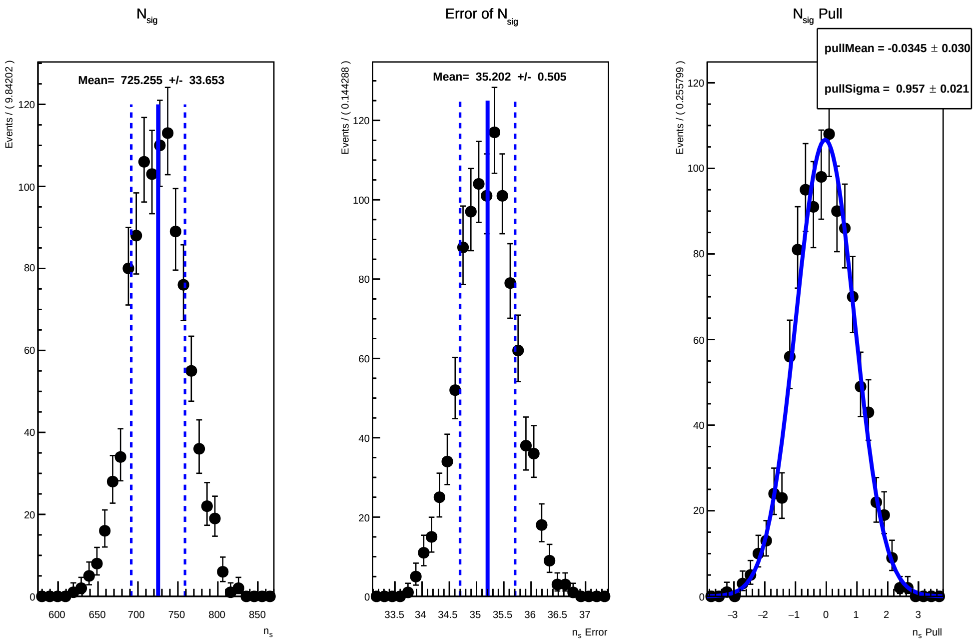

Figure A.4: In this figure, the results of the toy studies for the fit to the SM channel events of the MC sample are shown for the variable N_{sig}.

values for the full MC sample. The toys are created without including the constraints. The results are depicted in figure A.4 and in figure A.5. Furthermore, the range for the NLL and the upper limit plot is different compared to the reduced MC sample. The results for the NLL and profile NLL calculation by hand are shown in figure A.6.

A.3 Toys for Simultaneous Fit on $B^+ \to p\,\overline{\Lambda}\,\pi^+\,\pi^-$

In this chapter, the toy studies for the simultaneous fit on the reduced MC sample including only the direct decay $B^+ \to p\,\overline{\Lambda}\,\pi^+\,\pi^-$ as correctly reconstructed signal events are presented.
The results for the fit variable branching fraction $\mathcal{BR}_{SM}$ and the fit variable ratio $\mathcal{R}$ are presented in fig. A.7. The expected value for the branching fraction is $\mathcal{BR}_{SM} = 1.128 \times 10^{-5}$. Both the distribution of the $\mathcal{BR}_{SM}$ and its pull plot resemble a Gaussian function. The peak of the Gaussian for the $\mathcal{BR}_{SM}$ meets the expected value. In addition, a Gaussian function is fitted to the pull distribution. As is explained in the text, the mean of the Gaussian function is supposed to be zero and the width should be one. As is depicted in fig. A.7, both the mean and the sigma agree with their expectations within two standard deviations. For the pull of the ratio, the mean agrees within two standard deviations with zero and the width is closer to one than one standard deviation. Thus, the toy studies do not reveal a too large bias.

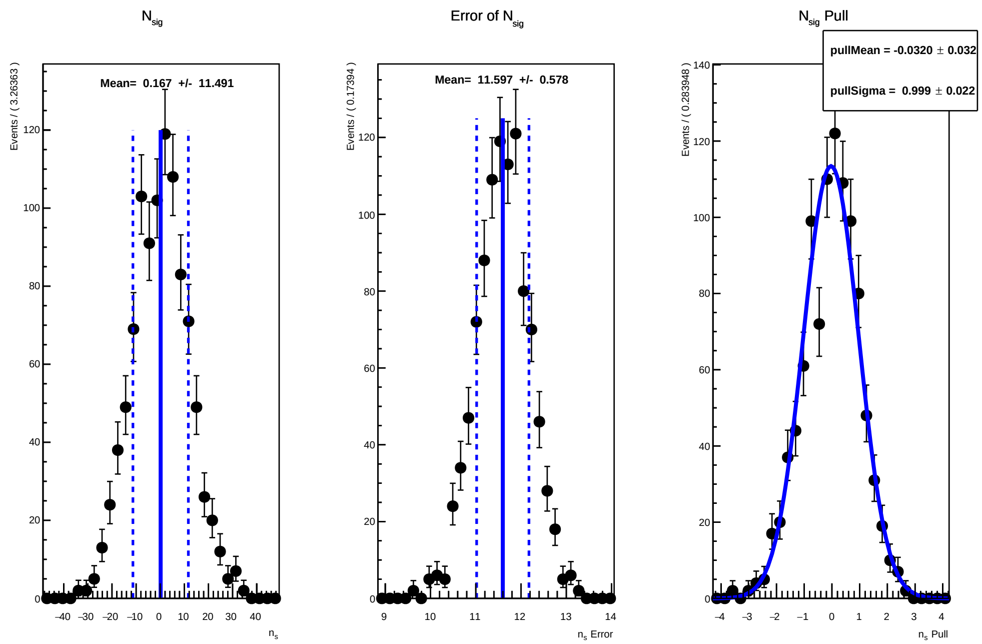

Figure A.5: In this figure, the results of the toy studies for the fit to the BSM channel events of the MC sample for the variable N_{sig} are shown.

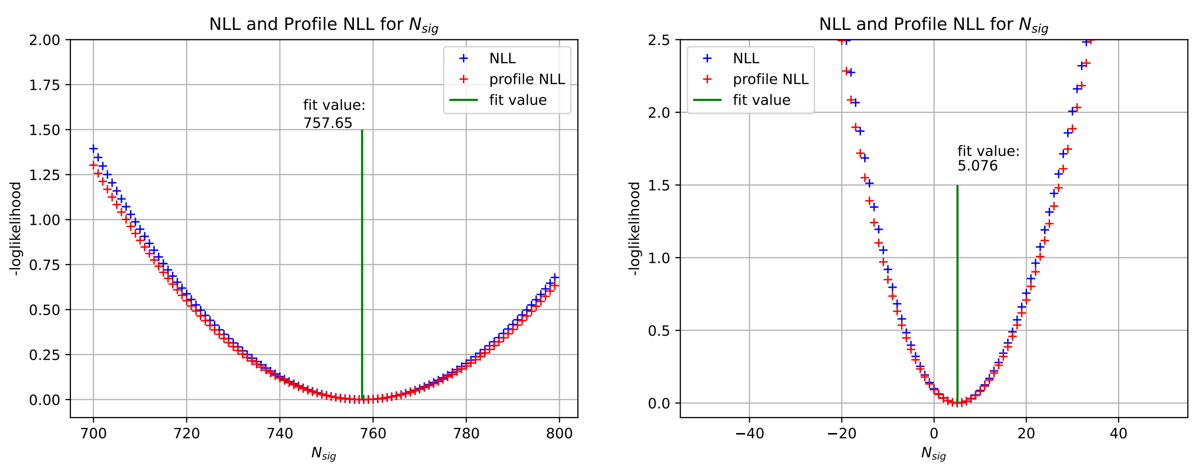

Figure A.6: These two pictures present the NLL and profile NLL results by hand for the SM channel events on the left and the BSM channel events on the right.

The results for the toy studies of the variables N_{sig} and $\mathcal{R}$ are depicted in fig. A.8. The expected value for N_{sig} is 345 events, which is roughly located at the maximum of the distribution. Again, a Gaussian function is fitted to the pull distribution and both the mean and the sigma agree with their corresponding values within one standard deviation.

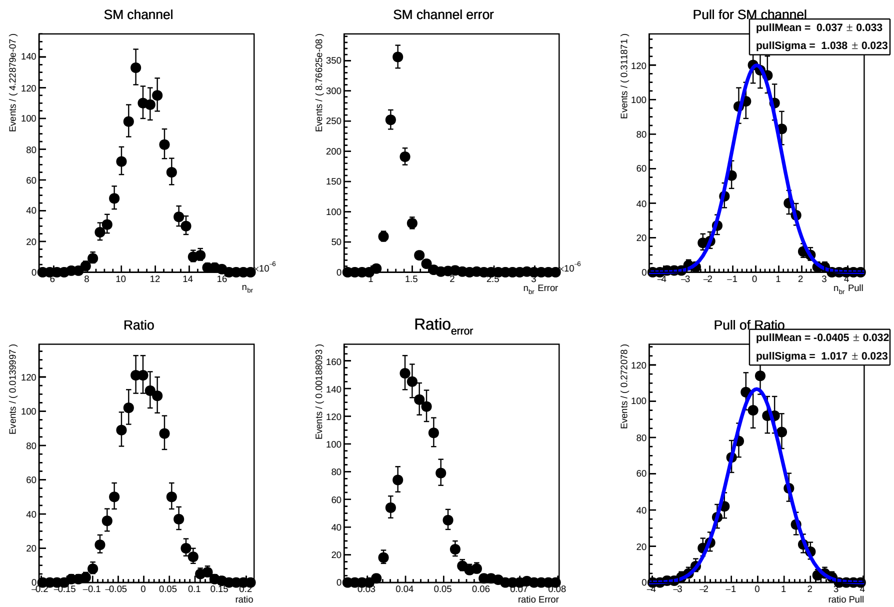

Figure A.7: This figure presents the results of the toy studies for the simultaneous fit on the reduced MC data sample including only the direct decay as correctly reconstructed signal events. The upper row depicts the result for the variable branching fraction $\mathcal{BR}_{SM}$ and the lower row completes it with the results for the variable ratio $\mathcal{R}$.

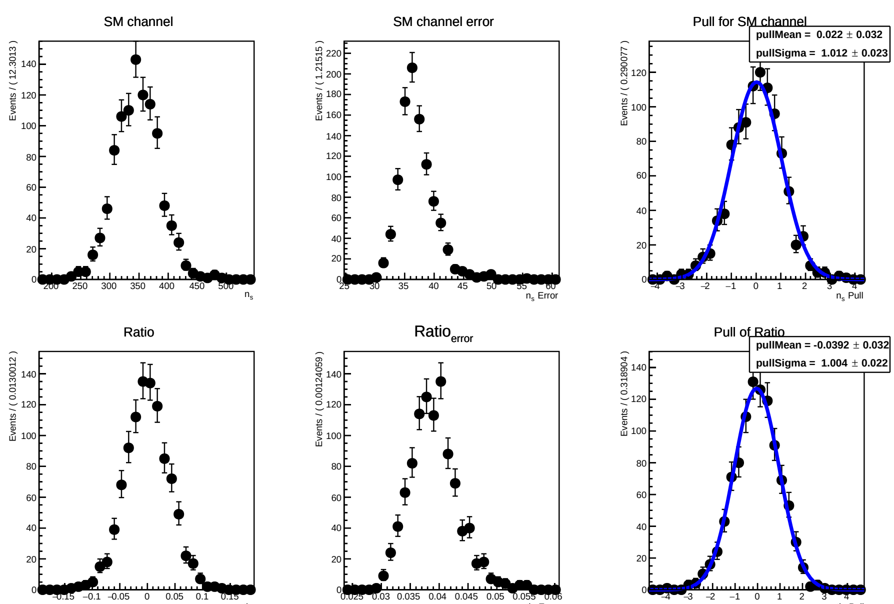

Figure A.8: In this figure, the results of the toy studies for the variables N_{sig} (first row) and $\mathcal{R}$ (second row) are visualized. The corresponding fit is the simultaneous fit on the reduced MC data sample excluding all decays except the direct decay as signal events.

The distribution of the ratio peaks around zero as expected and the Gaussian fit to the pull distribution results sigma being very close to one. In contrast to this, the mean value is outside of the one standard deviation interval around zero, but it still agrees with the expectations within two standard deviations.
To summarize the results of the toy studies, all values match the expectations within two standard deviations. Thus, the fit is validated.

A.4 Toys for Simultaneous Fit with Systematic Uncertainties

In this chapter, the results of the toy studies for the simultaneous fit on the reduced MC sample are analysed. In contrast to the last chapter, the systematic uncertainties are included in the fit. The signal events in the MC sample are the three decays $B^+ \to p\overline{\Lambda}\pi^+\pi^-$, $B^+ \to p\overline{\Lambda}\rho^0(\to \pi^+\pi^-)$ and $B^+ \to p\overline{\Lambda}f_2(\to \pi^+\pi^-)$.

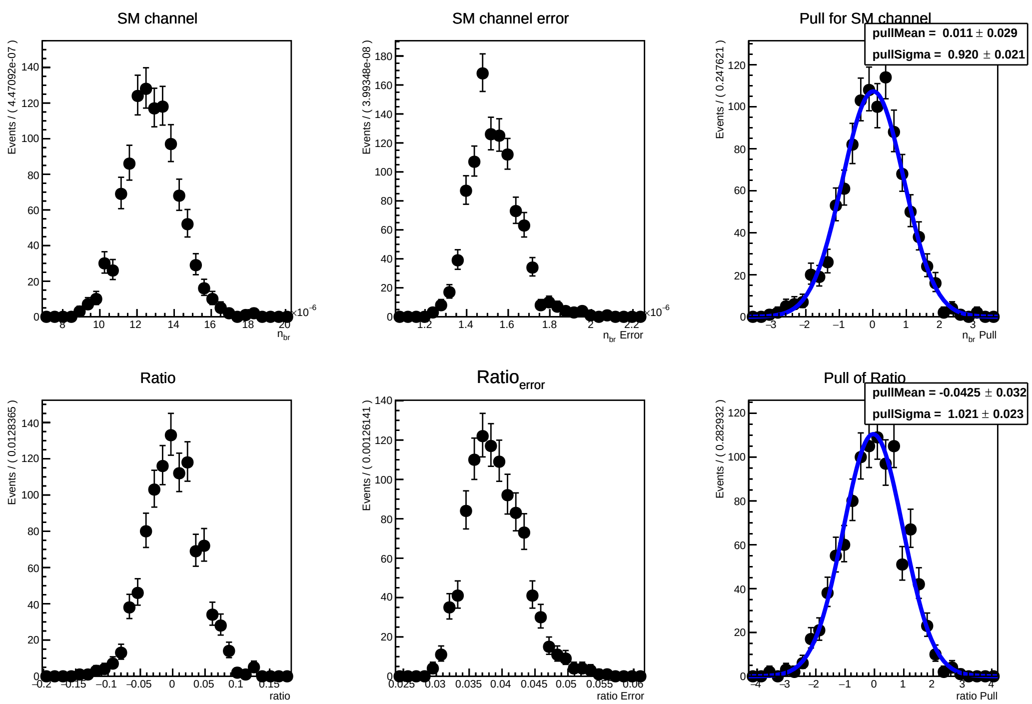

Figure A.9: This image shows the toy study results for $\mathcal{BR}_{SM}$ (first row) and $\mathcal{R}$ (second row) for the simultaneous fit on the reduced MC sample with systematic uncertainties included. The signal events contain just events out of the decays specified in ref. [26].

Starting with the toy study for $\mathcal{BR}_{SM}$ and $\mathcal{R}$, the expected value for the $\mathcal{BR}_{SM}$ is $1.273{\times}10^{-5}$. This is represented by the distribution of this variable presented in fig. A.9. The mean value of the Gaussian fit to the pull distribution of $\mathcal{BR}_{SM}$ agrees within one standard deviation with zero. Contrary, the sigma has a value of 0.920±0.021 and is thus more than three standard deviations away from the expectation. The interpretation of a smaller sigma is the overestimation of the uncertainties. This is fullfilled, as the included systematic uncertainties are overrated. Thus, the result is not optimal, but represents the input. For the Gaussian fit to the pull distribution of $\mathcal{R}$, the sigma is roughly the expectation and the mean value agrees with zero within two standard deviations. Overall, the toy studies presented here describe the expectations.

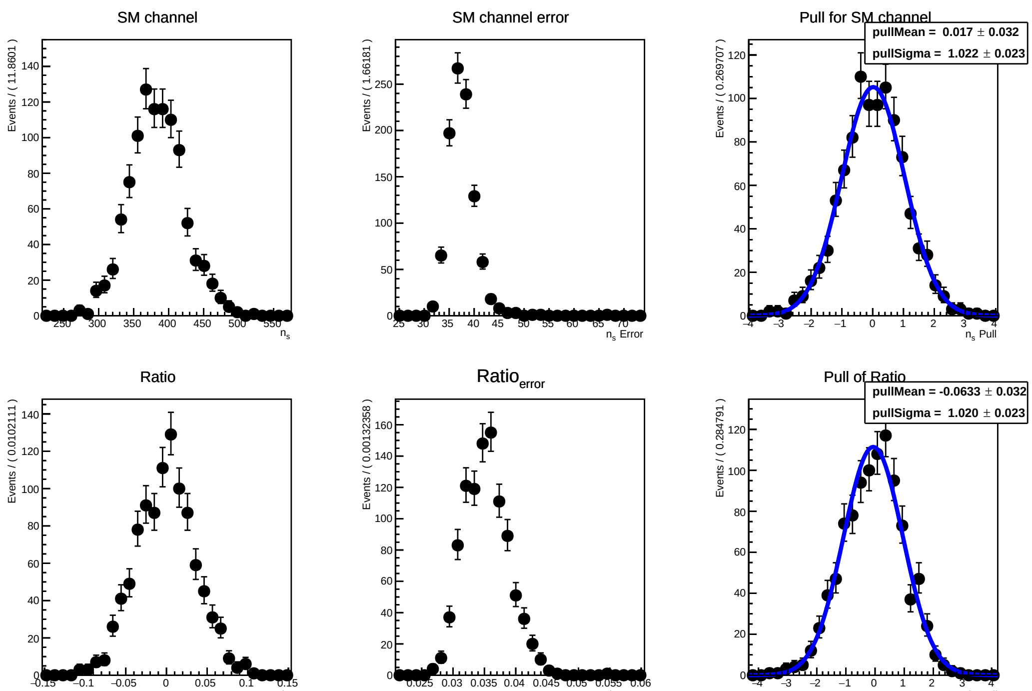

Figure A.10: In this figure, the first row presents the results of the toy studies for the variable N_{sig}, while the results for the ratio $\mathcal{R}$ are represented in the second row. The corresponding fit function includes the systematic uncertainties and is fitted to the reduced MC sample with the three decays of ref. [26] included as signal events.

Continuing now with the results of the toy studies for N_{sig} and $\mathcal{R}$, the results of the Gaussian fit to the pull distribution of N_{sig} match the expectations within one standard deviation. For the Gaussian fit to the pull distribution of the $\mathcal{R}$, the sigma agrees within one standard deviation with one and the mean value within two standard deviations with zero. The distributions of the variables peak at the expected values N_{sig}=381 and $\mathcal{R}$=0. Thus, the fit is validated.

A.5 Upper Limit Addition

In this chapter, another upper limit is shown. It was calculated using the full MC sample and the one dimensional fitting function.

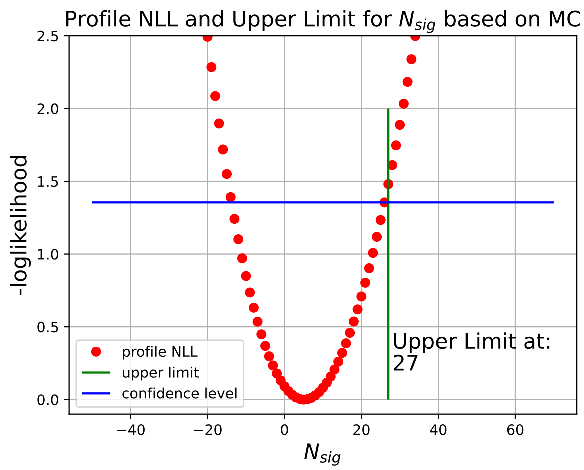

Figure A.11: This figure depicts the upper limit for the full MC sample and the one-dimensional fit.

The results are presented in fig. A.11. The procedure to determine the upper limit is described in the text. As a result, an upper limit of $N_{sig} = 27$ is determined. This is similar to fig. 5.32, where an upper limit of $N_{sig} = 28$ is calculated. Thus, the expectations are satisfied, since the only difference between these two results is the size of the MC sample.

Appendix B

Tables

B.1 BDT

A different number of files was used for the training of the BDT. These are listed in table B.1.

	$c\bar{c}$	$u\bar{u}$	$d\bar{d}$	$s\bar{s}$	τ-pair	$B^0\overline{B}^0$	B^+B^-	Signal MC (SM)
BDT training files	80	80	20	20	20	40	40	100
BDT test files	4	4	1	1	1	2	2	5
reduced MC [%]	96.41	96.39	96.39	96.38	96.43	96.40	96.42	60

Table B.1: This table provides an overview over the MC data used for the BDT training.

The different columns of the table are chosen to match the categories of the MC sample and the Signal MC. The second row states the number of files used for the BDT training. These files were excluded for the fourth row as were some more to have the same percentage for all categories in the reduced MC sample, which is at 96.4% for all categories of the MC sample, and thus still model the expected events in the detector. The Signal MC for the beyond Standard Model decay channel was not used for the BDT training, hence the sample is not reduced.

B.2 Cut Optimization

To estimate the quality of the cuts, the figure of merit is used on the BSM decay channel and the cuts are varied on a small scale to estimate the difference. The results are given in table B.2. The decreased MC sample (table B.1) is used for the analysis and the f.o.m., is used as reference and is calculated in the signal region. 1×10^6 signal events from the Signal MC for the beyond Standard Model decay are used for the calculation of the efficiency, while the N_{bkg} is extracted from the decreased MC sample. The applied procedure first

	+10%	+5%	+1%	-1%	-5%	-10%
Cont.Prob output	-4%	-3%	-2%			
χ^2 probability (vertex fit)	0.3%	0%	0%	0%	0.3%	0.3%
E (p_Λ)	-7%	-4%	-1%	0.6%	0.9%	-5%
$\lvert\Delta E\rvert$	-3%	-2%	-0.6%			
R2	0%	0%	0%	0%	0%	0%
cosTBTO	3%	1%	0.3%	0.3%	0%	-2%

Table B.2: This table depicts the results for the variation of the cuts evaluated with the figure of merit, defined in equ. 5.5.

selects one cut and adds 10% of the cut number to the cut and then continues with the columns until 10% of the cut value are subtracted from the limit, while the other cuts are not varied. For example adding 10% to Cont.Prob output < 0.44 would lead to Cont.Prob output < 0.484. The f.o.m. (equ. 5.5) for the initial cuts is subtracted from the f.o.m. for the varied cuts and the result is divided by the initial f.o.m. to evaluate the fluctuations of the f.o.m. in % of the initial value. Thus, also negative deviations meaning worse results can result out of the varied cuts. Empty spaces are left for variables, which are not varied in certain directions. This is due to the limitations on the cuts from the distribution of the Signal MC for the cut variable. Furthermore, two cuts are not listed here, since they are fixed. As a result, the potential increase in the cut optimization is found to be 3%.

B.3 Comparison of Signal MC for Standard Model Decay Channel and Beyond Standard Model Decay Channel

In order to compare the shapes of the event distribution of the SM decay channel and the BSM decay channel, the χ^2 test is used. The p-values are given in table B.3.
For the Standard Model decay channel, the reduced Signal MC sample B.1 was used. To the Signal MC sample of the beyond Standard Model decay channel, a weight was applied to scale it down to be comparable with the Signal MC of the Standard Model decay channel. The comparison took place for only correctly reconstructed events. The used bin number for the data ranges is forty. Again, the total number of counts for the Standard Model decay channel was normalized to the amount of counts for the beyond Standard Model decay channel. Sometimes, the MC data range for the χ^2 test is less than the range of the variable itself. This was chosen for the Signal MC data not filling out the whole range of the variable, since the χ^2 test is not applicable for regions without Signal MC.

cut variable	range	p-value
Cont.Prob output	(0, 1)	8.837×10^{-15}
χ^2 probability (vertex fit)	(0, 0.01)	0.013
E (p_Λ)	(0.95, 2.5) GeV	0.023
$\|\Delta E\|$	(-0.03, 0.03) GeV	0.088
R2	(0, 0.5)	4.102×10^{-5}
$p\_protonID$	(0.8, 1)	0.028
p_pionID	(0, 0.2)	0.037
$p_\Lambda\_protonID$	(0.8, 1)	0.051
p_Λ_pionID	(0, 0.2)	0.045
cosTBTO	(0, 1)	0.033

Table B.3: This table summarizes the p-values (equ. 5.3) of the χ^2 test (equ. 5.2) for the cut variables, which was applied to the comparison of the Signal MC for the Standard Model decay channel and for the beyond Standard Model decay channel.

B.4 Correlation Matrices of Simultaneous Fit

The correlation matrix for the simultaneous fit focusing on the branching ratio $\mathcal{BR}$ and the ratio $\mathcal{R}$ is depicted in table B.4.

	$\mathcal{BR}_{SM}$	N_{bkg}	N_{bsm}	$\mathcal{R}$	Θ	α	m	η_{SM}	η_{BSM}	σ	ξ	ξ_{BSM}
$\mathcal{BR}_{SM}$	1.00	-0.33	-0.02	0.00	-0.03	0.09	0.03	-0.03	0.00	0.51	0.48	0.03
N_{bkg}	-0.33	1.00	0.01	-0.01	0.01	-0.04	-0.02	0.00	0.00	-0.24	-0.23	-0.02
N_{bsm}	-0.02	0.01	1.00	-0.30	0.01	0.02	0.03	0.00	0.00	-0.04	-0.02	-0.14
$\mathcal{R}$	0.00	-0.01	-0.30	1.00	-0.02	-0.08	-0.10	0.00	0.00	0.10	0.01	0.45
Θ	-0.03	0.01	0.01	-0.02	1.00	0.16	0.09	0.00	0.00	-0.04	0.10	0.07
α	0.09	-0.04	0.02	-0.08	0.16	1.00	0.74	0.00	0.00	0.23	0.05	-0.02
m	0.03	-0.02	0.03	-0.10	0.09	0.74	1.00	0.00	0.00	0.15	0.03	-0.04
η_{SM}	-0.03	0.00	0.00	0.00	0.00	0.00	0.00	1.00	0.00	0.00	0.00	0.00
η_{BSM}	0.00	0.00	0.00	0.00	0.00	0.00	0.00	0.00	1.00	0.00	0.00	0.00
σ	0.51	-0.24	-0.04	0.10	-0.04	0.23	0.15	0.00	0.00	1.00	0.34	0.06
ξ	0.48	-0.23	-0.02	0.01	0.10	0.05	0.03	0.00	0.00	0.34	1.00	0.03
ξ_{BSM}	0.03	-0.02	-0.14	0.45	0.07	-0.02	-0.04	0.00	0.00	0.06	0.03	1.00

Table B.4: This table depicts the correlations for the simultaneous fit focusing on $\mathcal{BR}$. The variable N_{bsm} is the abbreviation of $N_{bkg,bsm}$.

The definition of the correlation is given in the text. The correlation table for the simultaneous fit parameters focusing on N_{sig} and $\mathcal{R}$ is given in table B.5. Correlations higher or equal $|10|\%$ are highlighted.

	N_{bkg}	$N_{bkg,bsm}$	N_{sig}	$\mathcal{R}$	$\mathcal{R}_\eta$	Θ	α	m	σ	ξ	ξ_{BSM}
N_{bkg}	1.00	0.01	-0.33	-0.01	0.00	0.02	-0.03	-0.01	-0.24	-0.22	-0.02
$N_{bkg,bsm}$	0.01	1.00	-0.02	-0.30	0.00	0.01	0.02	0.03	-0.04	-0.02	-0.14
N_{sig}	-0.33	-0.02	1.00	0.00	0.00	-0.03	0.06	0.01	0.50	0.47	0.03
$\mathcal{R}$	-0.01	-0.30	0.00	1.00	0.00	-0.02	-0.08	-0.10	0.10	0.01	0.45
$\mathcal{R}_\eta$	0.00	0.00	0.00	0.00	1.00	0.00	0.00	0.00	0.00	0.00	0.00
Θ	0.02	0.01	-0.03	-0.02	0.00	1.00	0.14	0.07	-0.05	0.10	0.07
α	-0.03	0.02	0.06	-0.08	0.00	0.14	1.00	0.74	0.21	0.03	-0.03
m	-0.01	0.03	0.01	-0.10	0.00	0.07	0.74	1.00	0.13	0.01	-0.04
σ	-0.24	-0.04	0.50	0.10	0.00	-0.05	0.21	0.13	1.00	0.33	0.06
ξ	-0.22	-0.02	0.47	0.01	0.00	0.10	0.03	0.01	0.33	1.00	0.03
ξ_{BSM}	-0.02	-0.14	0.03	0.45	0.00	0.07	-0.03	-0.04	0.06	0.03	1.00

Table B.5: In this table, the correlations between the fit parameters of the simultaneous fit focusing on N_{sig} and $\mathcal{R}$ are depicted.

B.5 PID Correction

The first analysed systematic is the PID correction. Two different tables are presented in the following.

	p			p_Λ			π^+			π^-		
	p	π	K	p	π	K	π	K	p	π	K	p
$B^+ \to p\overline{\Lambda}\pi^+\pi^-$	0.6	0.0	0.0	1.0	16.5	2.6	7.3	0.0	0.0	7.5	0.0	0.0
$B^+ \to p\Lambda\pi^+\pi^-$	0.5	0.0	0.0	0.5	19.0	5.3	10.4	0.0		9.8	0.0	0.0

Table B.6: This table summarizes the percentages of missing particles. For the empty bin the explanation is the absence of events (no p taken for a π^+).

The first table (B.6) depicts the percentage of missing particles both for the efficiency correction of the true particles and the fake rate correction of the false particles. The three particles considered are always p, π and K. The used reduced MC sample is utilised for both the reconstruction of the SM decay channel (first row) and the BSM decay channel (second row of the table B.7) The SM decay channel includes for the correctly reconstructed signal events just the three decays $B^+ \to p\overline{\Lambda}\pi^+\pi^-$, $B^+ \to p\overline{\Lambda}\rho^0(\to \pi^+\pi^-)$ and $B^+ \to p\overline{\Lambda}f_2(\to \pi^+\pi^-)$.
The second table gives an overview over the percentage of missing particles for the pid correction using the Signal MC samples for the three decays of paper [26]. It has to be noted, that the table does not include fake rate particles. This is due to the definition of the efficiency including just correctly reconstructed events. Thus, no fake rate particles are included by definition. Furthermore, the percentage for the two pions of the decay via the intermediate ρ^0 is the double amount compared to the other two decays. Further information can be found in the text.

	p_{miss}	$p_{\Lambda,miss}$	π^+_{miss}	π^-_{miss}
$B^+ \to p\overline{\Lambda}\pi^+\pi^-$	0.2%	0.3%	4.3%	4.4%
$B^+ \to p\overline{\Lambda}\rho^0(\to \pi^+\pi^-)$	0.1%	0.3%	10.2%	10.0%
$B^+ \to p\overline{\Lambda}f_2(\to \pi^+\pi^-)$	0.1%	0.3%	2.9%	3.1%

Table B.7: As only correctly reconstructed events are used for the efficiency correction resulting out of the PID correction, this table summarizes the missing particle percentage for true particles and not for fake rates. The missing particles are outside of the range of the variables used to create the pid table.

B.6 Slow Momentum Corrections Addition

The second systematic, which was analysed, is the slow pion momentum correction.

	$B^+ \to p\overline{\Lambda}\pi^+\pi^-$		$B^+ \to p\overline{\Lambda}\rho^0(\to \pi^+\pi^-)$		$B^+ \to p\overline{\Lambda}f_2(\to \pi^+\pi^-)$	
correction	0.9966621		0.9966689		0.9969949	
	abs	diff	abs	diff	abs	diff
bin 1 up	1.00241	0.00575	1.00213	0.00547	1.00214	0.00515
bin 1 down	0.99091	0.00575	0.99121	0.00546	0.99185	0.00515
bin 2 up	0.99567	-0.00099	0.99536	-0.00130	0.99607	-0.00093
bin 2 down	0.99765	-0.00099	0.99797	-0.00130	0.99792	-0.00093
bin 3 up	0.99661	-5.3967×10^{-5}	0.99664	-2.4367×10^{-5}	0.99692	-7.3105×10^{-5}
bin 3 down	0.99672	-5.4138×10^{-5}	0.99669	-2.4384×10^{-5}	0.99707	-7.3103×10^{-5}

Table B.8: This table depicts the results for the variations of the slow pion momentum corrections for each of the three bin variations. The difference values are computed with more digits than given in the table.

Table B.8 depicts the intermediate step of the analysis before calculating the uncertainty of the correction. The used sample is the Signal MC for the individual decay channels with a decreased sample for the direct decay (see Appendix table B.1). Only signal events passing the cuts and located in the signal region are taken into account. The numbers in the second row are the correction values summed up over all events and divided by the number of events. The same procedure is applied to the columns 'abs', but here the variation bin up and down are used. The column 'diff' gives the difference of the average up variation minus the average correction value and the difference between the average correction and the average down variation value, so basically the value of the column 'abs' minus the correction value of the second row or vice versa.

Bibliography

[1] https://software.belle2.org/development/sphinx/index.html. Accessed 04.09.2024.

[2] https://github.com/belle2/basf2. Accessed 02.09.2024.

[3] https://root.cern.ch. Accessed 30.08.2024.

[4] https://syscorrfw.readthedocs.io/en/latest/particleid_weight_production.html. Accessed 21.08.2024.

[5] https://gitlab.desy.de/william.sutcliffe/pidvar. Accessed 04.09.2024.

[6] R. Aaij, B. Adeva, et al. Evidence for the two-body charmless baryonic decay $B^+ \to p\overline{\Lambda}$. *Journal of High Energy Physics*, 04:162, 2017.

[7] R. Aaij et al. Evidence for CP violation in $B^+ \to p\overline{p}K^+$ decays. *arXiv:1407.5907v1*, 2014.

[8] R. Aaij et al. Search for the baryon-and lepton-number violating decays $B^0 \to p\mu^-$ and $B_s^0 \to p\mu^-$. *Physical Review D*, 108(1):012021, 2023.

[9] T. Abe, I. Adachi, K. Adamczyk, S. Ahn, H. Aihara, K. Akai, M. Aloi, L. Andricek, K. Aoki, Y. Arai, et al. Belle II Technical Design Report. *arXiv preprint arXiv:1011.0352*, 2010.

[10] M. Ablikim, M.N. Achasov, P. Adlarson, S. Ahmed, M. Albrecht, R. Aliberti, A. Amoroso, Q. An, Y. Bai, O. Bakina, et al. Search for $\overline{\Lambda} - \Lambda$ Baryon-Number-Violating Oscillations in the Decay $J/\psi \to pK^-\overline{\Lambda}$ + c.c. *Phyical Review Letters*, 131(12):121801, 2023.

[11] I. Adachi, T.E. Browder, P. Križan, S. Tanaka, and Y. Ushiroda. Detectors for extreme luminosity: Belle II. *Nuclear Instruments and Methods in Physics Research Section A: Accelerators, Spectrometers, Detectors and Associated Equipment*, 907:46–59, 2018.

[12] S. Agostinelli, J. Allison, K. Amako, J. Apostolakis, et al. GEANT4—a simulation toolkit. *Nuclear instruments and methods in physics research section A: Accelerators, Spectrometers, Detectors and Associated Equipment*, 506:250–303, 2003.

[13] B. Aharmim, S.N. Ahmed, A.E. Anthony, N. Barros, et al. Search for neutron-antineutron oscillations at the Sudbury Neutrino Observatory. *Physical Review D*, 96(9):092005, 2017.

[14] K. Akai, K. Furukawa, and H. Koiso. SuperKEKB collider. *Nuclear Instruments and Methods in Physics Research Section A: Accelerators, Spectrometers, Detectors and Associated Equipment*, 907:188–199, 2018.

[15] H. Albrecht, P. Böckmann, R. Gläser, G. Harder, A. Krüger, A. Nippe, M. Schäfer, W. Schmidt-Parzefall, H. Schröder, H.D. Schulz, et al. Observation of charmless B meson decays. *Physics Letters B*, 209(1):119–126, 1988.

[16] H. Albrecht, R. Gläser, G. Harder, A. Krüger, A.W. Nilsson, A. Nippe, T. Oest, M. Reidenbach, M. Schäfer, W. Schmidt-Parzefall, et al. Search for hadronic b $\rightarrow$ u decays. *Physics Letters B*, 241(2):278–282, 1990.

[17] D.M. Asner, M. Athanas, D.W. Bliss, W.S. Brower, G. Masek, H.P. Paar, et al. Search for exclusive charmless hadronic B decays. *Physical Review D*, 53(3):1039, 1996.

[18] K.S. Babu, E. Kearns, U. Al-Binni, S. Banerjee, D.V. Baxter, Z. Berezhiani, M. Bergevin, S. Bhattacharya, S. Brice, R. Brock, et al. Baryon number violation. *arXiv preprint arXiv:1311.5285v1*, 2013.

[19] C. Baltay, A. Bridgewater, W.A. Cooper, M. Habibi, and N. Yeh. Precision Measurement of the Lifetime and Decay Branching Rratio of the Λ^0 Hyperon. *Physical Review D*, 4(3):670–676, 1971.

[20] S. Behrends, K. Chadwick, J. Chauveau, P. Ganci, T. Gentile, et al. Observation of exclusive decay modes of b-flavored mesons. *Physical Review Letters*, 50(12):881, 1983.

[21] A. Belyaev and D.A. Ross. *The Basics of Nuclear and Particle Physics*. Springer, 2021.

[22] M. Beneke, G. Finauri, and A.A. Petrov. Indirect constraints on third generation baryon number violation. *arXiv preprint arXiv:2404.09642v1*, 2024.

[23] Ed. A.J. Bevan, B. Golob, Th. Mannel, S. Prell, and B.D. Yabsley. *The Physics of the B Factories*. Eur.Phys.J.C74 (2014) 3026, SLAC-PUB-15968, KEK Preprint 2014-3.

[24] C. Cecchi, G. De Nardo, E. Manoni, and M. Merola. B counting measurement of the Run 1 Belle II data sample. Available at `https://docs.belle2.org/record/3468/files/BELLE2-NOTE-PH-2023-011_v2.pdf`, Accessed: 2024-08-26.

[25] Y.-W. Chang et al. Observation of $B^0 \rightarrow \Lambda\overline{\Lambda}K^0$ and $B^0 \rightarrow \Lambda\overline{\Lambda}K^{*0}$ at Belle. *arXiv:0811.3826v2*, 2009.

[26] P. Chen, M.-Z. Wang, H. Aihara, A.M. Bakich, V. Balagura, V. Bhardwaj, M. Bischofberger, A. Bozek, M. Bračko, T.E. Browder, et al. Observation of $B^+ \to p\overline{\Lambda}\pi^+\pi^-$ at Belle. *Physical Review D*, 80(11):111103, 2009.

[27] S. Choudhury, S. Sandilya, K. Trabelsi, A. Giri, et al. Measurement of the B^+/B^0 production ratio in e^+e^- collisions at the Υ(4S) resonance using B $\to$ J/$\psi(\ell\ell)$K decays at Belle. *Physical Review D*, 107(3):L031102, 2023.

[28] G. Cowan. *Statistical Data Analysis.* Oxford University Press, 1998.

[29] F.S. Crawford, M. Cresti, R.L. Douglass, M.L. Good, G.R. Kalbfleisch, M.L. Stevenson, and H.K. Ticho. Evidence for the $\Delta I = \frac{1}{2}$ rule. *Physical Review Letters*, 2(6):266, 1959.

[30] N. Davidson, T. Przedzinski, and Z. Was. PHOTOS interface in C++: Technical and physics documentation. *Computer Physics Communications*, 199:86–101, 2016.

[31] P. del Amo Sanchez, J.P. Lees, V. Poireau, et al. Searches for the baryon-and lepton-number violating decays $B^0 \to \Lambda_c^+ l^-$, $B^- \to \Lambda l^-$, and $B^- \to \overline{\Lambda} l^-$. *Physical Review D*, 83(9):091101, 2011.

[32] D. Dorner, P. Rados, and C. Schwanda (Belle II Collaboration). Relative tracking efficiency study of charged, low momentum pions. Available at `https://docs.belle2.org/record/3694/files/BELLE2-NOTE-PH-2023-035.pdf`, Accessed: 2024-07-19.

[33] E. Farhi. Quantum chromodynamics test for jets. *Phyical. Review Letters*, 39(25):1587, 1977.

[34] R.A. Fisher. The use of multiple measurements in taxonomic problems. *Annals of eugenics*, 7(2):179–188, 1936.

[35] I. Fleck, M. Titov, C. Grupen, and I. Buvat. *Handbook of Particle Detection and Imaging.* Springer, Cham, 2021.

[36] G.C. Fox and S. Wolfram. Observables for the Analysis of Event Shapes in e^+ e^- Annihilation and Other Processes. *Physical Review Letters*, 41(23):1581, 1978.

[37] D Griffiths. *Introduction to Elementary Particles.* WILEY-VCH Verlag GmbH Co. KGaA, 2008.

[38] W.D. Hulsbergen. Decay chain fitting with a Kalman filter. *Nuclear Instruments and Methods in Physics Research Section A: Accelerators, Spectrometers, Detectors and Associated Equipment*, 552:566–575, 2005.

[39] W.E. Humphrey and R.R. Ross. Low-energy interactions of K$^-$ mesons in hydrogen. *Physical Review*, 127:1305–1323, 1962.

[40] H. Ikeda, A. Satpathy, B.S. Ahn, et al. A detailed test of the CsI (Tℓ) calorimeter for BELLE with photon beams of energy between 20 MeV and 5.4 GeV. *Nuclear Instruments and Methods in Physics Research Section A: Accelerators, Spectrometers, Detectors and Associated Equipment*, 441:401–426, 2000.

[41] S. Jadach, B.F.L. Ward, and Z. Wąs. The precision Monte Carlo event generator $\mathcal{KK}$ for two-fermion final states in e^+e^- collisions. *Computer Physics Communications*, 130(3):260–325, 2000.

[42] S. Jadach, B.F.L. Ward, and Z. Wąs. Coherent exclusive exponentiation for precision Monte Carlo calculations. *Physical Review D*, 63(11):113009, 2001.

[43] F. James and M. Winkler. Minuit user's guide. *CERN, Geneva*, 2004.

[44] T.M. Karbach and M. Schlupp. Constraints on yield parameters in extended maximum likelihood fits. *arXiv preprint arXiv:1210.7141v1*, 2012.

[45] T. Keck. FastBDT: A speed-optimized multivariate classification algorithm for the Belle II experiment. *Comput Softw Big Sci*, 1, 2017.

[46] E. Kou, P. Urquijo, W. Altmannshofer, F. Beaujean, G. Bell, M. Beneke, et al. *The Belle II Physics Book*. Progress of Theoretical and Experimental Physics, 2019.

[47] T. Kuhr, C. Pulvermacher, M. Ritter, T. Hauth, and N. Braun. The Belle II Core Software: Belle II Framework Software Group. *arXiv:1809.04299v2*, 2018.

[48] T.K. Kuo and S.T. Love. Neutron oscillations and the existence of massive neutral leptons. *Physical Review Letters*, 45(2):93, 1980.

[49] K. Lalwani. The Belle II experiment: Status and prospects. *SciPost Physics Proceedings*, 2023.

[50] D.J. Lange. The EvtGen particle decay simulation package. *Nuclear Instruments and Methods in Physics Research Section A: Accelerators, Spectrometers, Detectors and Associated Equipment*, 462(1-2):152–155, 2001.

[51] L. Lista. *Statistical Methods for Data Analysis: With Applications in Particle Physics*. Springer, Cham, 2023.

[52] F.G.K. Metzner. *Preparation of a measurement of $R\ (D^*)$ with leptonic τ and hadronic FEI tag at the Belle experiment*. PhD thesis, Karlsruher Institut für Technologie (KIT), 2022.

[53] T. Ohlsson. Proton decay. *Nuclear Physics B*, 993:116268, 2023.

[54] F. Oosterhof, B. Long, J. de Vries, R.G.E. Timmermans, and U. van Kolck. Baryon-number violation by two units and the deuteron lifetime. *Physical Review Letters*, 122(17):172501, 2019.

[55] G. Punzi. Sensitivity of searches for new signals and its optimization. *arXiv preprint physics/0308063v2*, 2003.

[56] P. Rados, G. Inguglia, L. Zani, A. Glazov, and A. Rostomyan. Tracking efficiency with taus. Available at `https://indico.belle2.org/event/8043/contributions/51113/attachments/20577/30471/tau_eff_f2f_31jan23.pdf`, Accessed: 2024-08-26.

[57] T. Sjöstrand, S. Ask, J.R. Christiansen, R. Corke, N. Desai, P. Ilten, S. Mrenna, S. Prestel, C.O. Rasmussen, and P.Z. Skands. An introduction to PYTHIA 8.2. *Computer Physics Communications*, 191:159–177, 2015.

[58] Y.-T. Tsai et al. Search for $B^0 \to p\overline{p}, \Lambda\overline{\Lambda}$ and $B^+ \to p\overline{\Lambda}$ at Belle. *Physical Review D*, 75(11):111101, 2007.

[59] W. Verkerke and D. Kirkby. The RooFit toolkit for data modeling. *arXiv:physics/0306116v1*, 2003.

[60] W. Waltenberger. Rave—a detector-independent toolkit to reconstruct vertices. *IEEE Transactions on Nuclear Science*, 58(2):434–444, 2011.

[61] M.Z. Wang et al. Study of $B^+ \to p\overline{\Lambda}\gamma, p\overline{\Lambda}\pi^0$ and $B^0 \to p\overline{\Lambda}\pi^-$. *Physical Review D*, 76(5):052004, 2007.

[62] (Particle Data Group) R.L. Workman et al. Review of particle physics. *Progress of Theoretical and Experimental Physics*, 2022:083C01, 2022.

Acknowledgements

First of all, I would like to thank Prof. Dr. Thomas Kuhr and Dr. Thomas Lück for the opportunity to work on such an interesting topic for my thesis. Their guidance and support on the development of the analysis provided me an amazing insight into methods and structures of data analysis.
A special thanks to Dr. Thomas Lück for his detailed explanations and his patience for all the questions I had.
I also want to thank the whole group for welcoming me in such a friendly environment. This made the work on my thesis an awesome experience.
Finally, I want to thank my family, friends and my boyfriend for their lasting support during this time.

Erklärung/Declaration

Hiermit erkläre ich, die vorliegende Arbeit selbständig verfasst zu haben und keine anderen als die in der Arbeit angegebenen Quellen und Hilfsmittel benutzt zu haben.

I hereby declare that this thesis is my own work, and that I have not used any sources and aids other than those stated in the thesis.

München, 09.09.2024
Melanie Hess